
**Improving one-dimensional
electro-acoustic models of the ear –
applications to
young infant's middle ear screening
and to
feedback cancellation in hearing aids**

Von der Fakultät VI für Medizin und Gesundheitswissenschaften
der Carl von Ossietzky Universität Oldenburg
zur Erlangung des Grades und Titels

Doktor der Ingenieurwissenschaften
(Dr.-Ing.)

angenommene Dissertation

von Herrn M. Tobias Sankowsky-Rothe
geboren am 15.11.1974 in Showa/Äthiopien

Gutachter: Prof. Dr. Steven van de Par
Weitere Gutachter*innen: Prof. Dr. Matthias Blau
Prof. Dr. Janina Fels
Tag der Disputation: 19.09.2023

Summary

This thesis is about the improvement of audiological applications by means of one-dimensional electro-acoustic models of the ear. One application, from the diagnostic field, is the middle ear screening for young infants. The second application, from the rehabilitative field, is the adaptive feedback cancellation in hearing aids. The use of one-dimensional electro-acoustic models allow the investigation of influences of physiological, pathological and/or environmental properties on acoustic quantities.

Middle ear screening is used to detect pathological conditions affecting sound conduction. It is based on the determination of a wideband acoustic immittance (WAI) quantity from an acoustical measurement in the ear canal. WAI comprises the quantities acoustic impedance, acoustic admittance and further quantities derived from these two. The measured WAI quantity is therefore intended to detect whether there is any abnormality regarding the middle ear. For children and adults, established methods exist to detect pathological middle ear conditions, however, for young infants, it is still difficult to make clear statements about the middle ear status based on WAI measurements. While the ear canal and the middle ear are very similar in children and adults, they differ significantly in infants.

One of the overall objective is to specify normative WAI data for young infants. To get closer to that objective, it is important to understand, on the one hand, WAI results in young infants with healthy middle ear and, on the other hand, in which way pathological middle ear conditions influence WAI quantities. In order to get insight into this, a one-dimensional electro-acoustic model of the ear canal and the middle ear of the healthy adult's ear is adapted to the young infant's ear. Furthermore, adaptations are made to improve the relation to physiology. In the next step, the model is enhanced so that two different pathological middle ear conditions can be reproduced. Moreover, in this study, measurements of the acoustic impedance were made in the ear canal of young infants with normal or pathological middle ear. These measurements are used, on the one hand, to trace general differences in the acoustic impedance caused by pathological middle ear conditions and by inter-individual differences. On the other hand, the impedance measurements are used for the development of the model.

With the one-dimensional electro-acoustic model of the infant's ear canal and middle ear, it is shown that the medium frequency range of the acoustic impedance between about 1 kHz to 3 kHz is dominated by the properties of the middle ear. At lower frequencies, properties of the ear canal are dominant. The range at higher frequencies is characterized by a strong inter-individual variability. Furthermore, the effect of the pathological middle ear condition of fluid in the middle ear is reproduced by the model. In addition, a proposal is made to model the pathological middle ear condition of a static air pressure difference between the ear canal and the middle ear cavities. Finally, it is shown for all relevant WAI quantities that the pathological middle ear conditions implemented in the model lead to characteristic differences compared to the healthy middle ear. However, it is also

shown that the WAI quantity of the acoustic absorbance, which is often used in studies, is extremely sensitive to the assumption of the ear canal's cross-sectional area at the probe tip necessary for its determination.

Adaptive feedback cancellation prevents the occurrence of acoustic feedback in hearing aids by using adaptive signal processing. It is based on the continuous estimation of the acoustic feedback path, i.e. the acoustic path from the speaker to the microphone of the hearing aid. In order to allow a fast adaptation, the feedback path is split up into a time-invariant fixed part and a time varying variable part.

The aim of this work is to determine a time-invariant fixed part so that the variable part can be adapted as fast as possible. Two different approaches to determine the time-invariant fixed part are compared. One is a novel approach based on a defined physical position and the other one a state-of-the-art position independent approach. Firstly, for the development of the defined physical position approach, a one-dimensional electro-acoustic model is designed which is used to identify those components of the acoustic feedback path which behave in a time-invariant manner. Based on the model, different variants of the fixed part according to this approach are developed. In general, it is assumed for this approach that the hearing aid is equipped with an ear canal microphone, so that a signal can be measured in the ear canal, which can then be used to determine the fixed part of the acoustic feedback path. The different variants according to the defined physical position approach are then compared with variants according to a position independent approach. A requirement for the latter is that at least two measured feedback paths are available, which differ for example with respect to slightly differing microphone positions. For all comparisons, real measured feedback paths are used. The performance is quantified by the added stable gain.

For the variants according to the defined physical position approach, it is shown that the variant in which the fixed part is directly derived from the measurement with the ear canal microphone slightly outperforms the other variants. The comparison of the two different approaches shows that a similar performance is achieved with both of them. Thus, the choice of which approach to use can be based on the respective requirements and advantages.

Zusammenfassung

In dieser Dissertation geht es um die Verbesserung audiologischer Anwendungen mithilfe von eindimensionalen elektroakustischen Modellen des Ohres. Eine Anwendung, aus dem diagnostischen Bereich, ist das Mittelohr-Screening bei Säuglingen. Die zweite Anwendung, aus dem rehabilitativen Bereich, ist die adaptive Rückkopplungsauslöschung in Hörgeräten. Der Einsatz von eindimensionalen elektroakustischen Modellen ermöglicht die Untersuchung von Einflüssen physiologischer, pathologischer und/oder umgebungsbedingter Eigenschaften auf akustische Größen.

Mittelohr-Screening dient der Erkennung pathologischer Zustände, die die Schalleitung beeinträchtigen. Es basiert auf der Bestimmung einer *wideband acoustic immittance* (WAI) Größe aus einer akustischen Messung im Gehörgang. Unter WAI sind die Größen akustische Impedanz, akustische Admittanz und weitere daraus abgeleitete Größen zusammengefasst. Aus der gemessenen WAI Größe soll somit erkannt werden, ob eine Auffälligkeit bezüglich des Mittelohres besteht. Für Kinder und Erwachsene existieren bewährte Methoden zur Detektion von pathologischen Mittelohrzuständen, für Säuglinge gilt es jedoch immer noch als schwierig, anhand von WAI Messungen klare Aussagen über den Mittelohrstatus zu treffen. Während der Gehörgang und das Mittelohr von Kindern und Erwachsenen sehr ähnlich sind, unterscheiden sie sich demgegenüber bei Säuglingen noch deutlich.

Eines der übergeordneten Ziele ist, normative WAI Daten für Säuglinge zu spezifizieren. Um diesem Ziel näher zu kommen, ist es wichtig zu verstehen, wie einerseits WAI Größen bei Säuglingen mit gesundem Mittelohr ausfallen und andererseits, in welcher Weise pathologische Mittelohrzustände WAI Größen beeinflussen. Um hier Einblick zu erlangen wird ein eindimensionales elektroakustisches Modell von Gehörgang und Mittelohr für das gesunde Ohr von Erwachsenen angepasst auf das Säuglingsohr. Darüber hinaus werden Anpassungen vorgenommen, um den Bezug zur Physiologie zu verbessern. Im nächsten Schritt wird das Modell erweitert, sodass zwei verschiedene pathologische Mittelohrzustände mit dem Modell nachgebildet werden können. Im Rahmen dieser Arbeit wurden außerdem Messungen der akustischen Impedanz im Gehörgang von Säuglingen mit normalem oder mit pathologischem Mittelohr durchgeführt. Diese Messungen werden einerseits genutzt, um generelle Einflüsse von pathologischen Mittelohrkonditionen und von interindividuellen Unterschieden auf die gemessene akustische Impedanz nachzuvollziehen. Andererseits werden die Impedanzmessungen zur Entwicklung des Modells genutzt.

Mit dem eindimensionalen elektroakustischen Modell des Gehörgangs und des Mittelohres von Säuglingen wird gezeigt, dass der mittlere Frequenzbereich der akustischen Impedanz zwischen ca. 1 kHz bis 3 kHz durch die Eigenschaften des Mittelohres dominiert wird. Bei tieferen Frequenzen dominieren Eigenschaften des Gehörgangs. Der Bereich der hohen Frequenzen ist geprägt von starken interindividuellen Unterschieden. Des Weiteren wird der Einfluss durch den pathologischen Zustand von Flüssigkeit im Mittelohr durch das Modell nachgebildet. Außerdem wird für den pathologischen Mittelohrzustand einer Differenz des statischen Luftdruckes zwischen Mittelohrkavitäten und

Gehörgang eine Modellierung vorgeschlagen. Schließlich wird für alle relevanten WAI Größen gezeigt, dass durch die im Modell implementierten pathologischen Mittelohrzustände charakteristische Unterschiede gegenüber dem gesunden Mittelohr auftreten. Allerdings wird auch gezeigt, dass die in Studien häufig herangezogene WAI Größe der akustischen Absorbanz extrem sensitiv ist gegenüber der zur Bestimmung notwendigen Annahme über den Gehörgangsquerschnitt an der Stelle der Messsonde.

Adaptive Rückkopplungsauslöschung verhindert das Auftreten von akustischen Rückkopplungen in Hörgeräten durch adaptive Signalverarbeitung. Sie basiert auf der kontinuierlichen Schätzung des akustischen Rückkopplungspfades, also des akustischen Pfades vom Lautsprecher zum Mikrofon des Hörgerätes. Damit die Adaption möglichst Schnell erfolgen kann, wird der Rückkopplungspfad in einen zeitinvarianten fixen Teil und einen zeitvarianten variablen Teil aufgeteilt.

Das Ziel in dieser Arbeit ist es, einen zeitinvarianten fixen Teil des akustischen Rückkopplungspfades zu bestimmen, sodass der der variable Teil so schnell wie möglich adaptiert werden kann. Es werden zwei verschiedene Ansätze zur Bestimmung des zeitinvarianten fixen Teils verglichen. Der eine ist ein neuer auf einer definierten physischen Position basierender Ansatz und der andere ein positionsunabhängiger Ansatz nach aktuellem Stand der Technik. Zunächst wird zur Entwicklung des auf einer definierten physischen Position basierenden Ansatzes ein eindimensionales elektroakustisches Modell entworfen, an dem Komponenten des akustischen Rückkopplungspfades identifiziert werden, die sich zeitinvariant verhalten. Anhand des Modells werden dann verschiedene Varianten des zeitinvarianten fixen Teils nach diesem Ansatz entwickelt und verglichen. Grundsätzlich wird für diesen Ansatz davon ausgegangen, dass das Hörgerät mit einem Gehörgangsmikrofon ausgestattet ist, sodass für die Bestimmung des fixen Teils des akustischen Rückkopplungspfades ein Signal im Gehörgang gemessen werden kann. Die verschiedenen Varianten nach dem auf einer definierten physischen Position basierenden Ansatz werden dann mit Varianten nach einem positionsunabhängigen Ansatz verglichen. Voraussetzung für letzteren Ansatz ist, dass mindestens 2 Messungen des akustischen Rückkopplungspfades vorliegen, die sich zum Beispiel durch leicht unterschiedliche Mikrofonpositionen unterscheiden. Für alle Vergleiche werden real gemessene Rückkopplungspfade verwendet. Die Performance wird quantifiziert anhand des *added stable gain*.

Für die Varianten des auf einer definierten physischen Position basierenden Ansatzes wird gezeigt, dass die Variante, bei der der fixe Teil direkt aus der Messung mit dem Gehörgangsmikrofon bestimmt wird, die anderen Varianten leicht übertrifft. Der Vergleich der beiden Ansätze zeigt, dass mit beiden eine vergleichbare Performance erzielt werden kann. Somit kann die Wahl welcher der beiden Ansätze zum Einsatz kommen soll, aufgrund der jeweiligen Voraussetzungen und Vorteile der Ansätze getroffen werden.

Contents

1	General introduction	1
1.1	Motivation	1
1.2	Diagnostic field	1
1.3	Rehabilitative field	3
1.4	One-dimensional electro-acoustic models of the human ear	3
1.5	Outline	4
2	Acoustic input impedance of infant ears	7
2.1	Introduction	8
2.2	Methods	9
2.2.1	Subjects	9
2.2.2	Impedance measurement technique	9
2.2.3	Protocol of ENT-specialists	9
2.2.4	General procedure	10
2.3	Results	10
2.4	Discussion	11
2.4.1	Problematic frequency ranges	11
2.4.2	Meaningful frequency range	12
2.5	Concluding remarks	13
	References for Chapter 2	13
3	Parametric outer/middle ear model part I	15
3.1	Introduction	16
3.2	Development of the model	18
3.2.1	Existing parametric model of the ear for adults (Hudde and Engel, 1998a)	18
3.2.2	Adaptation of the parametric model to infants' ears	19
3.2.2.1	Ear canal	19
3.2.2.2	Middle ear cavities	22
3.2.2.3	Eardrum, malleus and incus	23
3.2.2.4	Stapes and cochlea	27
3.3	Effect of proposed model adaptations on the eardrum impedance	27
3.4	Ear canal impedance of the proposed model	28
3.5	Experimental validation	32
3.6	Influence of ear canal shape	33
3.7	Comparison to similar models	34
3.8	Discussion	36

3.8.1	Current limitations of the model	36
3.8.2	Differences to similar models	37
3.9	Conclusions based on the model	37
3.10	Acknowledgment	38
3.11	Data Availability Statement	38
3.A	Appendix	38
3.A.1	Notes on damping models for compliant ear canal walls	38
3.A.2	Default parameter values	39
	References for Chapter 3	42
4	Parametric outer/middle ear model part II	47
4.1	Introduction	48
4.2	Predicting the effect of fluid in the middle ear	50
4.3	Predicting the effect of negative pressure difference	53
4.4	Comparison of immittance measures	57
4.5	Discussion	60
4.5.1	Implications for WAI-measurements	60
4.5.2	Age dependency	61
4.6	Concluding remarks	61
4.7	Data Availability Statement	62
	References for Chapter 4	62
5	Acoustic feedback path modeling	65
5.1	Abstract	66
5.2	INTRODUCTION	66
5.3	SCENARIO	68
5.4	FEEDBACK PATH MODELS	69
5.4.1	Feedback Path Model based on Digital Filter Design	69
5.4.2	Feedback Path Model based on Electro-Acoustic Modeling	71
5.4.2.1	Decomposition of the feedback path model based on electro-acoustic modeling	73
5.4.2.2	Parameters of the feedback path model based on electro-acoustic modeling	73
5.4.2.3	Parameter reduction of measured transfer functions and model variants of the fixed part model based on electro-acoustic modeling	77
5.4.3	Combined Feedback Path Model	77
5.4.3.1	Combined models using electro-acoustic modeling to derive the fixed part	77
5.4.3.2	Combined model using a measured transfer function as the fixed part	78
5.5	EXPERIMENTAL COMPARISON	78
5.5.1	Acoustic setup and performance measures	78
5.5.2	Algorithmic parameters	78
5.5.2.1	General parameters	79
5.5.2.2	Parameters of the feedback path model based on digital filter design	79

5.5.2.3	Parameters of the feedback path model based on a defined physical location for the decomposition	80
5.5.3	Comparison of the fixed part variants based on a defined physical location for the decomposition	80
5.5.4	Comparison of feedback path models	81
5.6	DISCUSSION	83
5.6.1	Practical considerations and robustness	83
5.6.2	Number of parameters	84
5.6.3	Difference in model structure to Ma et al., 2011	84
5.7	CONCLUSION	86
	References for Chapter 5	87
6	General discussion	91
6.1	Main findings of the thesis	91
6.2	Conclusions	93
6.2.1	Middle ear screening for young infants based on WAI	93
6.2.2	Adaptive feedback cancellation in hearing aids	94
6.3	Further implications and outlook	95
6.3.1	Middle ear screening	95
6.3.2	Ear canal microphones in hearing aids	96
	Bibliography	99
	Acknowledgments	101
	Curriculum Vitae	103

Chapter 1

General introduction

1.1 Motivation

A substantial permanent hearing impairment can have severe impact in every phase of life. Especially at the very early stages in life, a hearing loss can affect speech development negatively. Later, there is a risk of negative effects on social participation as well as educational and professional opportunities. In order to minimize negative effects from hearing impairment, firstly, diagnostic questions regarding the location (kind) and the severity (degree) of the impairment have to be answered. Based on these answers, rehabilitative measures can be applied. The most frequent intervention in case of a permanent hearing loss is a hearing aid. In both fields, diagnosis and rehabilitation, sophisticated methods and techniques have been developed over many decades, however, there is still room for improvement. The goal of this thesis is an improvement of existing diagnostic and rehabilitative applications and to gain a better understanding of them. In order to achieve such improvements, this thesis focuses on so called one-dimensional electro-acoustic models. One-dimensional electro-acoustic models allow predictions of acoustic quantities at any place within the model. Due to the manageable number of parameters, this kind of modeling is suited to investigate the impact of specific model components on these acoustic quantities.

1.2 Diagnostic field

The first question in the diagnostic field is whether there is a problem, i.e. a hearing impairment, or not. If this is the case, it has to be clarified where the problem is located within the auditory pathway, whether it is a persistent or temporary problem and how serious the hearing impairment is. For all these questions, often, objective test procedures are required. This is especially true if an active involvement of the person concerned is not possible.

The acoustic input impedance of the ear canal is a quantity which is used for diagnostic purposes to detect pathological middle ear conditions. In this context, the acoustic impedance, its reciprocal the acoustic admittance, and other quantities derived from these two are summarized under the term immittance. The broadband measures are referred to as wideband acoustic immittance (WAI). One of the topics of this thesis is the middle ear screening for young infants based on WAI. This screening is intended to detect those ears in which the sound conduction from the ear canal to the inner ear is affected. For children and adults, established methods exist, however, the ear canal and the middle ear of young infants are significantly different with different acoustic properties compared to those of

children and adults. With regard to the young infants' healthy ear, a first question to be answered is:

- How can the general differences between the adult's and the young infant's ear canal and middle ear be considered in a one-dimensional electro-acoustic model?

An important difference is the soft and flexible ear canal wall in young infant's ears, which later becomes acoustically rigid. This difference leads to the question:

- To what extent is the acoustic input impedance influenced by the soft and flexible ear canal wall?

WAI is determined from an acoustic measurement in the ear canal. For this purpose, a probe equipped with a speaker and a microphone is placed in the ear canal. Measured WAI data show a strong dependence on frequency. Eventually the question arises:

- Does an optimal frequency range of the acoustic impedance exist, which is sensitive to middle ear properties, without being too much affected by ear canal properties?

If such a frequency range exists, it might be possible to detect pathological middle ear conditions.

The term "pathological middle ear condition" instead of middle ear pathology is chosen intentionally because not every middle ear condition that affects sound conduction is a pathology. Nevertheless, these pathological conditions should still be detected. As an example, liquid in the middle ear is a frequently occurring pathological middle ear condition in young infants. A further question is:

- How can frequent pathological middle ear conditions be considered in the one-dimensional electro-acoustic model?

Such a model can then be used to answer the question:

- How do different middle ear conditions influence different WAI-measures?

The acoustic absorbance is one of the WAI-measures which has been proposed to be used for the detection of pathologic middle ear conditions. It is based on an assumptions about the ear canal cross-sectional area at the measurement position. In the literature, several studies containing absorbance data can be found among which the assumptions about the ear canal cross-sectional area differ. The one-dimensional electro-acoustic model could provide an answer to the question:

- How do different assumptions of the ear canal cross-sectional area affect the acoustic absorbance?

The development of the one-dimensional electro-acoustic model requires some data of the acoustic input impedance of the ear canal measured in young infants with healthy middle ears and with pathological middle ears. Such data provide knowledge about magnitude and phase of the complex acoustic input impedance of the ear. Questions to be answered from such impedance measurements are:

- Is it possible to trace general differences in the measured impedance caused by pathological conditions?
- Is it possible to distinguish such general differences from variations caused by inter-individual differences?

1.3 Rehabilitative field

The other topic of this thesis, which addresses the field of rehabilitation, is adaptive feedback cancellation in hearing aids. If the sound emitted from a hearing aid is picked up by the hearing aid microphone, a closed loop exists. The main task of a hearing aid is the amplification of the sound picked up by the microphone. On the way back from the hearing aid speaker to the microphone, the sound is attenuated passively. However, if the amplification by the hearing aid is larger than the attenuation, the level of the sound is increased by every run through the loop, resulting in acoustic feedback.

A generalized description of the problem to be tackled is as follows: Let us assume there is a small spatial region in which the sound transfer between two specific points has to be known precisely. Aggravatingly, the sound field in this area is governed by changes of the boundary conditions in time. Therefore, the acoustic path between the two points has to be adapted. In order to account for these changes as fast as possible, the most successful approach is to split the path between the two points in a time-invariant and a time varying part, allowing a decrease of computational complexity necessary for the adaptation. The question to be answered is:

- How to determine an optimal time-invariant part so that the time varying part can be adapted as fast as possible?

A one-dimensional electro-acoustic model can be used to get insight into the problem. It could be used to make decisions whether the time-invariant part can be assigned to physical locations on the path between the two points. The spatial region involved here is the immediate surrounding of a hearing aid worn by a person. The two specific points are the positions of the speaker and the microphone of the hearing aid. The path between the speaker and the microphone is referred to as acoustic feedback path and the desire of precise knowledge is based on the resulting opportunity to cancel feedback in the hearing aid, which offers a great benefit for the hearing aid user. To be clear on that, feedback in hearing aids is not only annoying due to the howling sounds and the functional failure when it occurs, most of all, the maximum amplification which can be provided by the hearing aid is limited by the threshold where feedback starts to emerge. With a one-dimensional electro-acoustic model and a certain knowledge about the individual model components it might be possible to assign some components to the time-invariant part, i.e. to assign some physical position based sections between the speaker and the microphone to the time-invariant part. The question to be answered here is:

- Which model components behave in a time-invariant manner?

More general questions to be addressed are:

- What are advantages and disadvantages of this physical position based approach compared to traditional approaches in adaptive feedback cancellation?
- Is there a benefit from combining the physical position based approach with a traditional approach?

1.4 One-dimensional electro-acoustic models of the human ear

One-dimensional electro-acoustic models in general are based on the electrical network theory. They exploit the analogies between the electrical, the mechanical and the acoustical domain, i.e. the

electrical quantities voltage and current are related to the mechanical quantities velocity and force, and to the acoustical quantities sound pressure and volume velocity. In these models, electrical, mechanical and acoustical components can be combined. The key feature of these models is that they are parametric models with a manageable number of parameters. The parameters typically are based on material properties and properties of simple parametric geometries. The models allow predictions of the complex quantities of the sound pressure and the volume velocity at any point in relation to excitation by one or more sources.

In these models, the ear canal is typically considered as a canal in which plane-wave-propagation can be assumed. This is acceptable if the cross-sectional area of the ear canal is small compared to the wave length, which is true up to several kHz. Further assumptions made for the modeling of the ear canal are that only smooth changes of the cross sectional area and the curvature occur over the length of the canal and often, but not always, the ear canal walls are assumed to be acoustically rigid. The one-dimensional electro-acoustic modeling of the ear canal has been applied in many studies with different application scenarios. One example can be found in Hudde et al. (1999) in which the modeling was used to predict the sound pressure at the eardrum.

Models of the middle ear typically can be divided into the physiological sections of the eardrum, the middle ear cavities, the malleus together with the incus and the stapes connected to the cochlea. The first one-dimensional electro-acoustic models of the middle ear have been proposed in Møller (1961), Onchi (1961), and Zwislocki (1957, 1962). Some further developments have been made in Shaw (1977) and Shaw and Stinson (1981), by improving the transmission characteristics of the middle ear, in Kringlebotn (1988), by adding an eardrum suspension and in Hudde and Engel (1998a,b,c), by improving the connection to the physiology. It is worth mentioning that more recent developments exist, e.g. O'Connor and Puria (2008) and Keefe (2015).

Of course, other techniques exist which are used to model the human ear. The most relevant techniques are finite-element (FE) models and statistical models. Compared to these techniques, one-dimensional electro-acoustic models have some clear limitations concerning accuracy. FE models are better suited for individual single-case models because geometrical properties can be represented in high detail. The sound propagation can be considered for all 3 spatial directions in this modeling technique. However, the usage of simple parametric geometries and the relatively small number of parameters in one-dimensional electro-acoustic models is advantageous compared to FE models, allowing to observe general effects on acoustic quantities caused by inter-individual differences, pathological changes and/or intentional modifications of the acoustic environment. Statistical models, of superior accuracy, might be derived from a large database of high quality. Conversely, an advantage of one-dimensional electro-acoustic models is that less data tends to be needed in the development.

1.5 Outline

In chapter 2, measurements of the acoustic input impedance of young infants' ears are presented. In addition to the measurements, the ears were assessed by ENT-specialists to have either a normal or a pathological middle ear status. A comparison of the measured impedance between the ears with normal and with pathological middle ear shows general differences. The measurement data are used in the chapters 3 and 4 for model development.

In chapter 3, a one-dimensional electro-acoustic model of young infants' eardrum and ear canal impedance for the healthy ear will be presented. The proposed model is based on an existing model

for adult ears. The acoustic input impedance of the ear predicted by the model is compared to the measurements on ears assessed to be normal from chapter 2. Finally, an optimal frequency range to sense middle ear properties from the acoustic input impedance of the ear is identified.

Chapter 4 introduces an extension of the previously proposed model for the healthy ear of young infants to account for specific frequent pathological middle ear conditions. Again, the acoustic input impedance of the ear predicted by the model is compared to measurements from chapter 2, this time using the measurements on the ears assessed to be pathological. The model is used to show the effects of different middle ear conditions on different WAI measures. Furthermore, the effects of different assumptions of the cross-sectional area of the ear canal at the measurement position on the acoustic absorbance is discussed.

Chapter 5 addresses the problem of acoustic feedback in hearing aids. Two different modeling approaches of the acoustic feedback path of hearing aids, namely physical position based and position independent models, are compared. A one-dimensional electro-acoustic model of the acoustic feedback path of a hearing aid is proposed. The model is used for the physical position based approach to define a time-invariant fixed part of the acoustic feedback path. As a result of the comparison of advantages and disadvantages of the two approaches, it is pointed out that they offer solutions for different requirements on the design and the fitting of a hearing aid.

In chapter 6 the main findings of this thesis are summarized and a suggestions for future work are given.

Chapter 2

Acoustic input impedance of infants with normal and pathological middle ear

This Chapter was published with identical content in:

Proceedings of the ICA 2019 and EAA Euroregio, pp. 5675–5680,

Sankowsky-Rothe, T., Becker, A., Plotz, K., Schönfeld, R., Radeloff, A., Van de Par, S. and Blau, M. (2019). "Acoustic input impedance of infants with normal and pathological middle ear"

Authors' contributions:

- Tobias Sankowsky-Rothe formulated the research question, developed the impedance measurement probe, implemented the measurement software, developed the medical questionnaire, analyzed and interpreted the data, and wrote the final paper,
- Andreas Becker developed the medical questionnaire, and carried out the medical examination.
- Karsten Plotz participated in the development of the medical questionnaire, and carried out the medical examination.
- Rüdiger Schönfeld carried out the medical examination.
- Andreas Radeloff managed administrative clinical tasks.
- Steven van de Par participated in interpretation of the data, and participated in writing the final paper.
- Matthias Blau formulated the research questions, participated in the development of the medical questionnaire, participated in interpretation of the data, and participated in writing the final paper.

Hereby I confirm that Tobias Sankowsky-Rothe contributed to the study as stated above.

.....
Date

.....
Steven van de Par (supervisor)

Abstract

Newborns and infants often suffer from pathological conditions of the middle ear. In many cases, those conditions comprise liquid in the middle ear, e.g. middle ear effusion, or amniotic fluid during the very first days of life. In order to check the middle ear status in a fast and simple manner, the measurement of the infant's ear acoustic input impedance could be a useful method.

In an ongoing study, the acoustic input impedance of infants' ears (aged from 2 weeks up to 5 months) was measured in the frequency range from 100 Hz to 10 kHz at ambient pressure. In addition, the middle ear status was assessed by ENT-specialists, yielding an expert classification of "normal" and "pathological" middle ears.

The results, on the one hand, show a great variability at low and very high frequencies, reflecting the susceptibility of the measurements to movements and noise of the subjects. On the other hand, there is a frequency range in which a clear discrimination between normal and pathological middle ears seems to be possible. This discrimination appears to profit from the consideration of both the magnitude and phase information of the measured acoustic impedance, indicating that power-based methods may miss important information.

Keywords: middle-ear, newborn, impedance, immittance

2.1 Introduction

The assessment of hearing ability in newborns and infants is a challenging task. Universal newborn hearing screening (UNHS) programs have the goal to identify infants with a permanent hearing loss in order to allow an early intervention.

Temporary pathological conditions of the middle ear are probably the most common cause of fails in UNHS-tests, but the results of these tests don't provide any information about the location of the problem.

In older children and adults tympanometry is the method of choice for detecting middle ear pathologies affecting the conductive path. In newborns and young infants tympanometry at 1 kHz is often used, but it seems that there is no commonly accepted method for interpreting the results.

Over the last years, other immittance-based measurements have been and still are investigated for their suitability to detect conductive problems in newborns and young infants, see e.g. (Aithal et al., 2015; Hunter et al., 2010; Keefe et al., 2000; Myers et al., 2018; Prieve et al., 2013). In contrast to the classical single frequency tympanometry, these modern methods make use of a broader frequency range. They can be grouped by two factors: 1) whether the static pressure in the ear canal is changed or not, and 2) by the resulting quantity to be analyzed. Some methods report complex-valued quantities, such as the acoustic impedance or its reciprocal the acoustic admittance. The others are power based methods reporting real-valued quantities such as power-reflectance or power-absorbance. So far only power based methods are used in clinics.

The present paper presents first results of an ongoing study, in which the acoustic input impedance of the ear of young infants with normal or pathological middle ear was measured. The status of the middle ear was assessed by ENT-specialists based on visual inspection of the ear together with results of a screening test and a 1 kHz tympanometry test.

2.2 Methods

2.2.1 Subjects

The infants age had to be less than 5 month to be included into the study. Furthermore infants were excluded in case of known trisomy 21, any pharyngeal arch syndromes with a somatically different ear canal structure, or a dysplasia of the outer or middle ear. The study was carried out at *Medizinisches Versorgungszentrum Oldenburg* (MEVO), which is an outpatient ENT department specialized to pediatric audiology. Parents, coming to a regular consultation-hour into MEVO because their infants failed at least one time the NHS, where asked for parental consent to participate in the study.

The study-design was approved by the medical ethics committee of the University of Oldenburg.

2.2.2 Impedance measurement technique

The acoustic input impedance of the ear was measured with a custom-made measurement probe. This impedance probe contains a miniature electret microphone (Knowles Electronic type FG-23652-P16) and a balanced armature driver (Knowles Electronic type TWFK-30017). Both, microphone and driver were connected to separate ducts in a cylinder. The cylinder can be equipped with standard silicon ear tips. A third duct in the cylinder with an inner diameter of 0.6 mm provides pressure equalization between the ear canal and ambient pressure.

Impedance was measured using a calibrated source method. The method is based on Stirnemann et al. (2003) with additional consideration of discontinuity and end corrections. It is described in detail in Blau et al. (2010). The resulting calibration parameters could then be used to compute the acoustic impedance from the transfer function between microphone and receiver signal measured in the ear canal. Random pink noise signals were used for the measurements at an A-weighted sound pressure level of 63 dB SPL measured in a high-frequency coupler with a volume of 0.4 cm³ (GRAS Sound & Vibration A/S type RA0252). The transfer functions were estimated using classical FFT-based estimation techniques (Bendat and Piersol, 2000).

Signal generation, recording and transfer function estimation were realized in Matlab. A multi channel sound card (RME type Fireface UC) was used for conversion between digital and analog signals.

2.2.3 Protocol of ENT-specialists

The regular examination comprised 1 kHz tympanometry, automated auditory brainstem response (AABR)-screening and/or otoacoustic emission (OAE)-screening, and visual inspection by microscopy.

For the tympanometry a Maico Race Car Tympanometer was used. With a stimulus frequency of 1 kHz at a level of 85 dB SPL, the static pressure was varied from 200 daPa to -300 daPa at an adaptive rate.

Two different devices were used for AABR screening tests depending on which one was available. One of the devices was a Maico MB 11 Beraphone with CE-chirp stimuli at a rate of 93/s and a level of 35 dB nHL. The other device was a GSI Novus which also utilizes CE-chirps at a level of 35 dB nHL. The stimulus rate of the latter device depends on the ear side, the probe for the left ear produces a rate of 88/s, while the right ear probe produces a rate of 92.5/s. In both devices an automated analysis reported either pass or fail.

OAE-screening was conducted using a GSI Corti. Transient evoked otoacoustic emissions were determined at six frequencies between 1.5 kHz and 4 kHz, the intensity of click stimuli was 80 dB SPL peak equivalent. A pass required a SNR of 4 dB at 3 out of 6 frequencies.

The visual inspection comprised examination of the outer ear, the ear canal and the eardrum. Findings of liquid in the middle ear or blockage of the ear canal with cerumen were noted for the study. Finally, the status of the middle ear was assessed, considering all results of the regular examination, to be *normal*, *pathological*, or to be *unclear* if a decision was not possible at that time.

2.2.4 General procedure

Infants first underwent the screening test (AABR and/or TEOAE), followed by the 1 kHz tympanometry. After that, parents were asked for parental consent to participate with their child in the study. If a consent was given, the acoustic impedance was measured. Usually all tests and measurements were conducted in both ears, while the infant was awake. Finally, the visual inspection was done.

2.3 Results

30 ears of 24 infants were assessed to have a normal middle ear and 13 ears were assessed to have a pathological middle ear. Figure 2.1 shows the numbers of ears for the normal and the pathological ears, respectively, grouped by age. As can be seen, in the group of normal middle ears the age of most subjects (80%) was less than 2 month. In the pathological group, only 37% were younger than 2 months and 40% were between 2 and 3 months.

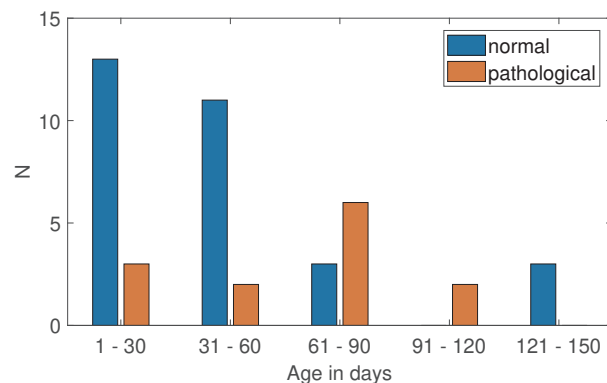


Figure 2.1: Numbers of normal and pathological ears, grouped by age.

It turned out that an assessment as “pathological” was always linked to middle ear effusion. While in one of the 13 middle ears the amount of secretion found was only small, in the other ears it was quite substantial.

Figure 2.2 shows the measured acoustic impedance of the normal ears on the left side and of the pathological ears on the right side. For the normal middle ears, a strong characteristic course of the acoustic impedance could be seen between about 1 kHz and 5 kHz, in both magnitude and phase. Below and above that frequency range, the variability increases. Furthermore, some artifacts (notches in impedance level and strong variations in phase) can be seen up to about 1.5 kHz, which are caused by a poor SNR in the measurement due to noise.

The acoustic impedance measured in the pathological middle ears shows substantially different characteristics. Except for two measurements, the level of the impedance has a minimum around 4 kHz with a steep gradient in phase. The first of the two exceptions, which is depicted as straight red line, has a decreasing impedance level and a phase near -90° . The ENT-specialist reported a very narrow ear canal with a protrusion at the posterior ear canal wall. The second exception is depicted by the green straight line. Both, level and phase of the acoustic impedance are quite similar to that of the normal ears with the level ranging in the upper limit of the impedances measured in normal ears. For that ear the ENT-specialist reported only a small amount of secretion in the middle ear.

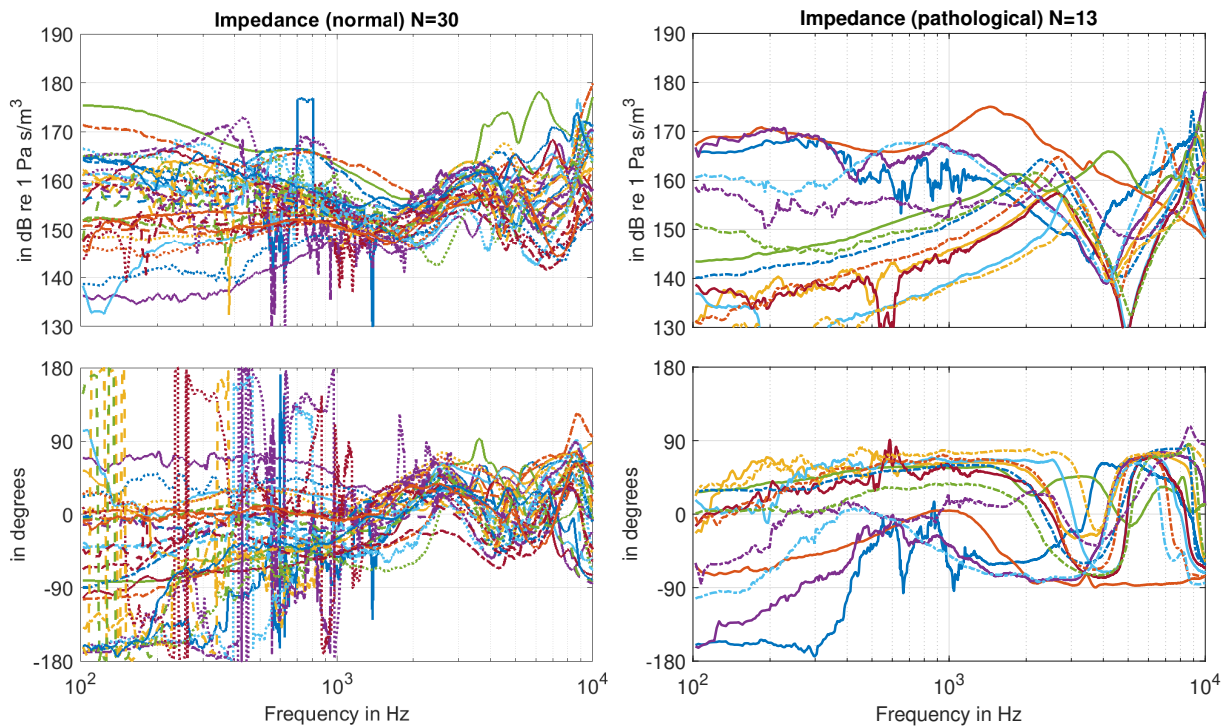


Figure 2.2: Acoustic input impedance of the ear measured on 30 infant ears with normal middle ear (left) and on 13 infant ears with pathological middle ear (right).

2.4 Discussion

2.4.1 Problematic frequency ranges

At low frequencies, results are widely spread in both magnitude and phase. One of the reason for that, as already mentioned in the previous section, is a poor SNR. Additionally to the noise produced by the infants during the measurement, the design of the probe is not optimal in terms of SNR. The third duct in the cylindrical probe tip, providing equalization of static air pressure between ear canal and environment, causes a low signal level at low frequencies. On the other hand, the pressure equalizing duct avoids overpressure that might be caused when inserting the probe into the ear. This was intended and supposed to help avoid erroneous influences on the acoustic impedance of the ear and increase the infant's acceptance of the measurement.

Another reason for the widely deviating results at low frequencies is that the sealing of the ear

canal by the probe differs between measurements. A highly sealed fitting of the probe results in a compliance like impedance at low frequencies, i.e. an impedance level decreasing with increasing frequency and a negative phase, which can be seen in some measurements. On the other hand, a loose fitting probe results in an acoustic leakage with a mass like impedance at low frequencies, i.e. an impedance level increasing with frequency and a positive phase. It should be noted that the pressure equalizing duct of the probe doesn't effect the measured impedance in terms of the sealing: As this duct is also present in the impedance calibration measurements, it is part of the source model.

Both problems, the poor SNR and the variations in sealing, result from challenges arising with measurements on very young infants. Of course, different actions could be taken to reduce these problems. However, it is assumed that the low frequency range isn't of much importance to detect pathological middle ear functions because at that age compliant ear canal walls affect the measured acoustic impedance, see Keefe et al. (1993).

At high frequencies (> 5 kHz), results are different between normal and pathological middle ears. Most impedance measurements on pathological middle ears show a peak in the impedance magnitude with a phase changing from positive to negative values at high frequencies, which is only shifted in frequency between different ears. Acoustic impedance measured on normal middle ears don't show a clear and simple characteristic course in that frequency range. It may be assumed that these variations are caused by individual differences in the middle ear and the residual ear canal. A further investigation of these effects will be part of future work.

2.4.2 Meaningful frequency range

The measured acoustic impedance in the frequency range from 1 kHz to 5 kHz showed clear characteristics, which can be assigned either to the middle ears assessed to be normal or to the ears assessed to be pathological due to middle ear effusion. These characteristics for the normal middle ears are a broad minimum in impedance level with gradually increasing phase at about 1.8 kHz, followed by a broad maximum of impedance level with gradually decreasing phase around 3.5 kHz. Characteristics of the pathological middle ears are a sharp minimum in impedance level with a steeply increasing phase around 4 kHz.

In Keefe et al. (1993) the acoustic input impedance of the ear on infants of different age groups was measured. These authors reported mean values for infants aged 1, 3, 6, 12, and 24 months old. The mean acoustic impedance reported for the 1, and 3 month groups showed the same characteristics, that were also found for the normal group in the present study.

In Prieve et al. (2013) wideband reflectance (WBR) was measured at infants aged from 3.1 to 25.6 weeks. WBR is a measure based on the acoustic impedance, it is also known as power-reflectance. The authors compared WBR measured on normal hearing (NH) infants with WBR measured on infant ears having a conductive hearing loss (CHL). Assessment of NH and CHL was achieved by determining the air-bone gap from air conduction thresholds and bone conduction thresholds measured with auditory brainstem response. WBR was determined at 15 $1/3$ octave bands in the frequency range from 211 Hz to 6 kHz. They found the frequency range around 1.6 kHz to be suitable to distinguish between NH and CHL, which is in agreement with the characteristics found in the present study. In contrast to the above presented results, the WBR-values didn't allow a distinction between NH and CHL around 4 kHz.

2.5 Concluding remarks

In the present contribution, measurements of the acoustic input impedance of the ear, measured at ambient pressure in young infants up to 5 months old, were presented. The infants were awake during the measurement. The middle ear status of the ears were assessed either to be normal or to be pathological, with the latter always being associated with middle ear effusion.

Different characteristics between normal and pathological middle ears could be found in both, impedance magnitude and phase. The results strongly indicate that the acoustic impedance measured at ambient pressure is suitable to detect middle ear effusion in young infants.

The impedance measured in the present study on normal assessed middle ears is in good agreement with mean values from literature.

At high frequencies (> 5 kHz), the acoustic impedance measured on ears where middle ears were assessed to be normal showed considerable inter-individual variations. The investigation of these variations will be part of future work.

Acknowledgements

This work was funded by the Jade University's research program Jade2Pro.

References for Chapter 2

- Aithal, S., Kei, J., Driscoll, C., Khan, A., and Swanston, A. (2015). "Wideband Absorbance Outcomes in Newborns: A Comparison With High-Frequency Tympanometry, Automated Brainstem Response, and Transient Evoked and Distortion Product Otoacoustic Emissions." In: *Ear and Hearing* 36.5, e237–e250. doi: [10.1097/AUD.000000000000175](https://doi.org/10.1097/AUD.000000000000175).
- Bendat, J. S. and Piersol, A. G. (2000). *Random Data: Analysis and Measurement Procedures*. 3rd ed. New York, NY (USA): John Wiley & Sons, Inc. isbn: 0471317330.
- Blau, M., Sankowsky, T., Roeske, P., Mojallal, H., Teschner, M., and Thiele, C. (2010). "Prediction of the sound pressure at the ear drum in occluded human cadaver ears". In: *Acta Acustica united with Acustica* 96.3, pp. 554–566.
- Hunter, L. L., Feeney, M. P., Lapsley Miller, J. A., Jeng, P. S., and Bohning, S. (2010). "Wideband reflectance in newborns: normative regions and relationship to hearing-screening results." In: *Ear and Hearing* 31.5, pp. 599–610. doi: [10.1097/AUD.0b013e3181e40ca7](https://doi.org/10.1097/AUD.0b013e3181e40ca7).
- Keefe, D. H., Bulen, J. C., Arehart, K. H., and Burns, E. M. (1993). "Ear-canal impedance and reflection coefficient in human infants and adults." In: *The Journal of the Acoustical Society of America* 94.5, pp. 2617–2638. doi: [10.1121/1.407347](https://doi.org/10.1121/1.407347).
- Keefe, D. H., Folsom, R. C., Gorga, M. P., Vohr, B. R., Bulen, J. C., and Norton, S. J. (2000). "Identification of neonatal hearing impairment: ear-canal measurements of acoustic admittance and reflectance in neonates." In: *Ear and Hearing* 21.5, pp. 443–461. doi: [10.1097/00003446-200010000-00009](https://doi.org/10.1097/00003446-200010000-00009).
- Myers, J., Kei, J., Aithal, S., Aithal, V., Driscoll, C., Khan, A., Manuel, A., Joseph, A., and Malicka, A. N. (2018). "Development of a Diagnostic Prediction Model for Conductive Conditions in Neonates Using Wideband Acoustic Immittance". In: *Ear and Hearing* 39.6, pp. 1116–1135. doi: [10.1097/aud.000000000000565](https://doi.org/10.1097/aud.000000000000565).

- Prieve, B. A., Vander Werff, K. R., Preston, J. L., and Georgantas, L. (2013). "Identification of Conductive Hearing Loss in Young Infants Using Tympanometry and Wideband Reflectance". In: *Ear and Hearing* 34.2, pp. 168–178. doi: [10.1097/aud.0b013e31826fe611](https://doi.org/10.1097/aud.0b013e31826fe611).
- Stirnemann, A., Graf, H., and Meier, H. (2003). "Akustische Impedanzmessungen in der Hörerätetechnik". In: *Fortschritte der Akustik DAGA 2003*. DEGA. Berlin, pp. 496–497.

Chapter 3

Parametric model of young infants' eardrum and ear canal impedances supporting immittance measurement results. Part I: Development of the model

This Chapter was published with identical content in:

Acta Acustica, vol. 6, pp. 53,

Sankowsky-Rothe, T., van de Par, S. and Blau, M. (2022). "Parametric model of young infants' eardrum and ear canal impedances supporting immittance measurement results. Part I: Development of the model", <https://doi.org/10.1051/aacus/2022047>

Authors' contributions:

- Tobias Sankowsky-Rothe formulated the research question, developed the model, interpreted the experimental and modeling data, and wrote the final paper,
- Steven van de Par participated in interpretation of the experimental and modeling data, and participated in writing the final paper.
- Matthias Blau formulated the research questions, participated in the development of the model, participated in interpretation of the experimental and modeling data, and participated in writing the final paper.

Hereby I confirm that Tobias Sankowsky-Rothe contributed to the study as stated above.

.....
Date

.....
Steven van de Par (supervisor)

Abstract

Wideband acoustic immittance (WAI) measurements provide an objective means to detect pathological middle ear conditions. However, for ears of young infants, it is still difficult to make clear statements about the middle ear status based on WAI measurements. In order to gain a better understanding of WAI data obtained in young infants' ears, a parametric electro-acoustic model of the ear canal and the middle ear of young infants is proposed. In this first part of the two-part paper, the development of the model for the healthy ear is presented. Based on an existing model for adult ears, the presented model is adapted to young infants' ears, uses parameters suited to represent physiological properties, and uses a smaller number of parameters in order to reduce model complexity. A comparison of the acoustic input impedance of the ear predicted by the model with real ear measurements in young infants' ears showed a good agreement in the main characteristics. Model predictions show that the medium frequency range (about 1–3 kHz) of the acoustic input impedance of the ear is dominated by the properties of the eardrum and the middle ear, indicating that pathological middle ear conditions can preferably be detected in this frequency range.

3.1 Introduction

Pathological middle ear conditions occur frequently in early infancy. In the first months of life, middle ear effusion, i.e. fluid in the middle ear resulting from otitis media, is the most frequent pathological middle ear condition. In Marchant et al. (1984) a prevalence of 74% for middle ear effusion was found for children in the first 6 months of life, and in Paradise et al. (1997) a prevalence of 47.8% was found for infants aged between 2 months and 6 months. Less frequent conditions are e.g. oedematous middle ear, negative pressure difference between middle ear and ear canal, and middle ear dysplasia. Besides treatments that may or may not be necessary as a result, such conditions also have consequences for diagnostic tests like those used within universal newborn hearing screening programs, because the sound has to travel through the middle ear in order to trigger a response. If an otoacoustic emissions test is applied, the middle ear has to be traveled even twice, first by the stimulus and second by the emission from the cochlea back to the ear canal. Such tests will also be affected by the non-pathological occurrence of amniotic fluid in the middle ear, typically present right after birth up to a few days.

Traditionally, tympanometry at a single frequency is used to detect pathological middle ear conditions. In the last years broadband immittance-based methods were investigated for their suitability and potential superiority in middle ear diagnostics. In this context the term immittance comprises the acoustic impedance, the acoustic admittance, as well as further measures derived from these quantities. The measures of these methods are grouped under the term “wideband acoustic immittance (WAI)”. In 2013 a consensus statement was formulated by several researchers in that field. It was concluded that WAI, as a tool to improve the diagnostics of middle ear disorders is very promising, however, further research is needed especially to increase the database for both, normative data and data for different pathologies (Feeney et al., 2013).

Today, it is still difficult to make clear statements about the middle ear status of young infants based on WAI measurements. One important aspect is that middle ears of young infants exhibit different acousto-mechanical properties in comparison to older children and adults. Furthermore, WAI is based on acoustic measurements in the ear canal and it is known that, in the first months of life, the acoustic properties of the ear canal also significantly differ from those at an older age.

In order to gain a better understanding of WAI, knowledge about the impact of different factors like compliant ear canal walls, ear canal shape, and the healthy middle ear versus different pathological middle ear conditions on WAI-measures would be valuable. While some early WAI studies with young infants (Keefe et al., 1993, 2000; Sanford et al., 2009; Sanford and Feeney, 2008; Werner et al., 2010) report complex impedance/admittance data together with measures derived from this data, in many recent WAI studies with young infants the only immittance measure reported is either the energy reflectance or the energy absorbance (Aithal et al., 2015; Blankenship et al., 2018; Pitaro et al., 2016; Prieve et al., 2013; Shahnaz et al., 2014). Both require an assumption or estimation regarding the value of the tube wave impedance associated with the ear canal area at the probe tip, which is often not consistent over studies and measurement devices, making the results hard to compare. In addition, they neglect phase information which could potentially be useful to identify acousto-mechanical properties of the residual ear canal and its termination by the eardrum and the middle ear.

In order to be able to verify the suitability of WAI as a diagnostic tool for young infants, certainty of the middle ear status and measures which are independent of the particular measurement device being used are needed. It would be helpful to have detailed knowledge of the transfer of sound in the ear canal to the eardrum, and more specifically to the middle ear. Acousto-mechanical transfer models would provide such detailed knowledge. Many models of this kind have been proposed, e.g. Hudde and Engel (1998a,b,c), Keefe (2015), Kringlebotn (1988), Shaw and Teranishi (1968), Shera and Zweig (1992), and Zwislocki (1962), which, in general, share many properties but differ in details. The more recent models in particular are mostly further developments of the earlier models. However, they have been developed specifically for adults. Since it is known that several potentially relevant properties of the ear canal and the middle ear differ significantly between adults and young infants, they can in general not be used for young infants.

Therefore, in this paper, a parametric electro-acoustic model of the ear canal and the middle ear of young infants, to be used to predict the acoustic input impedance at the eardrum at ambient pressure, will be presented. The model is based on the model for adults according to Hudde and Engel, 1998a,b,c with the following aims of adaptation: 1) differences between infants' and adults' ears should be taken into account, 2) model parameters should be suited to represent physiological properties, and 3) model complexity in terms of the number parameters should be reduced. The adult model from Hudde and Engel (1998a,b,c) was chosen as a starting point because it proved useful in previous studies of the authors on the development of individualized models for the prediction of the sound pressure at the eardrum (Blau et al., 2010; Sankowsky-Rothe et al., 2015a; Sankowsky-Rothe et al., 2011) and on the development of implantable middle-ear sensors (Blau et al., 2003). It should be noted that in this study we use the same concept of the drum impedance as in Hudde and Engel (1998a,b,c) and Rosowski et al. (1990), i.e. the impedance seen when exciting the eardrum by a plane wave impinging perpendicularly onto the drum surface, whereas in many other studies, the drum impedance is referred to as the impedance at or shortly behind the entrance to the so-called drum coupling region, which in turn is composed of the inclined eardrum and the air space below it.

The objective of the present work is that the adapted model can be used to predict the ability of immittance-based measurements in the ear canal to detect certain different pathological middle ear conditions. Hence its focus is the sound transfer in the ear canal and the acoustic input impedance of the eardrum and not the transfer through the middle ear.

In a companion paper, the model will be extended to predict the influence of pathological middle ear conditions in young infants' ears on the acoustic input impedance of the ear in order to investigate implications for WAI-measurements. A MATLAB-implementation of the complete model can be found in Sankowsky-Rothe (2022).

3.2 Development of the model

In the following, the proposed parametric electro-acoustic model of infants' middle ears and ear canals is described. The parameters of this model are linked to physiological properties. The starting point of the development was the model of the ear canal and middle ear for adults according to Hudde and Engel (1998a), which was adapted to model infants' ears. Furthermore, adaptations were made in order to reduce the model complexity by removing unimportant parameters. As will be explained in the following, reasons for parameters to be unimportant are (1) they are not needed for young infants' ears, (2) they model effects which were not strongly supported by the available measurement data in Hudde and Engel (1998a), or (3) their influence on the resulting input impedance of the eardrum is small.

3.2.1 Existing parametric model of the ear for adults (Hudde and Engel, 1998a)

The transmission-line model proposed in Hudde and Engel (1998a) is depicted in Figure 3.1. It consists of the acoustic two-port C representing the ear canal, the acoustic impedance of the middle ear cavities Z_{cav} , the acousto-mechanical kernel two-port K representing eardrum, malleus and incus, a mechanical admittance y_{is} representing the incudostapedial joint, the mechano-acoustical stapes two-port S and the mechanical admittance of the cochlea y_C . Additionally the model includes a Thévenin-equivalent acoustic source with the source sound pressure p_s and the source acoustic impedance Z_s connected to the ear canal two-port. As can be seen in Figure 3.1, a

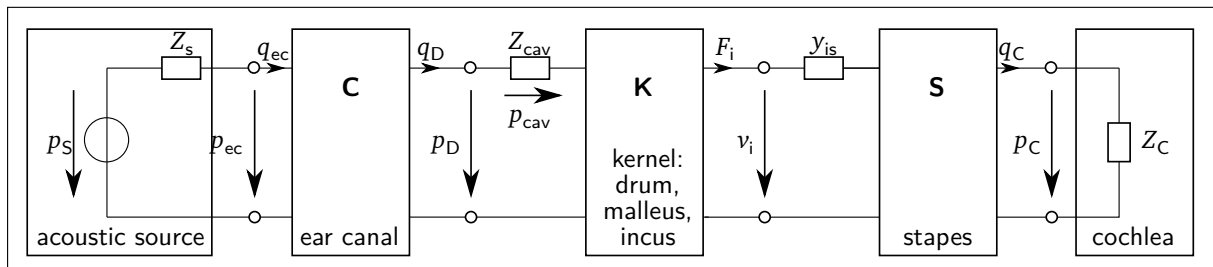


Figure 3.1: General model structure for sound transmission from the ear canal into the cochlea according to Hudde and Engel (1998a).

topology-preserving analogy between electric, acoustic and mechanic domain was used, where electrical voltage corresponds to acoustical pressure p and mechanical velocity v . The electrical current corresponds to acoustical volume velocity q and mechanical force F .

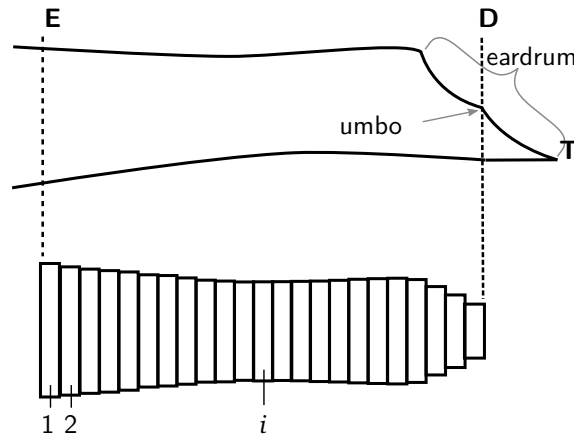


Figure 3.2: Sketch of the ear canal slice model showing the ear canal entrance E, the definition of the drum area D and the termination point T.

3.2.2 Adaptation of the parametric model to infants' ears

3.2.2.1 Ear canal

In Hudde and Engel (1998a) it was proposed to model the ear canal by a stepped circular duct with rigid walls. The sound transmission of the duct is defined by the width Δ_i and the cross sectional area A_i of each slice i , and is given by

$$\begin{bmatrix} p_{ec} \\ q_{ec} \end{bmatrix} = \left(\prod_i \begin{bmatrix} \cosh(\gamma_i \Delta_i) & \sinh(\gamma_i \Delta_i) Z_{twi} \\ \sinh(\gamma_i \Delta_i) / Z_{twi} & \cosh(\gamma_i \Delta_i) \end{bmatrix} \right) \begin{bmatrix} 1 & 0 \\ 1/Z_t & 1 \end{bmatrix} \begin{bmatrix} p_D \\ q_D \end{bmatrix}, \quad (3.1)$$

with γ the propagation constant, Z_{tw} the wave impedance, both depending on the cross-sectional area A , and with Z_t the impedance of the tapered end of the ear canal between the points D and T, see Figure 3.2. Both γ_i and Z_{twi} were computed according to Benade (1968), considering thermal and viscous losses for smooth wall surfaces, resulting in a complex tube wave impedance and a complex propagation constant with a real part α and an imaginary part β . In Hudde and Engel (1998b) it was proposed to increase the damping (i.e. the real part of the propagation constant) according to

$$\gamma = g\alpha + j\beta, \quad (3.2)$$

with $g = 3$ to account for non-smooth ear canal walls. The value of g was directly taken from Hudde and Engel (1998b) where it was estimated from reflectance measurements of rigidly terminated cadaver ear canal slices. The wave impedance is then approximated by

$$Z_{tw} = \frac{\rho c}{A} \gamma \frac{c}{j\omega}, \quad (3.3)$$

with ρ the mass density of air and c the speed of sound.

This model implies the first azimuthal mode being outside the relevant frequency range, the sound pressure at the umbo producing the most relevant contribution to the force acting on the manubrium, and rigid ear canal walls.

Physiological differences between adults' and infants' ear canals considered for our adaptation are the smaller dimensions and the much more compliant ear canal walls (Abdala and Keefe, 2011; Fels and Paprotny, 2013). From birth up to an age of 6 months, the typical distance from the tragus to the innermost point at the eardrum ranges from 21 mm to 26.1 mm (Keefe et al., 1993; Keefe et al., 1994; McLellan and Webb, 1957). The depth of the concha was reported to be between 7 mm and 8.6 mm in Keefe et al. (1994), resulting in an ear canal length ranging from 14 mm to 17.5 mm. In comparison, for adults a mean value of 23 mm ear canal length was reported in Keefe et al. (1993). The mean ear canal diameter for infants up to an age of 6 months ranges from 4.4 mm to 6.3 mm, see Keefe et al. (1993). For adults, a value of 10.4 mm diameter was reported in Keefe et al. (1993). It should be noted, that the mentioned values of ear canal geometry from Keefe et al. (1993), Keefe et al. (1994), and McLellan and Webb (1957) were determined from acoustic measurements with the underlying assumption of a cylindrical ear canal with rigid termination.

The walls of the ear canal are much softer and more flexible in young infants than in adults, see e.g. Holte et al. (1990). In Keefe et al. (1993) a resonant behavior of ear canal walls was found up to an age of 6 months. In order to consider the softer ear canal walls in the model, we propose to introduce a wall impedance

$$Z_{w,i} = W_{w,i} + j\omega M_{w,i} + 1/(j\omega N_{w,i}) \quad (3.4)$$

for every ear canal slice i with the wall resistance W_w , the acoustic mass M_w and the wall compliance N_w . Both the acoustic mass and the compliance are determined by the properties of the soft tissue in the ear canal, as

$$M_w = \frac{\rho_{st} d_{st}}{A_{st}}, \quad (3.5)$$

$$N_w = \frac{d_{st} A_{st}}{E_{st}}, \quad (3.6)$$

with ρ_{st} the density, d_{st} the thickness, A_{st} the surface area, and E_{st} the Young's modulus of the soft tissue. The damping is modeled with a frequency independent damping ratio given by

$$\zeta_{st} = 0.5 \left(\frac{\alpha}{\omega} + \beta \omega \right). \quad (3.7)$$

For the damping constants α and β it is assumed that $\alpha/\omega = \beta\omega$. The frequency-dependent wall resistance is then given by

$$W_w = \alpha M_w + \frac{\beta}{N_w}. \quad (3.8)$$

The proposed modeling of the damping is motivated by the work in Motallebzadeh et al. (2017a) in which a finite-element model of the ear canal and middle ear of a 22 days old infant was proposed. In Motallebzadeh et al. (2017a), three sets of values were given for the ear canal wall parameters E_{st} , ρ_{st} and ζ_{st} . The three sets, referred to as *low impedance*, *baseline* and *high impedance*, were chosen to cover a realistic range of values. The values given were E_{st} : 20 kPa, 210 kPa and 400 kPa, ρ_{st} : 1000 kg/m³, 1100 kg/m³ and 1200 kg/m³, ζ_{st} : 0.1, 0.25 and 0.4. No values were given in Motallebzadeh et al. (2017a) for the thickness d_{st} and the area A_{st} of the soft tissue in the ear canal. In order to reproduce the modeling results of the ear canal wall impedance Z_w in Motallebzadeh et al. (2017a), we adopt the values of E_{st} and ρ_{st} . For the damping ratio ζ_{st} modified values of

0.5, 0.6, 0.9 are used. The thickness d_{st} is assumed to be 3 mm and the area A_{st} is assumed to be 119 mm^2 (the lateral surface of a cylinder with a radius of 1.9 mm and a length of 10 mm). The

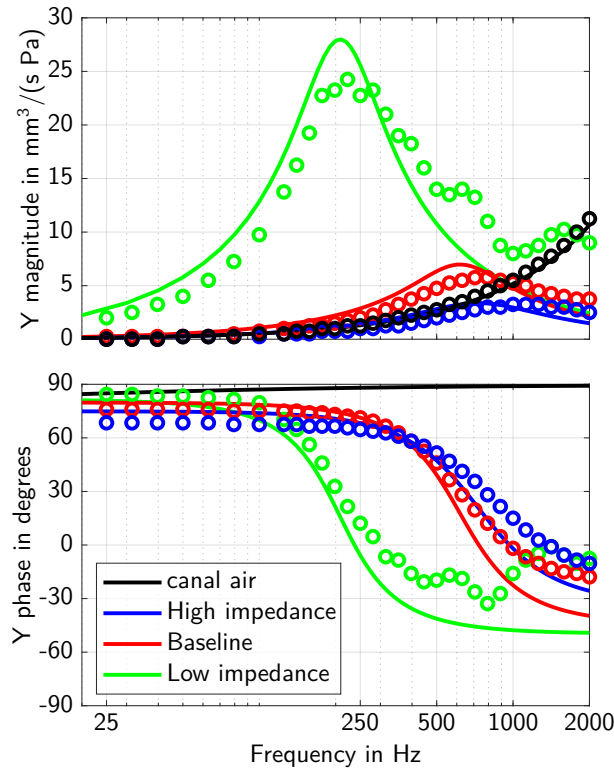


Figure 3.3: Reproduction of the modeling results in Motallebzadeh et al. (2017a) of the ear canal wall admittance and admittance of the air in the canal using equation 3.4. The circles correspond to Motallebzadeh et al. (2017a, Fig. 6) and the lines correspond to equation 3.4 using values of $\rho_{st} = \{1000 \text{ kg/m}^3, 1100 \text{ kg/m}^3 \text{ and } 1200 \text{ kg/m}^3\}$, $d_{st} = 3 \text{ mm}$, $A_{st} = 119 \text{ mm}^2$, $E_{st} = \{20 \text{ kPa}, 210 \text{ kPa} \text{ and } 400 \text{ kPa}\}$, $\zeta_{st} = \{0.1, 0.25 \text{ and } 0.4\}$, and $\frac{\alpha/\omega}{1.7} = \frac{\beta\omega}{0.3}$.

acoustic wall admittances $Y_w = 1/Z_w$ resulting from equation 3.4 for the three sets of values are depicted as straight lines in Figure 3.3 together with the modeling results from Motallebzadeh et al. (2017a, figure 6) depicted as open circles. Additionally the acoustic admittance of the air enclosed in the canal is depicted in black. Note that in Motallebzadeh et al. (2017a) a weighting of the damping constants α and β wasn't mentioned, however, the positive phase values at the resonant frequency of Y_w of their results indicate that they used a damping model which was dominated by mass rather than by compliance ($\alpha/\omega > \beta\omega$). In order to reproduce this effect in Figure 3.3 a weighting of $\frac{\alpha/\omega}{1.7} = \frac{\beta\omega}{0.3}$ is applied. For the model we propose here, a damping ratio ζ_{st} of 0.6 was chosen which leads to modeling results comparable to those in Motallebzadeh et al. (2017a) for their baseline set, see figure 3.3. Since no reason could be found that the damping is either dominated by mass or by compliance, $\alpha/\omega = \beta\omega$ is used in the model proposed here. It should be noted that the choice of a particular damping model is not critical with respect to the resulting immittance values, see discussion in appendix 3.A.1.

In order to account for the effect of the soft ear canal walls in the sound transmission eq. 3.1

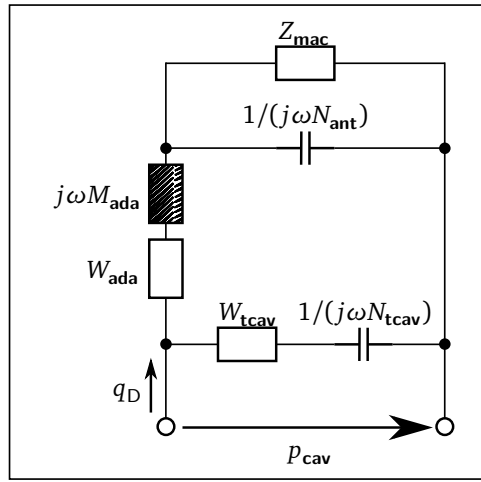


Figure 3.4: Equivalent circuit of the middle ear cavities model. The value of the impedance Z_{cav} results from the pressure p_{cav} divided by the volume velocity at the eardrum q_D .

changes to

$$\begin{bmatrix} p_{ec} \\ q_{ec} \end{bmatrix} = \left(\prod_i \left(\begin{bmatrix} \cosh(\gamma_i \Delta_i) & \sinh(\gamma_i \Delta_i) Z_{twi} \\ \sinh(\gamma_i \Delta_i) / Z_{twi} & \cosh(\gamma_i \Delta_i) \end{bmatrix} \right) \right) \begin{bmatrix} 1 & 0 \\ 1/Z_{w,i} & 1 \end{bmatrix} \begin{bmatrix} 1 & 0 \\ 1/Z_t & 1 \end{bmatrix} \begin{bmatrix} p_D \\ q_D \end{bmatrix}. \quad (3.9)$$

In comparison to models with rigid ear canal walls, the inclusion of the effects of soft ear canal walls will mainly affect frequencies below about 1.5 kHz, see discussion in section 3.4 (Figure 3.10).

3.2.2.2 Middle ear cavities

The middle ear cavities comprise the tympanic cavity, the aditus ad antrum, the antrum and the mastoid air cells. They are represented by the acoustic impedance Z_{cav} located between the ear canal two-port and the eardrum within the kernel two-port, see Figure 3.1. Generally, cavities are modeled using acoustic compliances representing volumes, acoustic masses representing air columns and resistive components introducing damping. The model of Z_{cav} for adults according to Hudde and Engel (1998a) is depicted in Figure 3.4. It contains the compliance N_{tcav} and the resistance W_{tcav} of the tympanic cavity, the acoustic mass M_{ada} and the resistance W_{ada} of the aditus ad antrum, the compliance N_{ant} of the antrum and the acoustic impedance Z_{mac} of the mastoid air cells.

With the acoustic compliance of a volume V given by $N = V/(\rho c^2)$, the resulting acoustic impedance of the middle ear cavities becomes

$$Z_{cav} = \left(\frac{1}{W_{tcav} + \rho c^2 / (j\omega V_{tcav})} + \frac{1}{W_{ada} + j\omega M_{ada} + \frac{1}{j\omega V_{ant} / (\rho c^2) + 1/Z_{mac}}} \right)^{-1}. \quad (3.10)$$

The acoustic impedance Z_{mac} of the mastoid air cells was modeled as a series resonant circuit in Hudde and Engel (1998a), defined by its resonant frequency f_{mac} , its quality factor Q_{mac} and its

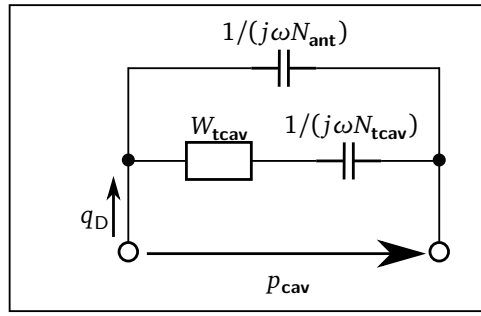


Figure 3.5: Equivalent circuit of the adapted middle ear cavities model. The value of the acoustic impedance Z_{cav} results from the pressure p_{cav} divided by the volume velocity at the eardrum q_D .

acoustic compliance N_{mac} associated with the volume V_{mac} of the air cells,

$$Z_{mac} = \frac{1 - (\omega/(2\pi f_{mac}))^2 + j\omega/(Q_{mac}2\pi f_{mac})}{j\omega V_{mac}/(\rho c^2)}. \quad (3.11)$$

Significant physiological differences in young infant's middle ear cavities, compared to those of adults, can be found in the sizes of the tympanic cavity and the antrum and in the status of pneumatization in the mastoid. In Ikui et al. (2000) the volume of the tympanic cavity was compared between infants aged ≤ 1 year and adults. It was found that the average infant's volume is about 2/3 of the volume in adults ($450 \text{ mm}^3/640 \text{ mm}^3$). The volume of all middle ear cavities of a 22 days old middle ear was estimated from CT-scans in Qi et al. (2008). The overall volume was estimated to be between 730 mm^3 and 930 mm^3 , with a volume of the tympanic cavity alone of 330 mm^3 . In the adult's model, a value of 500 mm^3 was used for the tympanic cavity volume and a value of 800 mm^3 was used for the antrum (Hudde and Engel, 1998c). Based on this, values of 330 mm^3 for the tympanic cavity and 500 mm^3 for the antrum were chosen for young infants in the present model.

According to Mansour et al. (2013, p. 107) pneumatization of the mastoid starts at the 33rd week of gestation. Starting with very few air cells in the mastoid, the surface of the antrum has an average value of 1 cm^2 at birth. In the first year of life, the surface increases due to the pneumatization to 4 cm^2 . In contrast, the mean adult mastoid air cell surface is about 12 cm^2 . Because of the weak degree of pneumatization of the mastoid in young infant, the effect is omitted in the model, i.e. Z_{mac} was removed from the model.

Furthermore, an additional modification in modeling the middle ear cavities is made. As will be shown in section 3.3, the influence of the components modeling the aditus ad antrum on the acoustic input impedance at the eardrum of the infant model is small. In order to reduce the overall complexity of the model, these components (namely W_{ada} and M_{ada}) were omitted.

The resulting model of the middle ear cavities for young infants is depicted in Figure 3.5.

3.2.2.3 Eardrum, malleus and incus

In Hudde and Engel (1998a) the eardrum, the malleus and the incus were aggregated in the kernel two-port, see Figure 3.1. The kernel comprises the acoustic properties, the transformation from the acoustical to the mechanical domain and the mechanical properties of eardrum, malleus and incus. The equivalent circuit of the kernel is depicted in Figure 3.6 with the acoustic properties represented

by the eardrum acoustic shunt impedance Z_{ac} on the left side. The two-port in the center models the acousto-mechanical transformation with the effective area A_D of the eardrum. On the right side, the mechanical properties are modeled by the mechanical admittances of the eardrum y_d , the malleus y_m , the incudomalleal joint y_{mi} and the incus y_i .

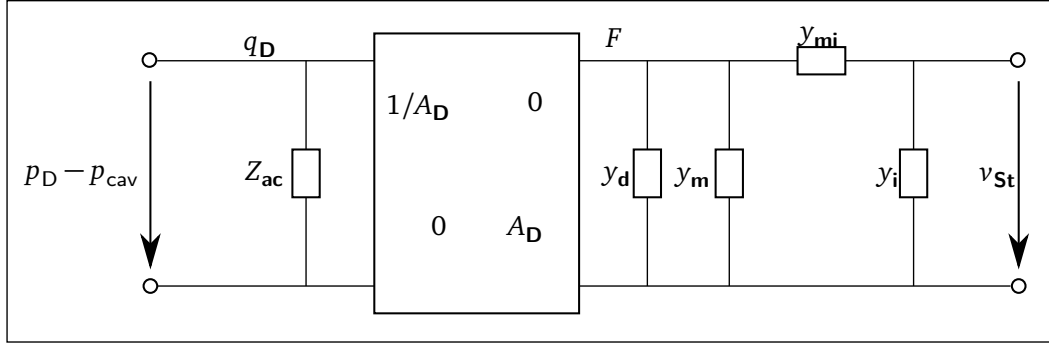


Figure 3.6: Equivalent circuit of the middle ear kernel two-port comprising the components of eardrum, malleus and incus according to Hudde and Engel (1998b).

The eardrum acoustic shunt impedance Z_{ac} was modeled as a series resonator with an additional correction of the phase. The resonator consists of a frequency independent acoustic resistance W_{ac} and a compliance N_{ac} , and an acoustic mass M_{ac} increasing with frequency, given by

$$M_{ac}(f) = M_{ac0} \left(1 + \sqrt{\frac{f}{f_{Ym}}} \right), \quad (3.12)$$

with the acoustic mass M_{ac0} at $f = 0$ Hz and the characteristic frequency f_{Ym} . The eardrum acoustic shunt impedance was given as

$$Z_{ac} = \frac{W_{ac} + j\omega M_{ac} + (j\omega N_{ac})^{-1}}{e^{j\omega\Phi_Y}}, \quad (3.13)$$

where

$$\Phi_Y(f) = s_{Yph} \log\left(1 + \frac{f}{f_{Yph}}\right) \quad (3.14)$$

is a phase correction with slope s_{Yph} and cut-off frequency f_{Yph} .

In the mechanical part, the admittance of the incudomalleal joint was defined as

$$y_{mi} = \left(w_{mi} + \frac{1}{j\omega n_{mi}} \right)^{-1}, \quad (3.15)$$

with the mechanical resistance w_{mi} and the mechanical compliance n_{mi} . The values of the other three mechanical admittances were determined from a common mechanical admittance y_{dmi} of eardrum, malleus and incus. The modeling of the admittance y_{dmi} is depicted in Figure 3.7. Herein, n_{oss} and m_{oss} are the mechanical compliance and mass of the ossicles, and w_{free} and m_{free} are the mechanical resistance and mass of the free vibrating part of the eardrum. The coupling between the ossicles and the free vibrating part of the eardrum is represented by the mechanical compliance n_{cpl} and resistance w_{cpl} . The mechanical admittance of the incus were then determined using

$$y_i = \frac{1}{3} y_{dmi} \quad (3.16)$$

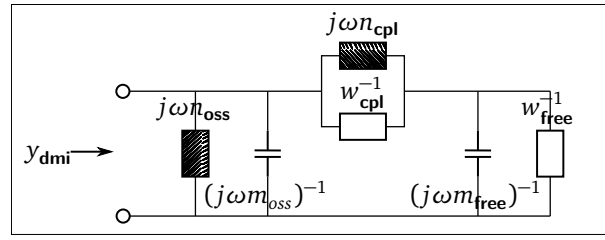


Figure 3.7: Equivalent circuit of the common mechanical admittance y_{dmi} comprising parts of the eardrum, the malleus and the incus.

and the mechanical admittance of the eardrum and the malleus using

$$y_{dm} = (1/y_d + 1/y_m)^{-1} = \frac{2}{3}y_{dmi} , \quad (3.17)$$

according to Hudde and Engel (1998c).

The acoustical to mechanical transformation as described in Hudde and Engel (1998b) is achieved by a gyrator two-port with a frequency-dependent, complex-valued effective eardrum area A_D . Specifically, A_D is given by a second order low-pass filter A'_D with an additional correction term Φ_A for the phase at higher frequencies, resulting in

$$A_D = A'_D e^{j\Phi_A} . \quad (3.18)$$

The low-pass filter was defined as

$$A'_D = \left(\frac{A_0 + A_\infty}{1 - (\omega/(2\pi f_A))^2 + j\omega/(Q_A 2\pi f_A)} - A_\infty \right) , \quad (3.19)$$

with the eardrum area A_0 at low frequencies ω , the area A_∞ for frequencies $\omega \rightarrow \infty$, the low-pass resonant frequency f_A and the low-pass quality factor Q_A . The phase correction term was defined as

$$\Phi_A = \begin{cases} 0 & \omega < 2\pi f_{Aph} \\ s_{Aph} \log\left(\frac{\omega}{2\pi f_{Aph}}\right) + \arg\{A'_D(f_{Aph})\} & \omega \geq 2\pi f_{Aph} \end{cases} \quad (3.20)$$

with the slope s_{Aph} , the cut-off frequency f_{Aph} and the phase angle of A'_D at f_{Aph} $\arg\{A'_D(f_{Aph})\}$.

In the present modeling approach, besides modifications that pertain to differences between infants and adults, two simplifications were made that are not related to differences between infants and adults. First, in Hudde and Engel (1998b), the parameters used to model the eardrum acoustic shunt impedance were derived from acoustic measurements, but they were not directly related to physiological properties. As explained above, basically a series resonator was used to model Z_{ac} , with a phase correction term comprising 3 additional parameters used to modify the impedance at high frequencies. The first one, f_{Ym} , causes a steeper slope of the acoustic impedance. The other two parameters, s_{Yph} and f_{Yph} , change the phase response from approaching -90° at high frequencies to positive phase values. A similar effect as caused by these three parameters can occur if an additional acoustic mass, acting in parallel to the resonator, e.g. a small air column between the acoustic impedance measurement device and the object to be measured, is introduced. In Hudde and Engel (1998b) the authors themselves remark that their measurement results are questionable at high frequencies (10 kHz). They explicitly refer to a minimum in the measured acoustic admittance

$(1/Z_{ac})$ which is not considered in their model. However, it would then be consequent to ignore the phase increase as well. Therefore, in the present approach, the phase correction term is omitted. Thus equation 3.13 simplifies to

$$Z_{ac} = W_{ac} + j\omega M_{ac} + (j\omega N_{ac})^{-1} . \quad (3.21)$$

Note that all parameters in equation 3.21 (W_{ac} , M_{ac} and N_{ac}) have values which do not depend on frequency. In order to be able to adapt at least the acoustic mass and the acoustic compliance to physiological conditions, the model of a stretched circular membrane according to Lenk (1977, pp. 71, 225–226) is used. The acoustic compliance is then given by

$$N_{ac} = \frac{\pi}{8} \frac{a_{ed}^4}{T_{0,ed} h_{ed}} , \quad (3.22)$$

with a_{ed} the radius of the eardrum, $T_{0,ed}$ the eardrum tension and h_{ed} the thickness of the eardrum. The acoustic mass is given by

$$M_{ac} = \frac{4}{3} \frac{\rho_{ed} h_{ed}}{\pi a_{ed}^2} , \quad (3.23)$$

with ρ_{ed} the membrane mass density.

The second simplification not related to differences between infants and adults is made in the effective eardrum area A_D . As will be shown in section 3.3, the influence of the three parameters high frequency eardrum area (A_∞), slope of the phase correction term (s_{Aph}) and cut-off frequency of the phase correction term (f_{Aph}) on the resulting acoustical eardrum impedance Z_D is very small. In order to reduce the overall complexity of the model, these parameters are omitted. The simplified effective eardrum area is then given by

$$A_D = \frac{A_0}{1 - (f/f_A)^2 + jf/(Q_A f_A)} . \quad (3.24)$$

Physiological differences of the eardrum between young infants and adults were reported in Ruah et al. (1991). It was found that the thickness of the pars flaccida (Shrapnell's Membrane) decreases with age, mainly during the first year of life. At an age of about 4 month the pars flaccida is about 3 times thicker compared to the thickness at an age of 21 years. Assuming the area of the pars flaccida is about 0.2 of the overall eardrum area, the parameters of acoustic and mechanic masses of the eardrum are multiplied by a factor of $3 \cdot 0.2 + 0.8 = 1.4$. According to equation 3.22, the acoustic compliance N_{ac} is inversely proportional to the thickness of the membrane and is therefore divided by 1.4.

Age-related changes of the ossicles were reported in Olszewski (1990), where the average weight of malleus and incus is roughly 25 % higher in adults than in the age group from 0 to 10 months. Since a reduction of the ossicles' mechanical mass in the model by 25 % has almost no effect on the acoustical eardrum impedance, this age-related difference is neglected.

There are some parameters in the model for which a direct physiological link is not obvious. This applies to the damping and to the low-pass used to model the effective eardrum area. By comparing the acoustic impedance predicted by the model with impedances measured in infant's ear canals from Sankowsky-Rothe et al. (2019), it was found that an adaption of three more parameters was necessary. Firstly, the resistance W_{ac} of the eardrum acoustic shunt impedance was reduced by

a factor of 0.7, secondly, the low-pass resonant frequency f_A of the effective eardrum area was increased by a factor of 2 and thirdly, the quality factor Q_A of the effective eardrum area was reduced to 1.

3.2.2.4 Stapes and cochlea

In Hudde and Engel (1998a) the stapes and the cochlea were represented by the mechanical admittance of the stapes y_{St} and the acoustic input impedance of the cochlea Z_C . Both were modeled by simple vibrators. The mechanical admittance of the stapes was given by

$$y_{St} = \left(w_{St} + \frac{1}{j\omega n_{St}} + j\omega m_{St} \right)^{-1}, \quad (3.25)$$

and the acoustic input impedance of the cochlea was given by

$$Z_C = \left(w_C + \frac{1}{j\omega n_C} + j\omega m_C \right) / A_{StF}, \quad (3.26)$$

with the respective mechanical elements resistance w , compliance n and mass m and with the area of the stapes footplate A_{StF} . The compliant element of y_{St} represents the annular ligament and the compliant element of Z_C is mainly caused by the round window membrane, see Hudde and Engel (1998c).

To our knowledge no physiological differences in stapes and cochlea input between infants and adults have been reported in literature. Therefore, we propose to retain the original model from Hudde and Engel (1998a) for this part of the overall model. However, it should be mentioned that in Abdala and Keefe (2011) it was stated that the developmental changes in the size of the middle ear cavities may be associated with a change in ossicular orientation.

3.3 Effect of proposed model adaptations on the eardrum impedance

In the previous section, several adaptations were proposed with respect to the model according to Hudde and Engel (1998a). In this section, the impact of the outlined adaptations on the acoustic impedance at the eardrum Z_D will be shown.

As discussed in section 3.2.2.3, the high-frequency eardrum area A_∞ , the slope of the phase correction term s_{Aph} and the cut-off frequency of the phase correction term f_{Aph} were proposed to be omitted in order to reduce the overall model complexity. As can be seen in Figure 3.8, by comparing the eardrum impedance of the original model (blue lines) with the red lines, the difference is indeed small and limited to the frequency range between 2 and 4 kHz.

In section 3.2.2.3 it was proposed to omit the parameters f_{Ym} , f_{Yph} and s_{Yph} manipulating the acoustic impedance Z_{ac} at high frequencies. The resulting eardrum impedance is depicted in Figure 3.8 (yellow line) including the previously mentioned simplifications. As can be seen, there is a significant difference in both, magnitude and phase of Z_D . The reason for omitting these parameters was that they were not strongly supported by the available data in Hudde and Engel (1998a), see section 3.2.2.3. In fact, the high frequency behavior of our proposed model is similar to that presented in Stirnemann (2011), in which a simple network-model of the middle ear was fitted to the occluded-ear simulator transfer impedance as defined in IEC-60318-4 (2007).

In Figure 3.9, the eardrum impedances Z_D of the adult model according to Hudde and Engel

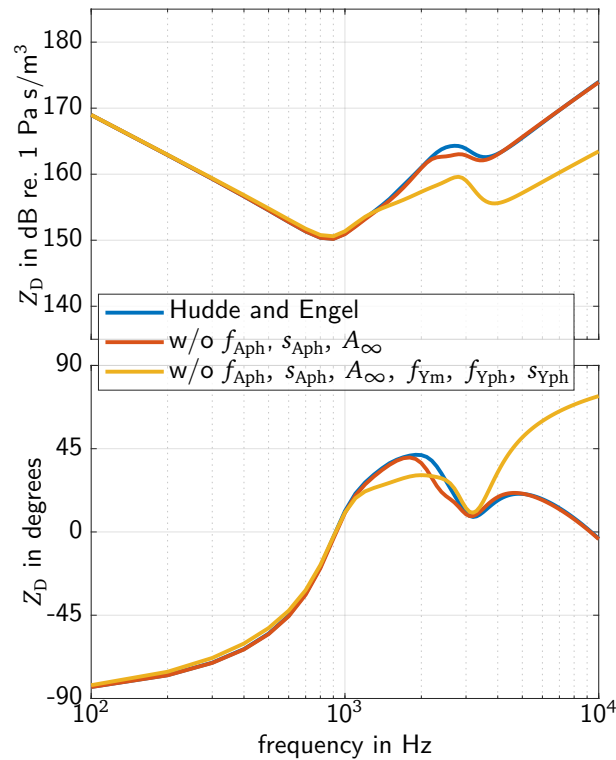


Figure 3.8: Impact of model simplifications in the kernel on Z_D for the model according to Hudde and Engel (1998c).

(1998c) (blue line), and of the model adapted to infants' ears (red line) are depicted. As can be seen, the most prominent difference is a shift of the global minimum in the magnitude from 800 Hz (adults) to about 2 kHz (infants) with a corresponding shift of the first zero crossing frequency in the impedance phase. Additionally, the eardrum impedance of the infants' model, extended by the model components of the aditus ad antrum, namely M_{ada} and W_{ada} , is depicted (yellow line). Since there are no known values for infant ears for M_{ada} and W_{ada} , the values of the adults model were used. It can be seen that the impact on Z_D is not very strong and mostly limited to a narrow frequency band around 5 kHz, which supports the omission of these parameters.

3.4 Ear canal impedance of the proposed model

To give insight into how the ear canal impedance Z_{ec} , which is the quantity measured in a WAI-measurement, of the newly proposed model for infants differs from the original model according to Hudde and Engel (1998a) for adults, some exemplary results are shown in Figure 3.10. For both, infant and adult, the ear canal is modeled assuming a constant cross section. Using the values of ear canal geometry given in section 3.2.2.1 with a probe insertion depth of 5 mm, which has to be subtracted from the ear canal lengths, for the infant's ear canal a length of 11 mm and a radius of 2.7 mm is assumed while for the adults' ear canal a length of 18 mm and a radius of 5.2 mm is assumed. In addition to the ear canal impedance of the infant's model ($Z_{ec, infant}$) the impedance of the same model neglecting the effect of compliant ear canal walls ($Z_{ec, infant rigid ec walls}$) is shown.

By comparing the ear canal impedances of the infants' model with and without compliant walls, it can be seen that the effect of compliant ear canal walls reduces the magnitude by several dB up to about 500 Hz. A substantial difference in the phase of Z_{ec} can be seen up to about 1.5 kHz. At

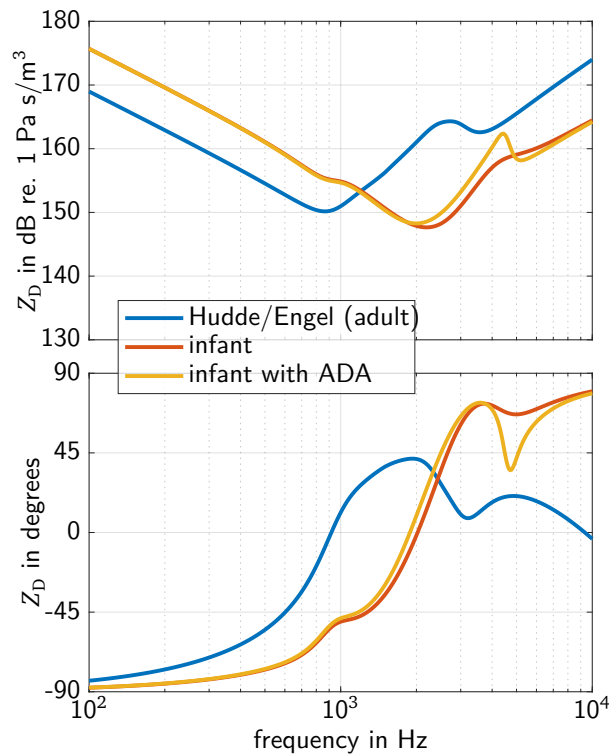


Figure 3.9: Eardrum impedances of the model according to Hudde and Engel (1998c), the model adapted to infants, and additionally the infant model extended by the model components of the aditus ad antrum (ADA).

higher frequencies, the effect of compliant ear canal walls can be ignored, provided our proposed model is valid.

A comparison of Z_{ec} with Z_D shows for the adult model that the magnitude of the eardrum impedance Z_D is high compared to that of the ear canal impedance. For the infant model, this is only true at frequencies up to about 1 kHz and above about 4 kHz. Conversely, between about 1.5 kHz and 3 kHz, Z_{ec} is governed by Z_D .

In Figure 3.11, the effect of varying either the ear canal radius (left) or the ear canal length (right) by $\pm 50\%$ can be seen. In both cases the ear canal volume varies, resulting in an increased low-frequency impedance magnitude with decreased volume. While a decreasing ear canal radius increases the impedance magnitude at higher frequencies, too, a decreasing ear canal length shifts the local extrema to higher frequencies.

The effects of varying the parameters modeling the compliant ear canal walls by $\pm 50\%$ on the ear canal impedance Z_{ec} are depicted in Figure 3.12. As already seen above, substantial differences in Z_{ec} are restricted to frequencies below about 1.5 kHz. As can be seen on the left side, increasing Young's modulus E_{st} shifts the magnitude minimum and the phase maximum to higher frequencies. As expected, increasing the damping ratio ζ_{st} results in a shallower magnitude minimum and phase maximum. On the right side it can be seen that increasing the thickness d_{st} shifts the magnitude minimum and the phase maximum to lower frequencies.

In summary, for the infant ear, the main characteristics of the ear canal impedance Z_{ec} and their underlying structures are as follows: At frequencies below about 1 kHz, the compliance of the air volume resulting from the ear canal geometry, together with the compliant ear canal walls and the compliant eardrum, determine the level of the magnitude. Additionally, the vibrating ear canal walls

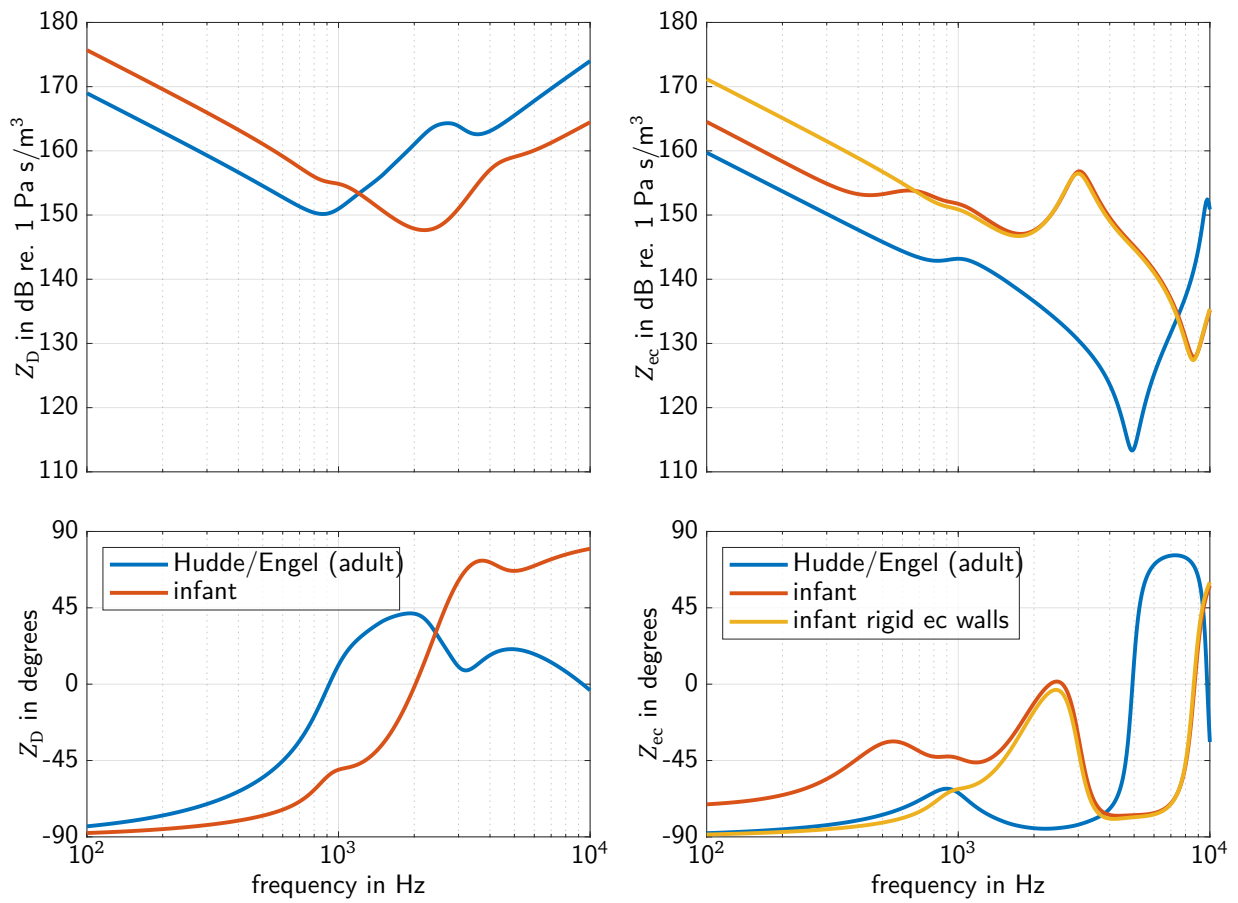


Figure 3.10: Eardrum impedances Z_D (left) and input impedances of the ear Z_{ec} (right) resulting from the model according to Hudde and Engel (1998c) and our model adapted to infant's ears.

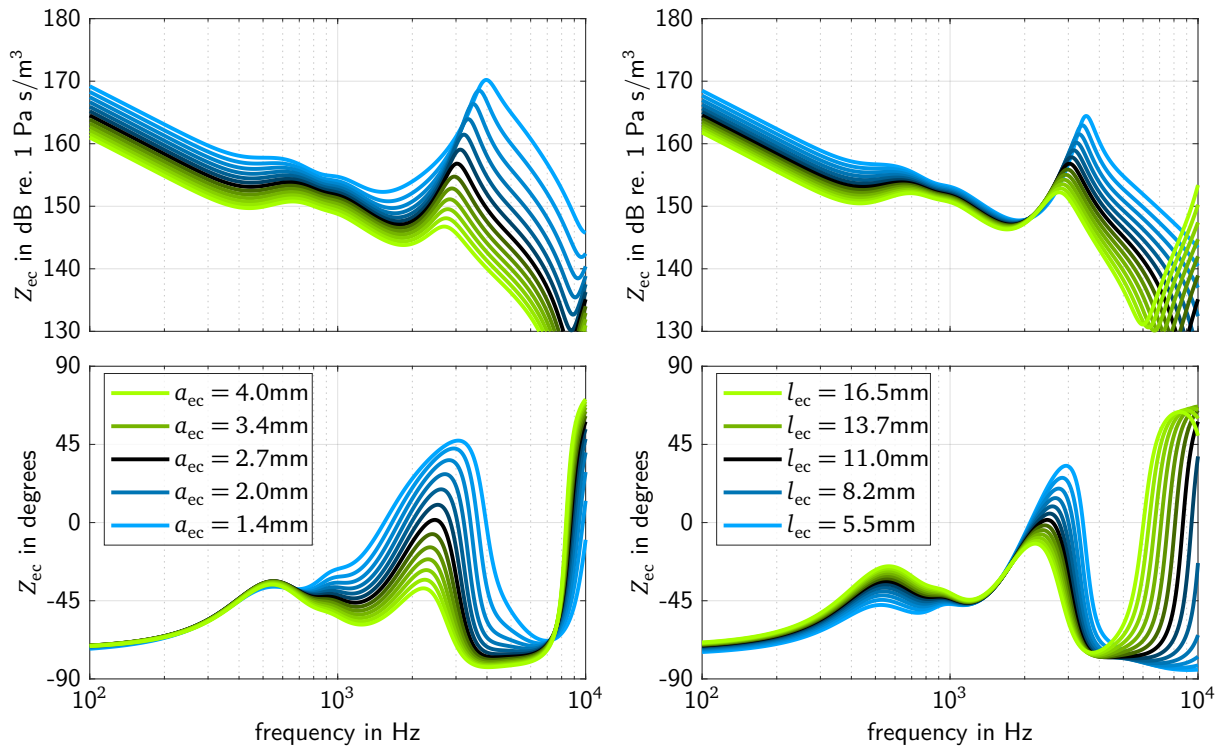


Figure 3.11: Ear canal impedances Z_{ec} resulting from our model adapted to infant's ears for different ear canal radii (left) and different ear canal lengths (right).

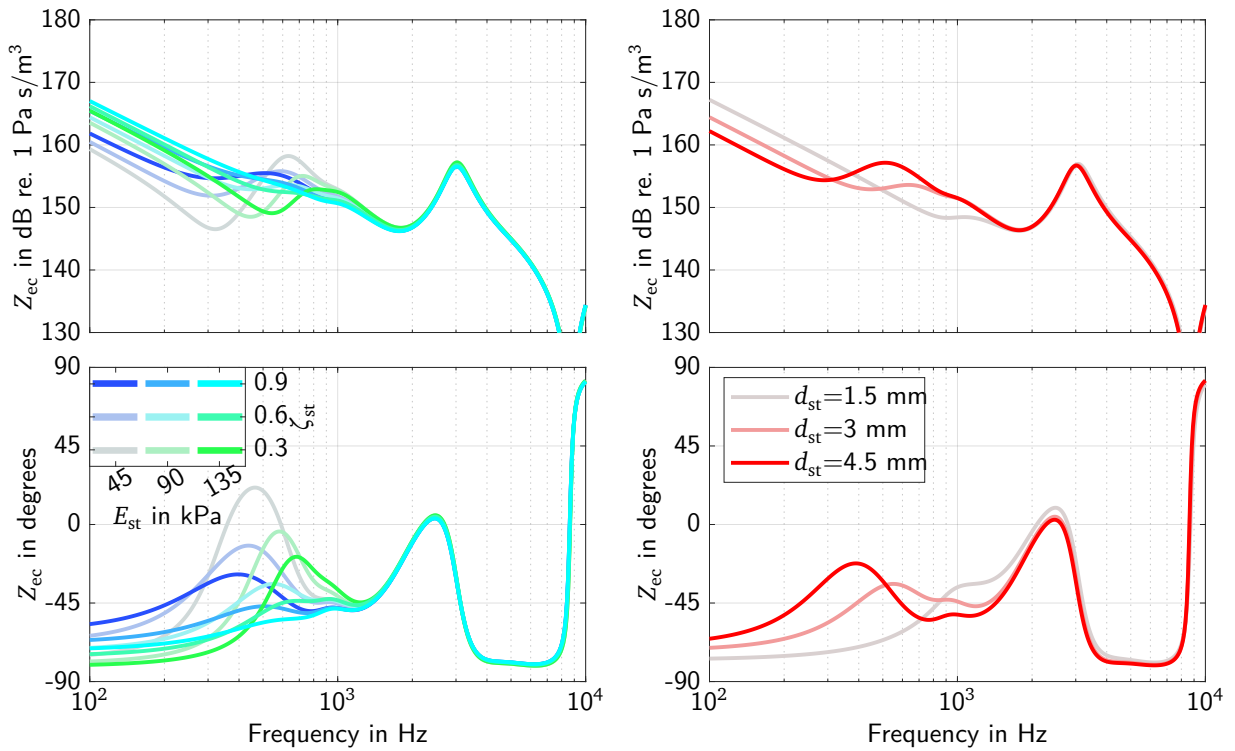


Figure 3.12: Ear canal impedances Z_{ec} resulting from the model adapted to infant's ears for different values of the parameters modeling the compliant ear canal walls.

cause a magnitude minimum or plateau and a maximum in phase around 400 – 700 Hz. Around 1.8 kHz, the acoustic input impedance at the eardrum causes a magnitude minimum with a phase increasing with frequency. At high frequencies above about 3 kHz, the ear canal geometry causes a magnitude minimum with a phase increasing with frequency.

3.5 Experimental validation

In this section, the model predictions of the ear canal impedance will be compared with measurements published in Sankowsky-Rothe et al. (2019). As described in Sankowsky-Rothe et al. (2019), the measurement method is based on Stirnemann et al. (2003), extended by consideration of discontinuity and end corrections in Blau et al. (2010). The method including the calibration procedure is described in detail in Blau et al. (2010). The measurements were performed using a custom-made impedance probe to measure the ear canal impedance on infant ears. The probe was designed to avoid over-pressure in the ear canal caused by inserting it into the ear canal at the cost of a decreased signal-to-noise ratio (SNR) at frequencies below about 1 kHz, further details can be found in Sankowsky-Rothe et al. (2019). This was realized by a pressure equalizing duct with an inner diameter of 0.6 mm. The subjects who participated in the study were aged between 2 weeks and 5 months. It should be noted that the infant ear undergoes developmental changes within the age range of the participants, i.e. an age-related effect is contained in the measurement data. The middle ear status of the participants was assessed by ENT-doctors specialized in pediatric audiology to be either normal, pathological or unclear at the time of testing. The assessment was based on the results of 1 kHz tympanometry, OAE- and/or AABR-screening, and ear-microscopy, see again Sankowsky-Rothe et al. (2019) for details. Note that in the following only the measurement data of the ears assessed to have a normal middle ear status are used. This comprised 30 ears from 24 infants in total.

In Figure 3.13, the measured ear canal impedances of 30 ears (pale colored lines), the modeled ear canal impedance, again using a constant ear canal cross section with 11 mm length and 2.7 mm radius (dashed black line) are depicted. Additionally, the modeled ear canal impedance using a constant ear canal cross section with 14 mm length and 1.7 mm radius is depicted (straight black line). All default parameter values used for the predictions are given in appendix 3.A.2. Since the impedance measurements in Sankowsky-Rothe et al. (2019) suffer from a bad SNR at low frequencies, due to noise generated by the subject during the measurement, only those impedance values are depicted in which the coherence between the signal applied to the probe speaker and the signal sensed by the probe microphone exceeded 0.5. Another effect that appeared in some measurements was acoustic leakage, which can be seen by phase values around 0 or larger below about 1 kHz. Although it would be easily possible to incorporate acoustic leakage into the model, this wasn't done here in order not to increase the number of parameters further.

Comparing the ear canal impedance (dashed line) of the model (using $a_{ec} = 2.7$ mm and $l_{ec} = 11$ mm) with those of the measurements, Figure 3.13 shows that the overall course of the impedance, with its main characteristics, is in agreement in both, magnitude and phase. At low frequencies up to about 1 kHz, the effect of compliant ear canal walls as described in section 3.4 can be seen in several measurements. The first minimum of the impedance magnitude at about 1.8 kHz is also present in the measurements, however, most measurements have a larger value compared to the model. Model and measurements have a phase increasing with frequency between 1.2 kHz and

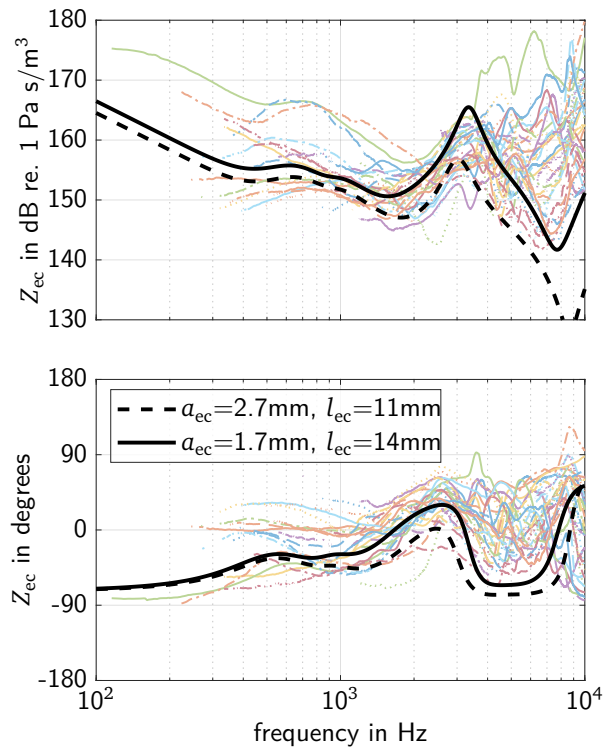


Figure 3.13: Ear canal impedance resulting from the model using two different sets of ear canal radius and diameter (black lines) together with ear canal impedances measured in $N = 30$ infant ears from Sankowsky-Rothe et al. (2019) (pale colored lines).

2.4 kHz, but in the model, the slope of the phase is smaller compared to the measurements. At higher frequencies, inter-individual differences in the measurements are quite large, but a significant difference between the measurements and the model is that the minimum in the impedance magnitude of the model is much steeper and the phase between about 2.5 kHz and 8 kHz lie below the measurements.

The high-frequency-minimum in the impedance magnitude is only caused by the ear canal dimensions, as can be seen in Figure 3.11. If the ear canal geometry is slightly changed, the agreement between model and measurement can be significantly increased. Z_{ec} , depicted as straight line in Figure 3.13, is modeled with an ear canal radius of 1.7 mm and an ear canal length of 14 mm. As can be seen, the agreement with the measurements is much better at high frequencies and, furthermore, also between 1.2 kHz and 2.4 kHz, in both magnitude and phase. However, between 3.5 kHz and 7 kHz, the model phase still lies below the measurements.

3.6 Influence of ear canal shape

So far, for all calculations of the impedance Z_{ec} , a cylindrical ear canal shape was assumed. As described in section 3.2.2.1, it is also possible to compute Z_{ec} for varying cross-sectional area functions of the ear canal. In Figure 3.14 the impedance of the ear Z_{ec} is depicted for three different ear canal shapes chosen to cover the range of possible shapes. From lateral to medial these shapes are: a cylindrical canal, a canal with linearly decreasing cross-sectional area, and a canal with linearly increasing cross-sectional area. All ear canals have the same volume and the same length. As can be seen, compared to the cylindrical canal, a conical shape with decreasing cross-sectional area shifts the magnitude minimum to higher frequencies. If the cross-sectional area

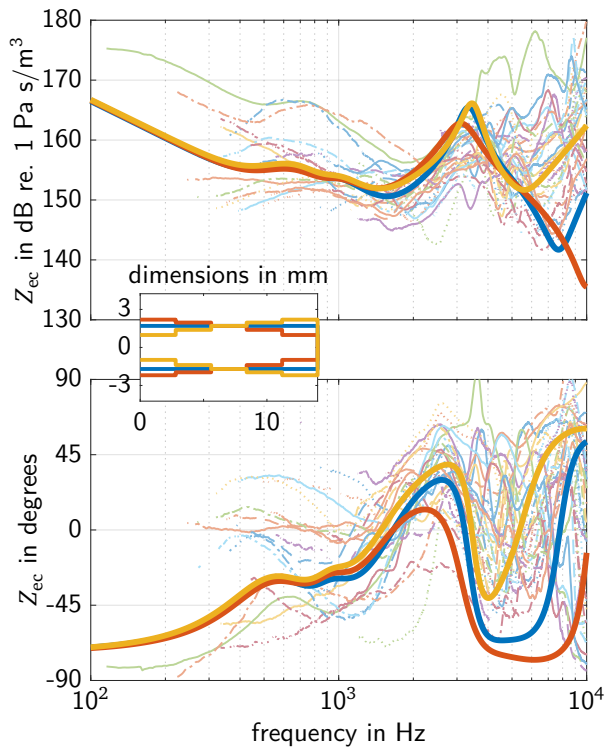


Figure 3.14: Input impedances of the ear Z_{ec} resulting from the model adapted to infant's ears for different ear canal shapes while preserving ear canal volume and length, together with ear canal impedances measured in infants ears with normal middle ear from Sankowsky-Rothe et al. (2019).

increases, the minimum is shifted to lower frequencies.

Changes in the ear canal shape without changing the ear canal volume mainly affect Z_{ec} at high frequencies. In the medium frequency range where Z_{ec} is dominated by Z_D , only a small effect can be observed for the magnitude and a slightly larger effect can be observed for the phase of Z_{ec} in the 2-3 kHz frequency range. Real ear canals will differ from the model by shapes that deviate from circular cross sections and by curvature. The effects shown above indicate that real ear canal shapes will have a strong influence on Z_{ec} at high frequencies, but at medium frequencies below about 3 kHz the influence on Z_{ec} will be rather small.

3.7 Comparison to similar models

One of the first models considering the effect of soft and flexible ear canal walls of young infants on WAI-measurements was proposed in Keefe et al. (1993). In that study, the authors presented measurement-based acoustic input impedances for different age groups. They used an electro-acoustic approach to model the acoustic input impedance Z_{ec} for the age group of 1 month in the frequency range from 125 Hz to 2 kHz. The ear canal walls were represented by a resonator with fixed values of the resonant frequency ($f_0 = 450$ Hz), the quality factor ($Q = 2$), and the compliance of the wall ($N_w = 1.6 \cdot 10^{-12}$ m³/(Pa s)). Compared to the model of the present study, provided that comparable ear canal dimensions are used, the effect of the ear canal wall on Z_{ec} is very similar at frequencies below the resonant frequency, see Figure 3.15. At higher frequencies, there are larger differences, mostly because at these frequencies the acoustic input impedance at the eardrum Z_D becomes dominant, which has a smaller magnitude in the present model. In contrast to the present modeling approach, beside being restricted to frequencies below 2 kHz, in Keefe

et al. (1993) neither a relation between ear canal dimensions and compliance of the wall, nor other relations to physiological properties are given.

In Qi et al. (2006), a finite-element model of a 22 days old newborn's ear canal was presented. The purpose of that model was to study the volume change in the ear canal under different static pressures of air as applied in tympanometry. The authors showed that using a Young's modulus of the soft tissue in the range from 30 kPa to 90 kPa and a Poisson's ratio of 0.475 resulted in plausible displacements and volume changes. The values used in the present model are in that range (90 kPa for Young's modulus) or very close since an incompressible medium is assumed (i.e. Poisson's ratio of 0.5).

Another finite-element model of the same ear as in Qi et al. (2006) was published in Motallebzadeh et al. (2017a). In that study, the sensitivity of the acoustic input admittance of the ear to changes in material properties was investigated up to frequencies of 2 kHz. Finally, a model with material properties adjusted to match some clinical data was proposed. A refined version of the model, in which the frequency range was extended up to 10 kHz, was proposed in Motallebzadeh et al. (2017b). Compared to the model of the present study, their first version model results in similar predictions, see Figure 3.15. Between about 500 Hz to 1.5 kHz the impedance magnitude of their model is about 3 dB greater. At about 800 Hz the phase responses start to deviate resulting in a difference of 46° at 2 kHz (-33° with the model in Motallebzadeh et al. (2017a) versus 13° with the model of the present study). The majority of the measurements depicted in Figure 3.15 have a positive phase value at 2 kHz and hence agree better with the model proposed here.

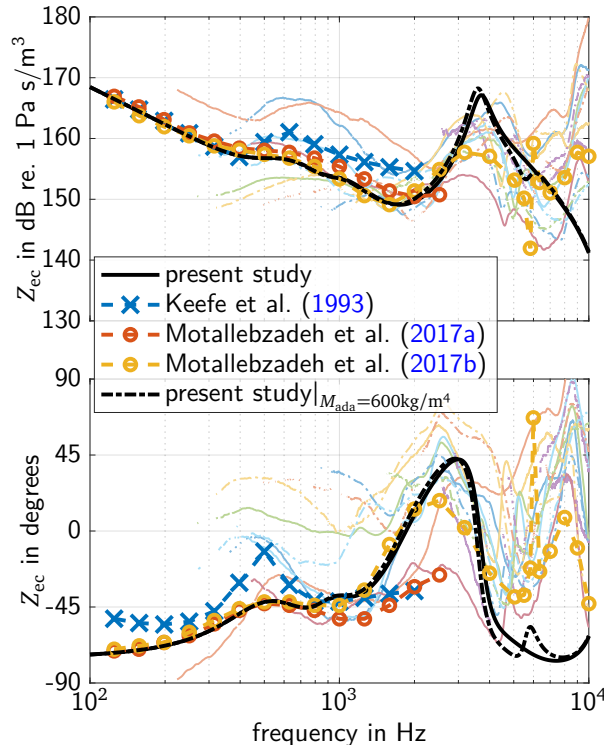


Figure 3.15: Input impedances of the ear Z_{ec} resulting from the models of the present study with $a_{ec} = 1.9$ mm, $L_{ec} = 8.5$ mm (black), according to Keefe et al. (1993) (blue), according to Motallebzadeh et al. (2017a) (red), and according to Motallebzadeh et al. (2017b) (yellow), together with ear canal impedances measured in infants ears with normal middle ear from Sankowsky-Rothe et al. (2019). The infants' age is between 16 and 28 days.

The prediction of their refined model is closer to that of the present study, especially in the frequency range from 1 to 2 kHz, as can be seen in Figure 3.15. At higher frequencies some substantial differences can be observed, in particular, at the magnitude maximum at 3.6 kHz and the phase maximum at 3 kHz. At these frequencies Z_{ec} transitions from dominance by Z_D to dominance by the ear canal geometry. Compared to the measurements, the prediction of the present study tends to the maximum values measured and the prediction according to Motallebzadeh et al. (2017b) tends to the lower values measured, however both predictions are within the range of measurements at frequencies between 2.4 kHz and 4 kHz. In the model according to Motallebzadeh et al. (2017b), a resonance at about 6 kHz and a local minimum at 7 kHz can be seen which are not predicted with the model of the present study. In Motallebzadeh et al. (2017b) it was explained that the resonance is caused by the first mode of the middle ear cavity and the minimum is caused by the first standing wave mode in the ear canal. A resonance in the middle ear cavities at about 6 kHz, but much less pronounced, could be predicted by the model of the present study if a value of 600 kg/m^4 for the acoustic mass of the aditus ad antrum M_{ada} would be used. However, a comparison with the measurements doesn't show an effect of much importance, therefore, omitting M_{ada} , as proposed in section 3.2.2.2, seems to be justified. The magnitude minimum at 7 kHz could be reproduced, but it would require an ear canal length of at least 16 mm which doesn't match the ear canal dimensions given in Motallebzadeh et al. (2017a). In summary, up to about 6 kHz the predictions of both models are comparable. However, the parametric model proposed here is easier to adapt to deviating properties, caused e.g. by inter-individual differences, than the single-case finite-element model from Motallebzadeh et al. (2017b).

3.8 Discussion

Based on an existing model for adults, a parametric electro-acoustic model has been developed, allowing predictions of acoustic input impedances of young infants' ears. Special attention has been paid to using model parameters representing physiological conditions whenever possible, and to reducing the number of parameters in comparison to the original model for adults according to Hudde and Engel (1998a,b,c). Predictions from the model showed that for frequencies below about 1 kHz, the ear canal impedance Z_{ec} is determined by the volume of air in the ear canal and by the compliant ear canal walls and that of the eardrum. At a medium frequency range around 1.8 kHz, Z_{ec} is determined by the eardrum impedance Z_D , and at high frequencies (above about 3 kHz) Z_{ec} is determined by the ear canal geometry. A comparison with impedances measured on infant's ears showed a good agreement in the main characteristics.

3.8.1 Current limitations of the model

The proposed model is developed to predict acoustic input impedances of the ears of young infants aged younger than 6 months. Known age-dependent physiological differences have been considered in the model, these differences are: 1.) the soft and flexible ear canal walls which will get acoustically rigid with increasing age. 2.) pneumatization of the mastoid, which increases with age and can be neglected for very young infants. 3.) the volume of the tympanic cavity and the antrum, which also increases with age. 4.) the thickness of the pars flaccida of the tympanic membrane, which decreases with age. It would be desirable to have the possibility of a continuous age-dependent adaptation of the model. However, this would require a more detailed knowledge about the developmental

processes, which is not available at present.

In the proposed model, the ear canal shape is restricted to consecutive cylindrical segments with different cross sections. Real ear canal shapes will deviate from circular cross sections and will have curvatures. It is assumed that these differences may have a noticeable effect on the acoustic input impedance of the ear Z_{ec} at high frequencies (≥ 4 kHz), but only very small effects at medium frequencies. However, at high frequencies, many of the measured Z_{ec} showed magnitudes larger than those predicted by the model. A higher magnitude of Z_{ec} in that frequency range means that the impact of Z_D on Z_{ec} is larger. The consequence for model predictions of the impact of specific middle ear conditions on immittance measurements is that the influence of specific middle ear conditions may not only be detectable at medium frequencies, but at higher frequencies as well.

The proposed model is currently limited to predictions at ambient pressure in the ear canal, whereas many WAI test are performed over a tympanometric range of air pressures in the ear canal. Nevertheless, the model is potentially extendable to account for differences in air pressure between ear canal and middle ear, by linearizing it to different static pressure states, as will be discussed in the companion paper (Sankowsky-Rothe et al., 2022b).

Although the structure of the model would permit predictions of middle ear transfer functions, such predictions weren't investigated. The aim of the proposed model is to support WAI-measurements by permitting statements about the acoustic input impedances Z_{ec} and Z_D . A verification of the model for the prediction of middle ear transfer impedances would require considerably different reference data. This may be part of future work.

3.8.2 Differences to similar models

The proposed model confirms that there are large differences in the acoustic input impedances of ear canal and eardrum between adults and young infants. Very few models for young infant ears exist. The electro-acoustic modeling approach in Keefe et al. (1993) was intended to simulate the effects of the soft and flexible ear canal walls of young infants. The predicted effects are somewhat comparable to those predicted by the model of the present study. However, the parts of the model in Keefe et al. (1993) representing the ear canal geometry and the eardrum are very basic and not related to physiological properties. In contrast, the model parameters of the present study are very close to physiological properties allowing predictions for different physiological conditions. On the other hand, finite-element models of young infant ears exist (Motallebzadeh et al., 2017a,b; Qi et al., 2008). The predictions of these models are very similar to those of the present model. The model proposed in Motallebzadeh et al. (2017b) allows predictions up to 10 kHz. Compared to the model of the present study, properties of ear canal shape can be reproduced much better with the finite-element model. However, predictions of the effects resulting from individual differences or different middle ear conditions would be extremely costly.

3.9 Conclusions based on the model

Based on the parametric model of young infants' eardrum and ear canal impedances proposed in this paper, the following conclusions can be made:

- The soft and flexible ear canal walls in young infant ears affect the measured acoustic input impedance of the ear Z_{ec} up to about 1.5 kHz, no significant effect is expected at higher

frequencies.

- At a medium frequency range around 1.8 kHz, the measured input impedance Z_{ec} is dominated by the eardrum impedance Z_D . Therefore, it can be expected that different middle ear conditions will have the largest effect on Z_{ec} in the medium frequency range.
- At high frequencies, the model predictions indicate that Z_{ec} is dominated by ear canal properties and therefore, it might not be possible to detect different middle ear conditions at high frequencies. However, predictions must be taken with caution at these frequencies because many measurements showed higher Z_{ec} magnitudes which could mean that in some cases middle ear conditions could still be detected.

In part II of this paper, the model will be extended to predict the influence of different pathological middle ear conditions on the acoustic input impedances of the ear canal and the eardrum of young infants in order to investigate implications for WAI-measurements.

3.10 Acknowledgment

We would like to thank the two anonymous reviewers for their thoughtful comments on an earlier version of the manuscript. This work was partly funded by the Jade University's research program Jade2Pro and partially supported by Deutsche Forschungsgemeinschaft (DFG, German Research Foundation) – Project-ID 352015383 – SFB 1330/2 C1.

3.11 Data Availability Statement

An implementation of the complete model is available on GitHub, under the reference https://github.com/tobiassankowsky/acoustic_impedance_infant_ear.

3.A Appendix

3.A.1 Notes on damping models for compliant ear canal walls

In order to account for the damping caused by the soft and flexible ear canal walls, in the present study, each slice i of the ear ear canal has a complex impedance $Z_{w,i}$ in parallel (see section 3.2.2.1). $Z_{w,i}$ is a series resonator with an acoustic mass, an acoustic compliance and an acoustic resistance. The acoustic resistance is modeled using a frequency independent damping ratio ζ_{st} (eq. 3.7) with damping constants α and β . The modeling is similar as in Motallebzadeh et al. (2017a,b), however, a significant difference is that in the present study the damping constants are chosen such that $\alpha/\omega = \beta\omega$ with the result that the undamped natural frequency equals the damped resonant frequency of $Z_{w,i}$, i.e. the minimum of the impedance magnitude coincide with a phase value of 0° (see left side of Figure 3.16 black line). In Motallebzadeh et al. (2017a,b), by contrast, the phase value of Z_w at the magnitude minimum is negative, i.e. $\alpha/\omega > \beta\omega$ or rather the resistive damping is dominated to a greater extent by mass than by compliance (see left side of Figure 3.16 red line). Another modeling approach is used in Keefe et al. (1993) in which Z_w is modeled by a resonator consisting of an acoustic mass in series with a resistance and a compliance in parallel. The resulting

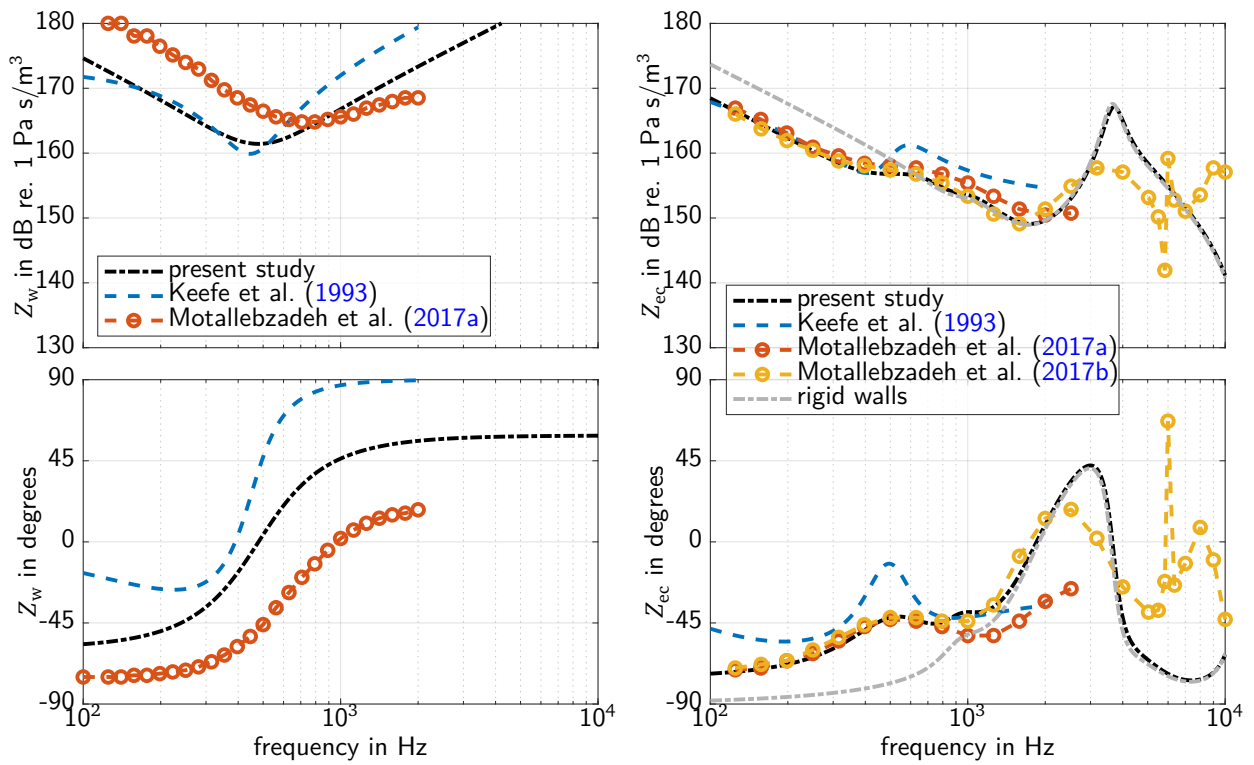


Figure 3.16: Ear canal wall impedance Z_w (left) and input impedances of the ear Z_{ec} (right) resulting from the models of the present study with $a_{ec} = 1.9$ mm, $L_{ec} = 8.5$ mm (black), according to Keefe et al. (1993) (blue), according to Motallebzadeh et al. (2017a) (red), and according to Motallebzadeh et al. (2017b) (yellow). Additionally, Z_{ec} resulting from the models of the present study assuming rigid ear canal walls is depicted (gray).

effect is that the resistive damping is dominated only by the compliance (see left side of Figure 3.16 red circles).

The input impedance of the ear Z_{ec} of the different models is depicted on the right side of Figure 3.16. For comparisons, Z_{ec} resulting from the model of the present study assuming rigid ear canal walls is depicted, additionally. A noticeable difference caused by the different approaches used to model Z_w results only in the phase of Z_{ec} at very low frequencies (< 400 Hz) with the model according to Keefe et al. (1993) compared to the other models. Note that the difference at about 500 Hz is mainly caused by the input impedance of the eardrum Z_D which is assumed to be larger in Keefe et al. (1993) compared to the other models.

It can be concluded that the effect of the different approaches which have been proposed to model the resistive component of the damping caused by the soft and flexible ear canal walls do not show a substantial different impact on Z_{ec} . If at all, differences are limited to the impedance phase at frequencies below about 400 Hz.

3.A.2 Default parameter values

Table 3.1: Default values of ear canal parameters.

Parameter	Infant value	Adult value
l_{ec} (or widths Δ_i)	14 mm	18 mm
a_{ec} (or areas A_i)	1.7 mm	5.3 mm
g_{ec}	10	3
ζ_{st}	0.6	–
E_{st}	90 kPa	–
ρ_{st}	1100 kg/m ³	–
d_{st}	3 mm	–

Table 3.2: Default values of middle ear cavities parameters.

Parameter	Infant value	Adult value
f_{mac}	–	3500 Hz
Q_{mac}	–	0.4000
V_{mac}	–	8 cm ³
M_{ada}	–	880 kg/m ⁴
W_{ada}	–	17e5 Pa s/m ³
V_{ant}	0.5 cm ³	0.8 cm ³
V_t	0.33 cm ³	0.5 cm ³
W_t	2e6 Pa s/m ³	2e6 Pa s/m ³

Table 3.3: Default values of middle ear kernel parameters.

Parameter	Infant value	Adult value	acc. to Hudde and Engel (1998c) (adult)
a_{ed}	4.3702 mm	4.3702 mm	–
$T_{0, ed}$	3.6465e+05 Pa	3.6465e+05 Pa	–
h_{ed}	0.112 mm	0.08 mm	–
ρ_{ed}	1100 kg/m ³	1100 kg/m ³	–
$(M_{ac0})^a$	2737.8 kg/m ⁴	1955.6 kg/m ⁴	2400 kg/m ⁴
$(N_{ac})^a$	3.5073e-12 m ⁵ /N	4.9102e-12 m ⁵ /N	5e-12 m ⁵ /N
f_{Ym}	–	–	1900 Hz
f_{Yph}	–	–	8000 Hz
s_{Yph}	–	–	4.3982
W_{ac}	275e5 Pa s/m ³	400e5 Pa s/m ³	400e5 Pa s/m ³
A_0	0.38 cm ²	0.38 cm ²	0.38 cm ²
A_{inf}	–	–	2 mm ²
f_A	4400 Hz	2200 Hz	2200 Hz
f_{Aph}	–	–	1500 Hz
s_{Aph}	–	–	-3.7699
Q_A	1	1.3	1.3
m_{free}	1.68e-05 kg	1.2e-05 kg	1.2e-05 kg
w_{free}	0.02 N s/m	0.02 N s/m	0.02 N s/m
n_{cpl}	0.0005 m/N	0.0005 m/N	0.0005 m/N
w_{cpl}	0.08 N s/m	0.08 N s/m	0.08 N s/m
m_{oss}	7e-06 kg	7e-06 kg	7e-06 kg
n_{oss}	0.003 m/N	0.003 m/N	0.003 m/N
n_{mi}	4e-05 m/N	4e-05 m/N	4e-05 m/N
w_{mi}	1 N s/m	1 N s/m	1 N s/m

^a not used as a parameter in the adapted model (see equations 3.23 and 3.22), values are given for comparisons to the model according to Hudde and Engel (1998c).

Table 3.4: Default values of stapes and cochlea parameters.

Parameter	Infant value	Adult value
m_{St}	3e-06 kg	3e-06 kg
n_{St}	0.0012 m/N	0.0012 m/N
w_{St}	0.018 N s/m	0.018 N s/m
m_C	1e-05 kg	1e-05 kg
n_C	0.011 m/N	0.011 m/N
w_C	0.07 N s/m	0.07 N s/m
not required		
A_C	3 mm ²	3 mm ²

References for Chapter 3

- Abdala, C. and Keefe, D. H. (2011). "Morphological and Functional Ear Development". In: *Human Auditory Development*. Springer New York, pp. 19–59. doi: [10.1007/978-1-4614-1421-6_2](https://doi.org/10.1007/978-1-4614-1421-6_2).
- Aithal, S., Kei, J., Driscoll, C., Khan, A., and Swanston, A. (2015). "Wideband Absorbance Outcomes in Newborns: A Comparison With High-Frequency Tympanometry, Automated Brainstem Response, and Transient Evoked and Distortion Product Otoacoustic Emissions." In: *Ear and Hearing* 36.5, e237–e250. doi: [10.1097/AUD.000000000000175](https://doi.org/10.1097/AUD.000000000000175).
- Benade, A. H. (1968). "On the Propagation of Sound Waves in a Cylindrical Conduit". In: *The Journal of The Acoustical Society of America* 44.2, pp. 616–623. doi: [10.1121/1.1911130](https://doi.org/10.1121/1.1911130).
- Blankenship, C. M., Hunter, L. L., Keefe, D. H., Feeney, M. P., Brown, D. K., McCune, A., Fitzpatrick, D. F., and Lin, L. (2018). "Optimizing Clinical Interpretation of Distortion Product Otoacoustic Emissions in Infants". In: *Ear & Hearing* 39.6, pp. 1075–1090. doi: [10.1097/aud.0000000000000562](https://doi.org/10.1097/aud.0000000000000562).
- Blau, M., Bornitz, M., Zahnert, T., Hofmann, G., and Hüttenbrink, K. (2003). *Entwicklung eines implantierbaren Mikrofons zum Einsatz in Cochlea-Implantaten und implantierbaren Hörgeräten, BMBF-Forschungsbericht. Bundesministerium für Bildung und Forschung*. Research rep. TIB Hannover, pp. 1–49. url: <https://www.tib.eu/de/suchen/id/tema%3ATEMA20040703524>.
- Blau, M., Sankowsky, T., Roeske, P., Mojallal, H., Teschner, M., and Thiele, C. (2010). "Prediction of the sound pressure at the ear drum in occluded human cadaver ears". In: *Acta Acustica united with Acustica* 96.3, pp. 554–566.
- Feeney, M. P., Hunter, L. L., Kei, J., Lilly, D. J., Margolis, R. H., Nakajima, H. H., Neely, S. T., Prieve, B. A., Rosowski, J. J., Sanford, C. A., Schairer, K. S., Shahnaz, N., Stenfelt, S., and Voss, S. E. (2013). "Consensus Statement". In: *Ear and Hearing* 34.Supplement 1, 78s–79s. doi: [10.1097/aud.0b013e31829c726b](https://doi.org/10.1097/aud.0b013e31829c726b).
- Fels, J. and Paprotny, J. (2013). "Ear Canal Properties of Children: Dimensions of Ear Canals and Simulation of the Input-Impedance". In: *Acta Acustica united with Acustica* 99.4, pp. 582–589. doi: [10.3813/AAA.918637](https://doi.org/10.3813/AAA.918637).
- Holte, L., Cavanaugh, R. M., and Margolis, R. H. (1990). "Ear canal wall mobility and tympanometric shape in young infants." In: *The Journal of pediatrics* 117.1 Pt 1, pp. 77–80.
- Hudde, H. and Engel, A. (1998a). "Measuring and Modeling Basic Properties of the Human Middle Ear and Ear Canal. Part I: Model Structure and Measuring Techniques". In: *ACUSTICA/acta acustica* 84.4, pp. 720–738.
- Hudde, H. and Engel, A. (1998b). "Measuring and Modeling Basic Properties of the Human Middle Ear and Ear Canal. Part II: Ear Canal, Middle Ear Cavities, Eardrum, and Ossicles". In: *ACUSTICA/acta acustica* 84.5, pp. 894–913.
- Hudde, H. and Engel, A. (1998c). "Measuring and Modeling Basic Properties of the Human Middle Ear and Ear Canal. Part III: Eardrum Impedances, Transfer Functions and Model Calculations". In: *ACUSTICA/acta acustica* 84.6, pp. 1091–1108.
- IEC-60318-4 (2007). *Electroacoustics - Simulators of Human Head and Ear - Part 4: Occluded-ear simulator for the measurement of earphones coupled to the ear by ear inserts*. International Electrotechnical Organisation. Standard. International Electrotechnical Organisation.

- Ikui, A., Sando, I., Haginomori, S.-I., and Sudo, M. (2000). "Postnatal Development of the Tympanic Cavity: a Computer-aided Reconstruction and Measurement Study". In: *Acta Oto-Laryngologica* 120.3, pp. 375–379. doi: [10.1080/000164800750000595](https://doi.org/10.1080/000164800750000595).
- Keefe, D. H., Bulen, J. C., Arehart, K. H., and Burns, E. M. (1993). "Ear-canal impedance and reflection coefficient in human infants and adults." In: *The Journal of the Acoustical Society of America* 94.5, pp. 2617–2638. doi: [10.1121/1.407347](https://doi.org/10.1121/1.407347).
- Keefe, D. H., Folsom, R. C., Gorga, M. P., Vohr, B. R., Bulen, J. C., and Norton, S. J. (2000). "Identification of neonatal hearing impairment: ear-canal measurements of acoustic admittance and reflectance in neonates." In: *Ear and Hearing* 21.5, pp. 443–461. doi: [10.1097/00003446-200010000-00009](https://doi.org/10.1097/00003446-200010000-00009).
- Keefe, D. H. (2015). "Human middle-ear model with compound eardrum and airway branching in mastoid air cells." In: *The Journal of the Acoustical Society of America* 137 (5), pp. 2698–2725. doi: [10.1121/1.4916592](https://doi.org/10.1121/1.4916592).
- Keefe, D. H., Bulen, J. C., Campbell, S. L., and Burns, E. M. (1994). "Pressure transfer function and absorption cross section from the diffuse field to the human infant ear canal". In: *The Journal of the Acoustical Society of America* 95.1, pp. 355–371. doi: [10.1121/1.408380](https://doi.org/10.1121/1.408380).
- Kringlebotn, M. (1988). "Network Model for the Human Middle Ear". In: *Scandinavian Audiology* 17.2, pp. 75–85. doi: [10.3109/01050398809070695](https://doi.org/10.3109/01050398809070695).
- Lenk, A. (1977). *Elektromechanische Systeme Band 2. Systeme mit verteilten Parametern*. Berlin: VEB Verlag Technik.
- Mansour, S., Magnan, J., Haidar, H., Nicolas, K., and Louryan, S. (2013). *Comprehensive and Clinical Anatomy of the Middle Ear*. 1st ed. Springer-Verlag Berlin Heidelberg. doi: [10.1007/978-3-642-36967-4](https://doi.org/10.1007/978-3-642-36967-4).
- Marchant, C. D., Shurin, P. A., Turczyk, V. A., Wasikowski, D. E., Tutihasi, M. A., and Kinney, S. E. (1984). "Course and outcome of otitis media in early infancy: A prospective study". In: *The Journal of Pediatrics* 104.6, pp. 826–831. doi: [10.1016/s0022-3476\(84\)80475-8](https://doi.org/10.1016/s0022-3476(84)80475-8).
- McLellan, M. and Webb, C. (1957). "Ear studies in the newborn infant". In: *The Journal of Pediatrics* 51.6, pp. 672–677. doi: [10.1016/s0022-3476\(57\)80102-4](https://doi.org/10.1016/s0022-3476(57)80102-4).
- Motallebzadeh, H., Maftoon, N., Pitaro, J., Funnell, W. R. J., and Daniel, S. J. (2017a). "Finite-Element Modelling of the Acoustic Input Admittance of the Newborn Ear Canal and Middle Ear." In: *Journal of the Association for Research in Otolaryngology* 18, pp. 25–48. doi: [10.1007/s10162-016-0587-3](https://doi.org/10.1007/s10162-016-0587-3).
- Motallebzadeh, H., Maftoon, N., Pitaro, J., Funnell, W. R. J., and Daniel, S. J. (2017b). "Fluid-Structure Finite-Element Modelling and Clinical Measurement of the Wideband Acoustic Input Admittance of the Newborn Ear Canal and Middle Ear". In: *Journal of the Association for Research in Otolaryngology* 18.5, pp. 671–686. doi: [10.1007/s10162-017-0630-z](https://doi.org/10.1007/s10162-017-0630-z).
- Olszewski, J. (1990). "The morphometry of the ear ossicles in humans during development". In: *Anatomischer Anzeiger* 171.3, pp. 187–191.
- Paradise, J. L., Rockette, H. E., Colborn, D. K., Bernard, B. S., Smith, C. G., Kurs-Lasky, M., and Janosky, J. E. (1997). "Otitis Media in 2253 Pittsburgh-Area Infants: Prevalence and Risk Factors During the First Two Years of Life". In: *Pediatrics* 99.3, pp. 318–333. doi: [10.1542/peds.99.3.318](https://doi.org/10.1542/peds.99.3.318).

- Pitaro, J., Al Masaoudi, L., Motallebzadeh, H., Funnell, W. R. J., and Daniel, S. J. (2016). “Wide-band reflectance measurements in newborns: Relationship to otoscopic findings.” In: *Int. J. Pediatr. Otorhinolaryngol.* 86, pp. 156–160. doi: [10.1016/j.ijporl.2016.04.036](https://doi.org/10.1016/j.ijporl.2016.04.036).
- Prieve, B. A., Vander Werff, K. R., Preston, J. L., and Georgantas, L. (2013). “Identification of Conductive Hearing Loss in Young Infants Using Tympanometry and Wideband Reflectance”. In: *Ear and Hearing* 34.2, pp. 168–178. doi: [10.1097/aud.0b013e31826fe611](https://doi.org/10.1097/aud.0b013e31826fe611).
- Qi, L., Funnell, W. R. J., and Daniel, S. J. (2008). “A nonlinear finite-element model of the newborn middle ear.” In: *The Journal of the Acoustical Society of America* 124.1, pp. 337–347. doi: [10.1121/1.2920956](https://doi.org/10.1121/1.2920956).
- Qi, L., Liu, H., Lutfy, J., Funnell, W. R. J., and Daniel, S. J. (2006). “A nonlinear finite-element model of the newborn ear canal.” In: *The Journal of the Acoustical Society of America* 120.6, pp. 3789–3798. doi: [10.1121/1.2363944](https://doi.org/10.1121/1.2363944).
- Rosowski, J. J., Davis, P. J., Merchant, S. N., Donahue, K. M., and Coltrera, M. D. (1990). “Cadaver middle ears as models for living ears: comparisons of middle ear input immittance.” In: *Annals of Otology, Rhinology and Laryngology* 99.5 Pt 1, pp. 403–412. doi: [10.1177/000348949009900515](https://doi.org/10.1177/000348949009900515).
- Ruah, C. B., Schachern, P. A., Zelterman, D., Paparella, M. M., and Yoon, T. H. (1991). “Age-related morphologic changes in the human tympanic membrane. A light and electron microscopic study.” In: *Archives of otolaryngology–head & neck surgery* 117.1 (6), pp. 627–634. doi: [10.1121/1.2920956](https://doi.org/10.1121/1.2920956).
- Sanford, C. A., Keefe, D. H., Liu, Y.-W., Fitzpatrick, D., McCreery, R. W., Lewis, D. E., and Gorga, M. P. (2009). “Sound-conduction effects on distortion-product otoacoustic emission screening outcomes in newborn infants: test performance of wideband acoustic transfer functions and 1-kHz tympanometry.” In: *Ear and hearing* 30 (6), pp. 635–652. doi: [10.1097/AUD.0b013e3181b61cdc](https://doi.org/10.1097/AUD.0b013e3181b61cdc).
- Sanford, C. A. and Feeney, M. P. (2008). “Effects of maturation on tympanometric wideband acoustic transfer functions in human infants”. In: *The Journal of the Acoustical Society of America* 124.4, pp. 2106–2122. doi: [10.1121/1.2967864](https://doi.org/10.1121/1.2967864).
- Sankowsky-Rothe, T., Blau, M., Köhler, S., and Stirnemann, A. (2015a). “Individual Equalization of Hearing Aids with Integrated Ear Canal Microphones”. In: *Acta Acustica united with Acustica* 101.3, pp. 552–566. doi: [10.3813/AAA.918852](https://doi.org/10.3813/AAA.918852).
- Sankowsky-Rothe, T. (2022). *Parametric model of young infants’ eardrum and ear canal acoustic input impedances*. Code. Version v1.0. url: https://github.com/tobiassankowsky/acoustic_impedance_infant_ear.
- Sankowsky-Rothe, T., Becker, A., Plotz, K., Schönfeld, R., Radeloff, A., Van de Par, S., and Blau, M. (2019). “Acoustic input impedance of infants with normal and pathological middle ear”. In: *Proceedings of the ICA 2019 and EAA Euroregio. 23rd International Congress on Acoustics, integrating 4th EAA Euroregio 2019* (Sept. 2019). Aachen, Germany. isbn: 978-3-939296-15-7.
- Sankowsky-Rothe, T., Blau, M., Rasumow, E., Mojallal, H., Teschner, M., and Thiele, C. (2011). “Prediction of the sound pressure at the ear drum in occluded human ears”. In: *Acta Acustica united with Acustica* 97.4, pp. 656–668. doi: [10.3813/AAA.918445](https://doi.org/10.3813/AAA.918445).
- Sankowsky-Rothe, T., van de Par, S., and Blau, M. (2022b). “Parametric model of young infants’ eardrum and ear canal impedances supporting immittance measurement results. Part II: Predic-

- tion of eardrum and ear canal impedances for frequent pathological middle ear conditions". In: *submitted to: Acta Acustica*.
- Shahnaz, N., Cai, A., and Qi, L. (2014). "Understanding the Developmental Course of the Acoustic Properties of the Human Outer and Middle Ear Over the First 6 Months of Life by Using a Longitudinal Analysis of Power Reflectance at Ambient Pressure". In: *Journal of the American Academy of Audiology* 25.5, pp. 495–511. doi: [10.3766/jaaa.25.5.8](https://doi.org/10.3766/jaaa.25.5.8).
- Shaw, E. A. G. and Teranishi, R. (1968). "Sound Pressure Generated in an External-Ear Replica and Real Human Ears by a Nearby Point Source". In: *The Journal of the Acoustical Society of America* 44.1, pp. 240–249. doi: [10.1121/1.1911059](https://doi.org/10.1121/1.1911059).
- Shera, C. A. and Zweig, G. (1992). "Middle-ear phenomenology: The view from the three windows". In: *The Journal of the Acoustical Society of America* 92.3, pp. 1356–1370. doi: [10.1121/1.403929](https://doi.org/10.1121/1.403929).
- Stirnemann, A. (2011). "Ein Mittelohrmodell basierend auf der Außenohr Transferimpedanz". In: *Fortschritte der Akustik DAGA 2011*. DEGA.
- Stirnemann, A., Graf, H., and Meier, H. (2003). "Akustische Impedanzmessungen in der Hörerätetechnik". In: *Fortschritte der Akustik DAGA 2003*. DEGA. Berlin, pp. 496–497.
- Werner, L. A., Levi, E. C., and Keefe, D. H. (2010). "Ear-Canal Wideband Acoustic Transfer Functions of Adults and Two- to Nine-Month-Old Infants". In: *Ear and Hearing* 31.5, pp. 587–598. doi: [10.1097/aud.0b013e3181e0381d](https://doi.org/10.1097/aud.0b013e3181e0381d).
- Zwislocki, J. (1962). "Analysis of the middle-ear function. Part I: Input impedance". In: *The Journal of the Acoustical Society of America* 34.8, pp. 1514–1523. doi: [10.1121/1.1918382](https://doi.org/10.1121/1.1918382).

Chapter 4

Parametric model of young infants' eardrum and ear canal impedances supporting immittance measurement results. Part II: Prediction of eardrum and ear canal impedances for frequent pathological middle ear conditions

This Chapter was submitted with identical content to:

Acta Acustica,

Sankowsky-Rothe, T., van de Par, S. and Blau, M. (2022). "Parametric model of young infants' eardrum and ear canal impedances supporting immittance measurement results. Part II: Prediction of eardrum and ear canal impedances for frequent pathological middle ear conditions"

This Chapter was since published after revision in:

Acta Acustica (2023), vol. 7, pp. 21, <https://doi.org/10.1051/aacus/2023017>

Authors' contributions:

- Tobias Sankowsky-Rothe formulated the research question, developed the model, interpreted the experimental and modeling data, and wrote the final paper,
- Steven van de Par participated in interpretation of the experimental and modeling data, and participated in writing the final paper.
- Matthias Blau formulated the research questions, participated in the development of the model, participated in interpretation of the experimental and modeling data, and participated in writing the final paper.

Hereby I confirm that Tobias Sankowsky-Rothe contributed to the study as stated above.

.....
Date

.....
Steven van de Par (supervisor)

Abstract

In order to gain a better understanding of wideband acoustic immittance (WAI) measurements, in this second part of a two-part paper, the parametric electro-acoustic model of the ear canal and the middle ear of young infants proposed in the first part is extended. The extension allows predictions of the influence of the pathological middle ear conditions middle ear effusion and negative static air pressure difference between the middle ear and the ear canal. Comparisons of the acoustic input impedance of the ear predicted by the model with real ear measurements in young infants' ears with middle ear effusion show that the effects due to the pathology can be predicted well. For the negative static air pressure, a modeling approach was proposed but could not be confirmed yet, due to a lack of available measurement data. Furthermore, comparisons between different middle ear states (healthy, middle ear effusion and static air pressure difference) predicted by the model showed characteristic differences in all relevant WAI measures. However, it is also shown that WAI measures requiring an estimate of the cross-sectional area at the measurement position, i.e., absorbance and reflectance, are highly sensitive to this estimate.

4.1 Introduction

The aim of this work is to investigate the use of the model presented in Sankowsky-Rothe et al. (2022a), which predicts wideband acoustic immittance (WAI) measured within the ear canal, for detecting certain pathological middle ear conditions in young infants. WAI comprises measures like the acoustic impedance, the acoustic admittance, as well as measures derived from these quantities like the reflectance or the absorbance. WAI has been identified to be a promising tool in middle ear diagnostics (Feeney et al., 2013). In this context it is important to note that several properties of the ear canal and the middle differ between young infants on the one hand and older children and adults on the other hand, resulting in significantly different WAI results (Sankowsky-Rothe et al., 2022a).

In the accompanying paper Sankowsky-Rothe et al. (2022a), a parametric electro-acoustic model of the ear canal and the middle ear of healthy young infants was proposed. The model parameters represent physiological properties wherever possible. The model was used to predict the ear canal acoustic impedance Z_{ec} , the quantity which is measured in a WAI-measurement, and the acoustic input impedance at the eardrum Z_D , the interesting quantity in terms of middle ear diagnostics which can, however, not directly be measured. Three main findings were identified in the study.

- The soft and flexible ear canal walls in young infants' ears affect Z_{ec} up to about 1.5 kHz with no significant effect for higher frequencies.
- At medium frequencies around 1.8 kHz, Z_{ec} is dominated by the input impedance at the eardrum Z_D . Thus, the largest effects of pathological middle ear conditions on Z_{ec} is expected at medium frequencies.
- At high frequencies, the model prediction of Z_{ec} has a much smaller magnitude compared to Z_D indicating that Z_{ec} is dominated by ear canal properties and therefore, it might be difficult to detect different middle ear conditions at these frequencies. However, the predictions must be taken with caution at high frequencies because many measurements on real ears showed higher Z_{ec} magnitudes than the predictions. The relatively smaller difference between the

measured Z_{ec} magnitudes and Z_D could mean that in some cases middle ear conditions could still be detected.

The objectives of the present paper are a) the extension of the model in order to predict the influence of different pathological middle ear conditions on the acoustic input impedances of the ear canal and the eardrum, and b) the investigation of implications for WAI-measurements. Two pathological middle ear conditions have been chosen for the model extension:

- Firstly, middle ear effusion, resulting from otitis media, is the most frequent pathological middle ear condition in young infants with prevalence rates of 74% found in Marchant et al. (1984) for children in the first 6 months of life and 48.8% found in Paradise et al. (1997) for children aged between 2 and 6 months.
- Secondly, a negative static air pressure difference between middle ear and ear canal will be considered. It is often one of the earlier symptoms of otitis media, see e.g. Dirckx et al. (2013) and Hoth (2011).

The model predictions will be compared with ear canal acoustic impedances measured in infant ears published in Sankowsky-Rothe et al. (2019). The aspects of the measurement procedure relevant for this study will be described here in detail. As described in Sankowsky-Rothe et al. (2022a), the measurement method is based on Stirnemann et al. (2003), extended by consideration of discontinuity and end corrections in Blau et al. (2010). The method including the calibration procedure is described in detail in Blau et al. (2010). The measurements were performed using a custom-made impedance probe to measure the ear canal impedance on infant ears. The probe was designed to avoid over-pressure in the ear canal caused by inserting it into the ear canal at the cost of a decreased signal-to-noise ratio (SNR) at frequencies below about 1 kHz, further details can be found in Sankowsky-Rothe et al. (2019). This was realized by a pressure equalizing duct with an inner diameter of 0.6 mm.

The subjects who participated in the study were aged between 2 weeks and 5 months. It should be noted that the infant ear undergoes developmental changes within the age range of the participants, i.e. an age-related effect is contained in the measurement data. The middle ear status of the participants was assessed by ENT-doctors specialized in pediatric audiology to be either normal, pathological or unclear at the time of testing. The assessment was based on the results of 1 kHz tympanometry, OAE- and/or AABR-screening, and ear-microscopy, see again Sankowsky-Rothe et al. (2019) for details. While in Sankowsky-Rothe et al. (2022a) the measurement data of the ears that were assessed to have a normal middle ear status were used, in this paper, we concentrate on the ears that were assessed to have a pathological middle ear status. This comprised 13 ears from 9 infants.

Models predicting the effects of fluid in the middle ear have been proposed in Gan and Wang (2007) and in Wang et al. (2016). In contrast to the present paper, both models differ in the modeling approach and in the targeted age. In Gan and Wang (2007), a finite-element model of an adult ear was presented and in Wang et al. (2016) a finite-element model of the ear of an infant aged 4 years was presented. It is known from literature, that the acoustic input impedance of the ear significantly differs between those ages and the age range from 0.5 to 5 months, which is addressed here, see e.g. Keefe et al. (1993).

The paper is organized as follows. In sections 4.2 and 4.3, the model extensions and comparisons of predicted and measured Z_{ec} are given for the conditions of fluid in the middle ear and negative

pressure difference between the ear canal and the middle ear, respectively. In section 4.4, model predictions for normal and pathological middle ear conditions are compared for various WAI-measures. In section 5.6, implications for WAI-measurements are given. A MATLAB-implementation of the model can be found in Sankowsky-Rothe (2022).

4.2 Predicting the effect of fluid in the middle ear

Fluid in the middle ear may occur as remaining amniotic fluid after birth or as middle ear effusion. In both cases, a substantial part of the middle ear cavities is filled with liquid, covering partly the eardrum.

The representation in the model should comprise a reduced volume of the tympanic cavity, resulting in a smaller value of the acoustic compliance of the tympanic cavity N_{tcav} , and a reduced area of the eardrum that is vibrating, resulting in modified values of the effective eardrum area A_0 , the eardrum acoustic shunt impedance Z_{ac} , and the mechanical eardrum parameters, namely the mechanical mass and resistance of the free vibrating portion of the eardrum m_{free} and w_{free} .

A first approach to implement the effect of fluid in the middle ear is proposed as follows: The effective eardrum area is decreased using a factor $x_A < 1$, such that

$$A_0|_{\text{fluid}} = x_A A_0 . \quad (4.1)$$

According to Sankowsky-Rothe et al. (2022a, equation 21)

$$Z_{\text{ac}} = W_{\text{ac}} + j\omega M_{\text{ac}} + (j\omega N_{\text{ac}})^{-1} , \quad (4.2)$$

the eardrum acoustic shunt impedance Z_{ac} is determined by the acoustic compliance N_{ac} , the acoustic mass M_{ac} and the acoustic resistance W_{ac} . For simplicity it is assumed that the eardrum geometry remains circular when the area is decreased, i.e., only the radius of the vibrating membrane is reduced by $\sqrt{x_A}$. From Sankowsky-Rothe et al. (2022a, equation 22),

$$N_{\text{ac}} = \frac{\pi}{8} \frac{a_{\text{ed}}^4}{T_{0,\text{ed}} h_{\text{ed}}} , \quad (4.3)$$

with a_{ed} the radius of the eardrum, $T_{0,\text{ed}}$ the eardrum tension and h_{ed} the thickness of the eardrum, one can infer that the acoustic compliance should change with x_A^2 , i.e. the acoustic compliance decreases if the eardrum area decreases. The acoustic mass should then change with $1/x_A$ according to Sankowsky-Rothe et al. (2022a, equation 23),

$$M_{\text{ac}} = \frac{4}{3} \frac{\rho_{\text{ed}} h_{\text{ed}}}{\pi a_{\text{ed}}^2} , \quad (4.4)$$

with ρ_{ed} the membrane mass density, i.e. the acoustic mass increases if the eardrum area decreases. Because a simple relation between the acoustical resistance and the area of the eardrum is not known, in a first approach W_{ac} is kept constant. The mechanical mass of the free vibrating part of the eardrum m_{free} is changed by multiplying it with x_A assuming that the free vibrating portion of the eardrum decreases with x_A . A relation between the eardrum area and the mechanical resistance w_{free} is not known, therefore the value is kept constant.

The volume change of the tympanic cavity can also be linked to the parameter x_A , by letting

$$V_{\text{tcav}}|_{\text{fluid}} = V_{\text{tcav}} \cdot x_A, \quad (4.5)$$

effectively assuming that the volume of the tympanic cavity results from protruding the reduced area of the vibrating eardrum.

The impact of different values of x_A on the acoustic input impedance at the eardrum Z_D and the eardrum acoustic shunt impedance Z_{ac} is depicted on the left side of Figure 4.1. It can be seen that the smaller the eardrum area gets, the more Z_D is dominated by Z_{ac} . Furthermore, a smaller eardrum area shifts the magnitude minimum and the phase change to higher frequencies. At frequencies smaller and larger than the minimum, the magnitude increases with decreasing eardrum area.

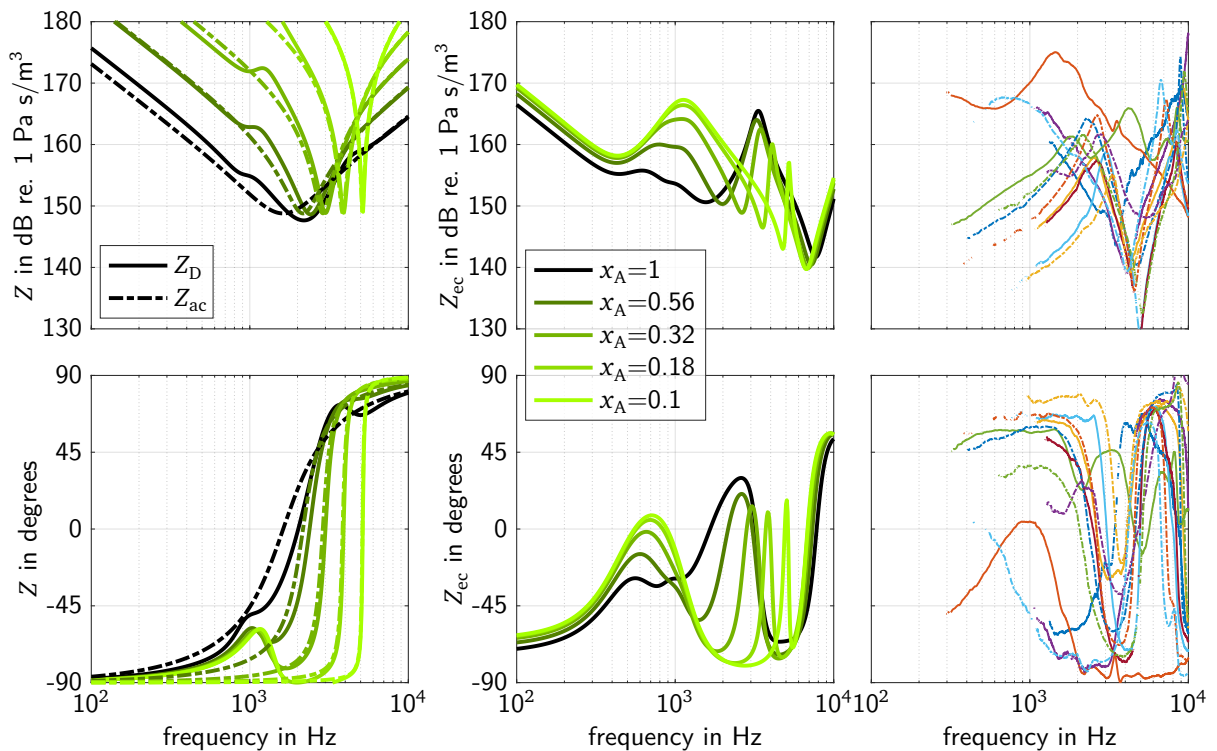


Figure 4.1: First approach to model the effects of fluid in the middle ear. Left: Acoustic input impedance at the eardrum Z_D and eardrum acoustic shunt impedance Z_{ac} for different factors of eardrum area. Middle: Ear canal impedance for different factors of eardrum area resulting from the model using an ear canal radius of 1.7 mm and an ear canal length of 14 mm. Right: Ear canal impedances measured in infants' ears with middle ear effusion from Sankowsky-Rothe et al. (2019).

In the middle column of Figure 4.1, the ear canal impedance Z_{ec} is depicted for different values of x_A . The ear canal is modeled using a constant ear canal radius of 1.7 mm and an ear canal length of 14 mm. In the right column of Figure 4.1, measurement results from Sankowsky-Rothe et al. (2019) of ear canal impedances measured in infants' ears with diagnosed middle ear effusion are depicted. The measurements suffer from a bad signal-to-noise ratio (SNR) at low frequencies, therefore, only those values are depicted in which the coherence between the signal applied to the probe speaker and the signal sensed by the probe microphone exceeded 0.5. Another effect that is present in the majority of the measurements is acoustic leakage resulting in an impedance magnitude

increasing with increasing frequency and positive phase values up to about 2 kHz. In the modeling, a tightly sealed ear canal is assumed, i.e. without leakage, therefore, in the following comparisons between measurements and predictions concentrate on higher frequencies, while differences up to about 2 kHz are ignored. The predicted shift of the first magnitude minimum below 2 kHz to higher frequencies is well reflected in the measurements. Above this first minimum, there is a mismatch between model and measurements. In the model output, the second minimum, which is mainly determined by the ear canal geometry, is only weakly affected by the variation of x_A . In the measurements, however, no second minimum can be seen up to 10 kHz. The only magnitude minimum in the measurements is broader than the first minimum of the model. It is located at lower frequencies than the second minimum of the model.

Based on these observations, the previously described approach of modeling the effects of fluid in the middle ear is amended. Firstly, in order to obtain a greater shift of the magnitude minimum of Z_{ac} , the acoustic mass M_{ac} is not changed with changing x_A . Which can be interpreted as the acoustically effective part of the vibrating mechanical mass of the eardrum being proportional to x_A^2 instead of x_A , which was expected in the first place. Secondly, the acoustic resistance W_{ac} is decreased with decreasing x_A , using

$$W_{ac|fluid} = x_A W_{ac} . \quad (4.6)$$

The result of this final approach used to model the effects of fluid in the middle ear can be

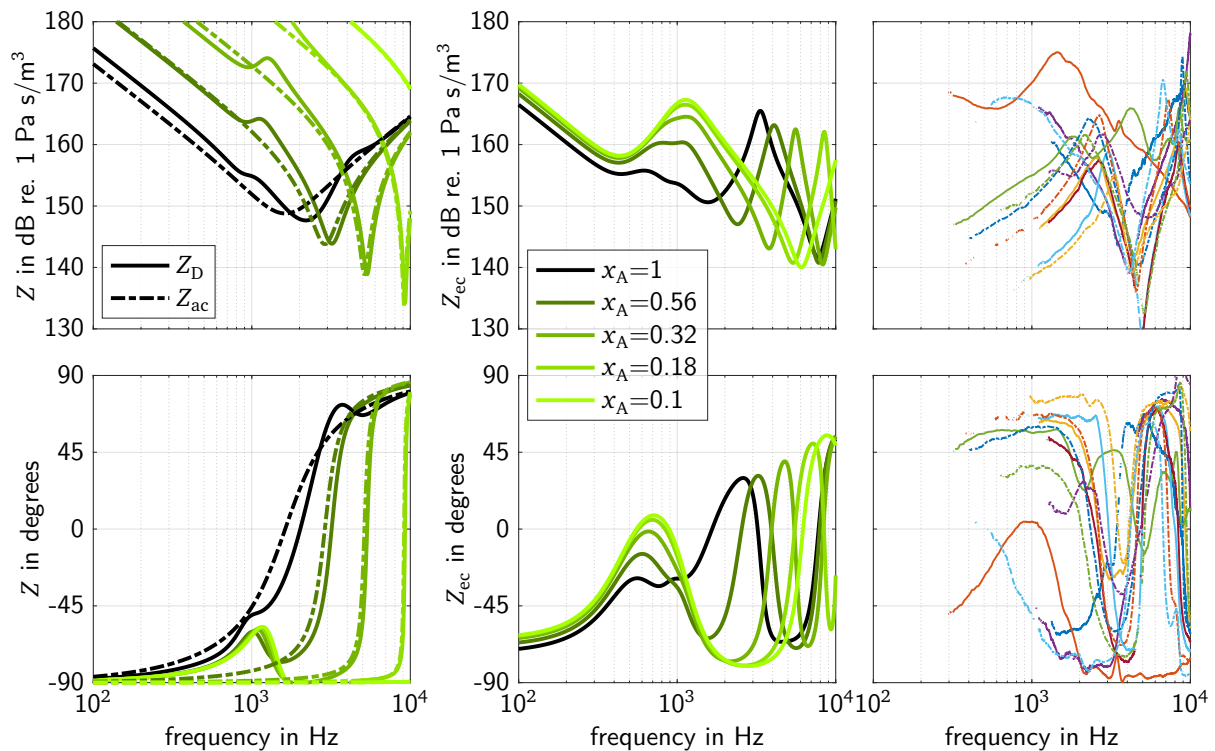


Figure 4.2: Final approach to model the effects of fluid in the middle ear. Left: Acoustic input impedance at the eardrum Z_D and ear drum acoustic shunt impedance Z_{ac} for different factors of eardrum area. Middle: Ear canal impedance for different factors of eardrum area resulting from the model using an ear canal radius of 1.7 mm and an ear canal length of 14 mm. Right: Ear canal impedances measured in infants' ears with middle ear effusion from Sankowsky-Rothe et al. (2019).

seen in Figure 4.2. Again, on the left side the acoustic input impedance at the eardrum Z_D and the eardrum acoustic shunt impedance Z_{ac} are depicted for different eardrum area factors x_A . The differences compared to the first approach are a shift of the magnitude minimum to higher frequencies and a smaller value of the impedance at the minimum, both for $x_A < 1$. In the middle column, the ear canal impedance Z_{ec} of the model for different factors of x_A can be seen. For a factor $x_A = 0.18$ it can be seen that the course of the impedance is very similar to that of the measurements at high frequencies, which are depicted in the right column of Figure 4.2. At about 5 kHz, there is a magnitude minimum and a phase increasing with frequency with a slope much like the measurements. A further minimum appears at a frequency slightly smaller than 10 kHz which is a little less than in the measurements. If the eardrum area is further decreased, both minima are shifted to higher frequencies. It can be concluded that the distance between the two minima at high frequencies might be a little underestimated, but an eardrum area decreased by a factor of about 1/5 results in a good estimation of the effects of fluid in the middle ear. This can be seen in Figure 4.3 in which the prediction of Z_{ec} using a factor $x_A = 0.2$ is depicted together with all measured impedances of infant's ears with middle ear effusion from Sankowsky-Rothe et al. (2019).

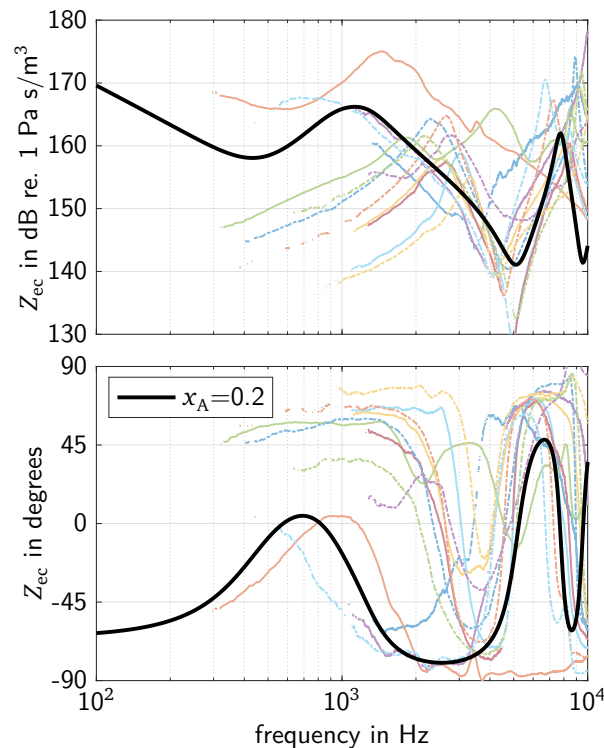


Figure 4.3: Final approach to model the effects of fluid in the middle ear. Ear canal impedance for a factor of $x_A = 0.2$ eardrum area resulting from the model using an ear canal radius of 1.7 mm and an ear canal length of 14 mm together with all ear canal impedance measurements on infants' ears with middle ear effusion from Sankowsky-Rothe et al. (2019).

4.3 Predicting the effect of negative pressure difference between the middle ear cavities and the ear canal

Due to a dysfunction of the eustachian tube and the gas resorption of the mucosa, the static pressure of air in the middle ear cavities $p_{0, ME}$ can be decreased. Compared to the ambient static

pressure of air p_0 , the pressure difference $\Delta p_0 = p_{0, ME} - p_0$ gets negative. Consequences of the negative Δp_0 are a retracted eardrum with an increased tension of the membrane, a reduced density of air in the middle ear cavities, and a slightly decreased volume of the tympanic cavity. A relevant range of Δp_0 can be obtained from the measurement range in tympanometry, which reaches down to -400 daPa (-4 kPa).

In the model, the tension of the eardrum is represented in the acoustic compliance N_{ac} which is part of the eardrum acoustic shunt impedance Z_{ac} . As described in part I Sankowsky-Rothe et al. (2022a, section 2.2.3), Z_{ac} is modeled as a stretched circular membrane (Sankowsky-Rothe et al., 2022a). According to Lenk (1977, p. 68), the displacement ξ_z orthogonal to the membrane-plane due to a pressure difference Δp_0 at a normalized radial distance from the center r/a is given by

$$\xi_z\left(\frac{r}{a}\right) = \Delta p_0 \frac{a^2}{4T_0 h} \left(1 - \left(\frac{r}{a}\right)^2\right), \quad (4.7)$$

with T_0 the tension of the non-displaced membrane and h the membrane thickness. Therefore, the displacement at the center of the membrane is given by

$$\xi_z(0) = \Delta p_0 \frac{a^2}{4T_0 h}. \quad (4.8)$$

The membrane takes the shape of an elliptical paraboloid. The area of the membrane with the displacement $\xi_z(0)$ is given by

$$A' = \pi \frac{a}{6\xi_z^2(0)} \left((a^2 + 4\xi_z^2(0))^{3/2} - a^3 \right), \quad (4.9)$$

corresponding to an area of a circle with a radius of

$$a' = \sqrt{\frac{a}{6\xi_z^2(0)} \left((a^2 + 4\xi_z^2(0))^{3/2} - a^3 \right)}. \quad (4.10)$$

The in-membrane strain S for a given displacement $\xi_z(0)$ is given by

$$S = \frac{a'}{a} - 1, \quad (4.11)$$

resulting, by using equations 4.8 and 4.10, in

$$S(\Delta p_0) = \sqrt{\frac{\left(a^2 + 4 \left(\Delta p_0 \frac{a^2}{4T_0 h} \right)^2 \right)^{3/2} - a^3}{6a \left(\Delta p_0 \frac{a^2}{4T_0 h} \right)^2}} - 1. \quad (4.12)$$

With the relation between strain and tension of the membrane given in Lenk (1977)

$$T = \frac{E}{(1-\nu)} S, \quad (4.13)$$

with Young's modulus E and Poisson's ratio ν , the membrane tension T'_0 for a static Δp_0 can be

calculated using

$$T'_0 = T_0 + \frac{E}{(1-\nu)} \left(\sqrt{\frac{\left(a^2 + 4\left(\Delta p_0 \frac{a^2}{4T_0 h}\right)^2\right)^{3/2} - a^3}{6a\left(\Delta p_0 \frac{a^2}{4T_0 h}\right)^2}} - 1 \right). \quad (4.14)$$

The acoustic compliance of the displaced membrane is then given by

$$N'_{ac} = \frac{\pi}{8} \frac{a_{ed}^4}{T'_{0,ed} h'_{ed}}, \quad (4.15)$$

with the thickness h'_{ed} of the stretched eardrum. If an incompressible isotropic medium of the membrane ($\nu = 0.5$, see e.g. Silva (2006)) is assumed, the volume of the membrane remains unchanged. With eq. 4.11, the thickness of the stretched eardrum is given by

$$h'_{ed} = \frac{h_{ed}}{(1+S)^2}. \quad (4.16)$$

As mentioned above, the negative pressure difference affects the middle ear cavities by decreasing the density of air in the middle ear, and by decreasing the volume of the tympanic cavity. The decrease in density of air in the middle ear cavities increases the compliance of the tympanic cavity N_{tcav} and the compliance of the antrum N_{ant} . The density is given by

$$\rho_{me} = \rho_{air} \frac{(p_0 + \Delta p_0)}{p_0}. \quad (4.17)$$

The volume occupied by the statically displaced membrane, i.e. the volume decrease of the tympanic cavity, is given by

$$\Delta V_{tcav} = \frac{\pi}{2} a_{ed}^2 \xi_z(0). \quad (4.18)$$

Both effects are very small and for the compliance of the tympanic cavity, given by $N_{tcav} = V_{tcav}/(\rho_{me} c^2)$, with the speed of sound c , the decreased density and the decreased volume cancel each other out.

The only parameter value needed to model a negative pressure difference between the middle ear cavities and the ear canal, is the Young's modulus E of the membrane, see eq. 4.14. Note that Poisson's ratio ν was already chosen to be 0.5. Unfortunately, there is no easy way to determine E . In the literature, values of Young's modulus of real tympanic membranes can be found, at least for adult ears. However, those values can't be used directly for the modeling approach of a stretched circular membrane because of the different membrane shapes and in-plane tensions. This means that a value of E could only be determined indirectly, e.g. from impedance measurements at different strain levels. It would, however, be necessary that the effect of membrane stress could be separated from other effects like e.g. those caused by compliant ear canal walls in tympanometry. To the best of our knowledge, no studies exist in which the effect of negative pressure difference in young infants' middle ears on immittance measurements is investigated. Therefore, we had to estimate a reasonable value of E . Assuming that E has a substantial effect on Z_D for Δp_0 in the range from 0 to -2.5 kPa, we chose a value of $E = 100$ MPa. On the left side of Figure 4.4, both, the eardrum acoustic shunt impedance Z_{ac} , and the acoustic input impedance at the eardrum Z_D are depicted for different Δp_0 . As can be seen, the minimum in the magnitude of Z_{ac} shifts to

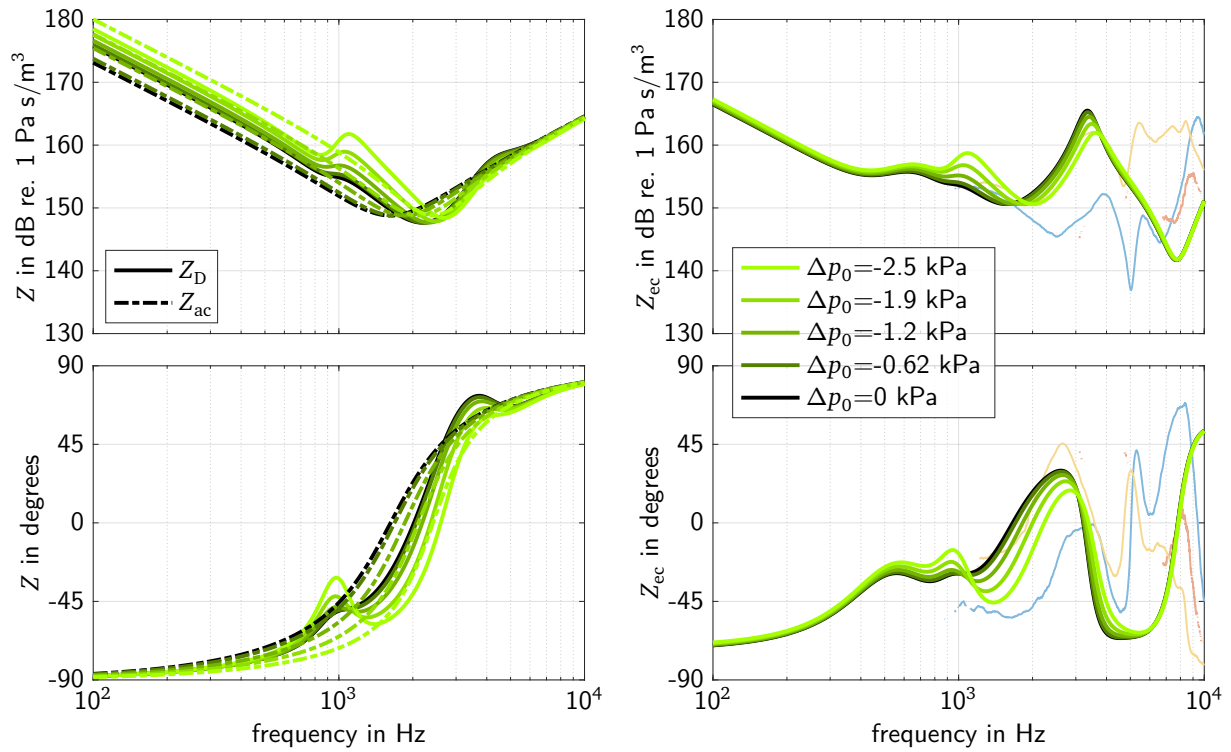


Figure 4.4: Modeling of the effect of negative pressure difference between ear canal and middle ear using a Young’s modulus of $E = 100$ MPa. Left: Acoustic input impedance at the eardrum Z_D and eardrum acoustic shunt impedance Z_{ac} for different pressure differences Δp_0 in kPa between ear canal and middle ear. Right: Ear canal impedance for different pressure differences Δp_0 in kPa resulting from the model using an ear canal radius of 1.7 mm and an ear canal length of 14 mm, together with ear canal impedances from Sankowsky-Rothe et al. (2019) measured in infants’ ears where the tympanometric peak pressure was smaller -1 kPa (-100 daPa).

higher frequencies when Δp_0 is decreased from 0 to negative values. This can also be observed for the global minimum in Z_D . If the minimum in Z_{ac} is shifted to higher frequencies, a new magnitude minimum in Z_D at about 800 Hz emerges followed by a maximum at about 1.2 kHz. This minimum is caused by the mechanical middle ear components, in particular by the ossicles. The ear canal impedance Z_{ec} of the model is depicted on the right side of Figure 4.4. Additionally, measurements from Sankowsky-Rothe et al. (2019) on infants’ ears where the tympanometric peak pressure was smaller than -1 kPa (-100 daPa) are depicted, unfortunately, there were only two ears in which this was clearly the case. As can be seen in the magnitude, a local maximum appears at about 1.1 kHz if Δp_0 gets negative. This can also be observed in the measurements. In the phase of Z_{ec} , the increase with frequency between 1.2 kHz and 2.5 kHz is shifted to higher frequencies with a steeper slope for negative Δp_0 . Regarding the modeling approach, an assessment of the choice of parameters is not possible at this time due to a lack of available measurement data, therefore, it can only be seen as a first proposal. However, the resulting effects show at least some similarities with the few measurements.

In summary, an approach to model the effect of negative pressure difference between the middle ear cavities and the ear canal was proposed. However, there are several simplifications in the modeling approach. First of all, using a stretched circular membrane is obviously a significant simplification, which among other things has the consequence that a physiologically correct value of Young’s

modulus can't be used. Furthermore, the assumption of the eardrum behaving linear-elastically may not fully hold in practice, even in the range of typically observed tympanometric pressures. Despite these assumptions some characteristics observed in the few available measurements are captured by the model. More data involving negative tympanic pressures would be required for a more in-depth validation.

4.4 Comparison of immittance measures for normal and pathological middle-ear conditions

There is an on-going discussion of the suitability of different immittance measures for screening or diagnostic purposes of young infants' middle ears. All these measures are derived from the acoustic impedance in the ear canal (Z_{ec}) or its reciprocal, the acoustic admittance. Most investigations concentrate either on the energy reflectance (also called power reflectance) which is given by $|R|^2 = |(Z_{ec} - Z_{tw}) / (Z_{ec} + Z_{tw})|^2$, with the tube wave impedance Z_{tw} of the ear canal cross section at the measurement position, or on the energy absorbance given by $1 - |R|^2$. Sometimes, the phase or group delay of the pressure reflectance R is also discussed (Hunter et al., 2016; Keefe et al., 2015).

The model output for different immittance measures is depicted in Figure 4.5 for three different states of the middle ear, namely normal, fluid in the middle ear ($x_A = 0.2$), and a negative pressure difference of $\Delta p = -2500$ Pa between the middle ear cavities and the ear canal. In the left column, the acoustic input impedance at the eardrum (Z_D) is depicted. Z_D directly reflects the state of the middle ear and hence is the desired measure, however, it is not directly available. In the second column of Figure 4.5, the acoustic input impedance (Z_{ec}) is depicted as it would be measured in the ear canal. The complex-valued pressure reflectance R is depicted in the third column with its magnitude (top) and its group delay (bottom). Finally the energy reflectance is depicted in the top and the energy absorbance in the bottom panel of the last column. All of the selected immittance measures show characteristic differences between the three states.

The most important changes compared to the normal middle ear condition in the case of fluid in the middle ear are a massively increased magnitude of Z_D up to a frequency of 6 kHz and a large difference in the phase of Z_D between 1.5 kHz and 8 kHz. The magnitude of Z_{ec} differs largely between 500 Hz and 2 kHz where a local maximum appears and at high frequencies due to a shift of the minimum to lower frequencies. The phase of Z_{ec} has a significantly different slope at frequencies higher than 500 Hz. The magnitude of the reflectance is much larger at frequencies between 500 Hz and 5 kHz and the group delay has significantly smaller values between about 1 kHz and 3 kHz.

In the case of a negative pressure difference between middle ear and ear canal, the magnitude of Z_D is significantly larger between 900 Hz and 2 kHz. The phase of Z_D has a local maximum at 900 Hz and the phase change in mid-frequency range is shifted to higher frequencies. The magnitude of Z_{ec} has a conspicuous maximum at 1.1 kHz and the phase of Z_{ec} has smaller values between about 1.1 kHz and 3 kHz. The magnitude of the reflectance has a peak at 1.2 kHz and a minimum at 3 kHz. The group delay does not show the maximum at 1.7 kHz.

In conclusion, all of these quantities should be included in the search for an objective classification of middle-ear disorders in humans. This is particularly true for phase (or alternatively, group delay) quantities, which have mostly been ignored so far.

Measurement-based data of the mean energy absorbance for age groups between 1 and 3 months

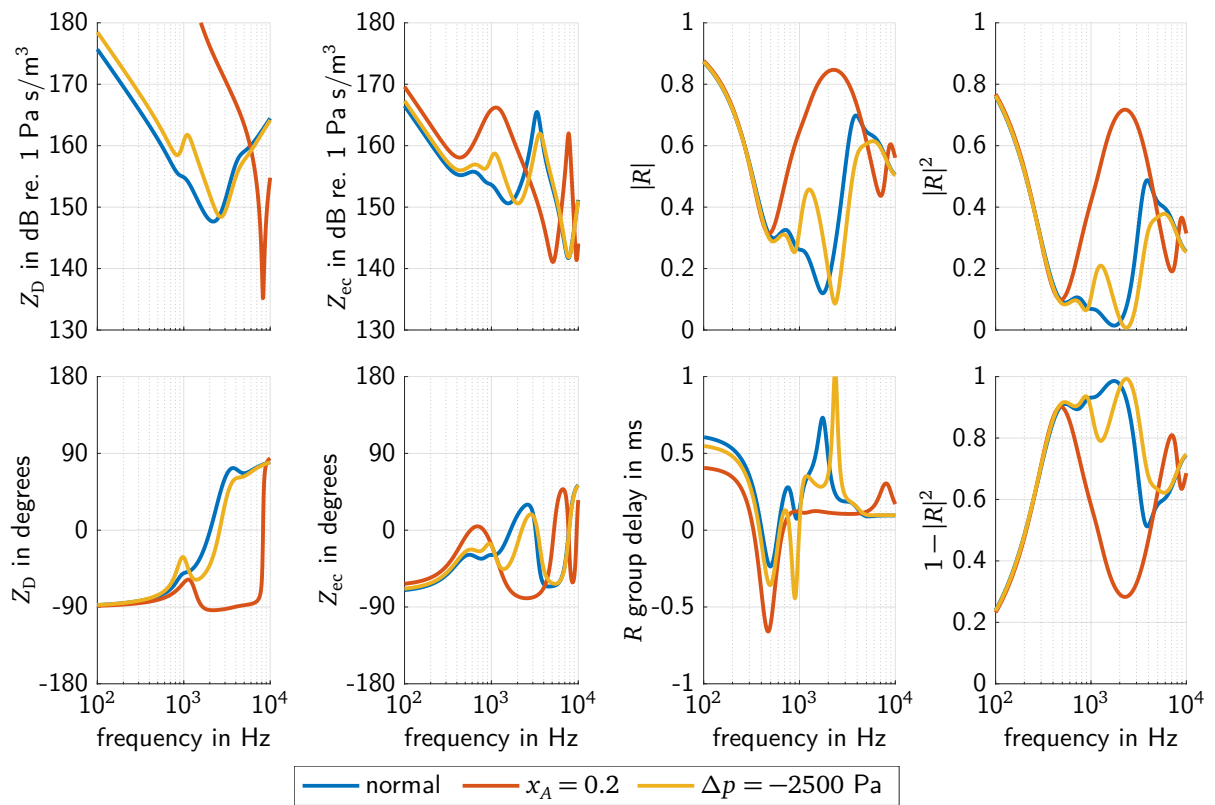


Figure 4.5: Comparison of predicted immittance measures for ears with normal middle ear, fluid in the middle ($x_A = 0.2$), and negative pressure difference between middle ear and ear canal ($\Delta p = -2500$ Pa). Left column: acoustic input impedance at the eardrum; second column: input impedance of the ear; third column: magnitude and group delay of the reflectance; right column top: energy reflectance; right column bottom: energy absorbance.

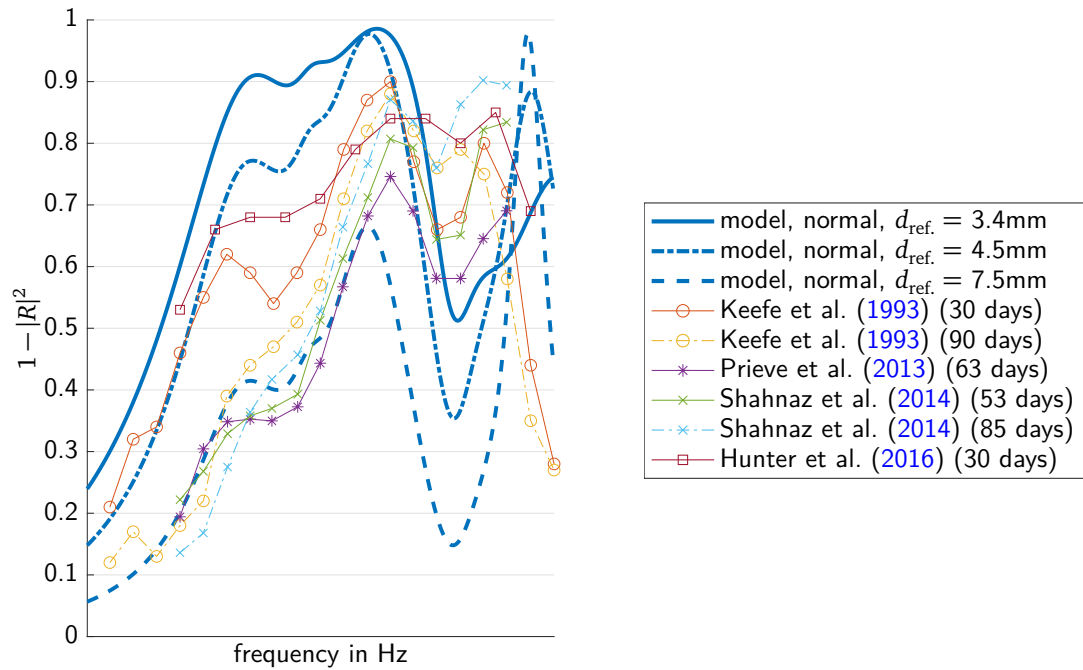


Figure 4.6: Energy absorbance predicted by the model using different areas to compute Z_{tw} , together with measurement based data from Hunter et al. (2016), Keefe et al. (1993), Prieve et al. (2013), and Shahnaz et al. (2014) for different age groups with the mean or median age in days given in parentheses.

have been published in Hunter et al. (2016), Keefe et al. (1993), Prieve et al. (2013), and Shahnaz et al. (2014). In Figure 4.6 these data are depicted with thin lines together with the energy absorbance predicted by the model (thick lines) using three different areas to compute the tube wave impedance: 1) the correct ear canal cross section with a diameter of 3.4 mm, 2) an area with a diameter of 4.5 mm, and 3) an area with a diameter of 7.5 mm. The selection of diameters is based on values used in the commercially available devices for WAI-measurements. Some agreements can be found in all predictions and measurement-based data: At low frequencies absorbance increases with frequency, and a maximum value at about 2 kHz is followed by a notch between 3 and 4 kHz. However, large differences can be seen in both, predictions and measurement-based data. As can be seen in the predictions, the reference area used for the tube wave impedance largely affects the value of the energy absorbance in the whole frequency range between 100 Hz and 10 kHz. It should be noted that these differences in energy absorbance are only the result for one single idealized (cylindrical) ear canal geometry. They do not specify something like a normative range since other ear canal geometries will result in other differences caused by the selected reference area. In Hunter et al. (2016) and Keefe et al. (1993) an acoustic estimate of the ear canal area at the probe tip was used, and in Prieve et al. (2013) and Shahnaz et al. (2014) a reference area with a diameter of 7.5 mm was used. It can be seen that the measurement-based data differ and that effects of age (e.g. the effect of compliant ear canal walls) can possibly not be distinguished from effects due to a mismatch in reference area. The model predictions suggest that, if the energy absorbance is used as the immittance measure of choice, it might be more valuable to look at the variation with frequency in a range from 1 to 6 kHz rather than to look at absolute values.

4.5 Discussion

The parametric electro-acoustic model of young infants' eardrum and ear canal impedances proposed in Sankowsky-Rothe et al. (2022a) has been extended to account for selected pathological middle ear conditions. Firstly, the condition of fluid in the middle ear, which is the most frequent pathological middle ear condition in young infants, has been considered in the model. It has been realized by a single factor x_A decreasing the effective eardrum area and the volume of the tympanic cavity. Secondly, the condition of negative pressure difference Δp_0 between the middle ear cavities and the ear canal has been implemented. Comparisons between model predictions for a normal middle ear status and for these pathological middle ear conditions showed characteristic differences for all WAI-measures, including quantities that have mostly been ignored, i.e., phase quantities. Furthermore, it was shown that different reference diameters used to compute the acoustic absorbance lead to large differences for the same ear.

4.5.1 Implications for WAI-measurements

For those immittance measures which can easily be determined by acoustic measurements in the ear canal (Z_{ec} and R), the effects of the different pathological middle ear conditions showed large differences at frequencies between 600 Hz and 6 kHz. In part I Sankowsky-Rothe et al. (2022a) it was found that the ear canal properties (geometry and compliant walls) dominate Z_{ec} at frequencies below about 1.5 kHz and above about 4 kHz, therefore, the frequency range from 1.5 kHz to 4 kHz should be suited to detect pathological middle ear conditions in young infants' ears. This is in agreement with results of studies in which WAI was measured on young infants' ears classified to have either a normal or a pathological middle ear status (Blankenship et al., 2018; Prieve et al., 2013; Sankowsky-Rothe et al., 2019). In Prieve et al. (2013), the energy reflectance ($|R|^2$) measured on infants aged between 0.7 and 5.9 months (median 2.1 months) was compared. It was found that a discrimination between normal hearing and conductive hearing loss was possible at frequencies around 1.6 kHz. In Blankenship et al. (2018), the absorbance ($1 - |R|^2$) was measured on infants aged from birth up to 4 months (mean 1.3 months). A mixed-model ANOVA showed significant different mean absorbance values between the normal hearing group and combined groups of ears having a conductive or a mixed hearing loss at frequencies from 1 to 8 kHz. In Sankowsky-Rothe et al. (2019), the ear canal impedance (Z_{ec}) was measured on infants aged between 0.5 and 4.8 months (mean 1.8 months). Characteristic differences of Z_{ec} between normal ears and ears with middle ear effusion were found in the frequency range from 1 to 5 kHz. All these studies show that discriminating between normal and pathological middle ears of young infants based on WAI seems to be possible. Therefore, the goal should be the specification of normative WAI-data for young infants. However, as was shown in section 4.4, reflectance measures are strongly sensitive to the choice of the reference area. In order to make WAI measures less dependent on this choice (and thus less dependent on the measurement device being used), impedance (or admittance) quantities which do not require area information should be used to arrive at normative data. When reflectance quantities are used in studies, it is essential that complex quantities are specified and that the assumed reference area is also specified to at least allow comparisons with other data.

4.5.2 Age dependency

The model initially proposed in Sankowsky-Rothe et al. (2022a) and extended in this paper targets young infants aged between about 1 to 5 months. The parameter values are partly based on physiological data found in literature. However, the few physiological data available do not allow a more detailed age dependency to be implemented yet. Comparisons of model predictions have been made with ear canal impedances measured on infants aged between 0.5 and 4.8 months. Our model does not account for age dependent effects within these age range yet.

Some age-dependent WAI data can be found in the literature. In Keefe et al. (1993) absorbance values for the age groups of 1 month, 3 months and 6 months showed that up to about 630 Hz the absorbance significantly decreases with increasing age. This was explained by a decrease of the effects due to the soft and flexible ear canal walls. In Shahnaz et al. (2014), absorbance values for the age groups roughly at 0.5, 2, 3, 4, 5 and 6 months showed that below about 500 Hz the absorbance slightly decreases with increasing age. At high frequencies around 3 to 4 kHz, the absorbance increases with increasing age. A comparison of absorbance values for age groups of 1 month and of 6 months shows that an absorbance decreasing with increasing age at low frequencies was found in Hunter et al. (2016), Keefe et al. (1993), and Shahnaz et al. (2014). However, in Keefe et al. (1993) this low-frequency-behavior was observed up to about 2 kHz, in Shahnaz et al. (2014) this was only true up to 500 Hz. In Hunter et al. (2016), in turn, the decreasing absorbance with increasing age was observed in the whole frequency range, but in Keefe et al. (1993) and Shahnaz et al. (2014) an absorbance increasing with increasing age was observed at frequencies around 3 to 4 kHz. It can be concluded that: (1) effects caused by the soft and flexible ear canal walls decrease in the first months of life. (2) age dependency at high frequencies around 3 to 4 kHz can be expected. (3) unfortunately, the results of various studies in which absorbance values were determined for age groups contradict each other.

Furthermore, in Hunter et al. (2016) median absorbance values for newborns and for infants aged 1, 6, 9, and 12 month were published. Significant differences were found between the group of newborns, the age group 1 month and the group 6-12 months. For clinical applications, the authors recommended to use separate normative references for these age groups. Therefore, in the future, an extension of our model to newborns might be valuable for the application of WAI in combination with the universal newborn hearing screening (UNHS). In this context, the effects of fluid in the middle ear are of special interest because UNHS-tests can be affected if amniotic fluid is still present in the middle ear shortly after birth.

4.6 Concluding remarks

In this paper, the parametric electro-acoustic model of eardrum and ear canal impedances of young infants (Sankowsky-Rothe et al., 2022a) was extended to account for specific pathological middle ear conditions:

- The effect of fluid in the middle ear on Z_{ec} was modeled by a single factor x_A decreasing the effective eardrum area and the volume of the tympanic cavity. A factor of about 1/5 showed a good estimation of the effects of fluid in the middle ear observed in measurements on infants' ears aged between 0.5 and 4.8 months.
- For the pathological middle ear condition of negative pressure difference Δp_0 between the

middle ear cavities and the ear canal, a modeling approach was proposed. Characteristic effects in the modeled Z_{ec} caused by a negative Δp_0 were found in the medium frequency range. At about 1.1 kHz, a local magnitude maximum appeared if Δp_0 got negative. The increase of the phase value between 1.2 kHz and 2.5 kHz was shifted to higher frequencies. A confirmation of these effects by measurements wasn't yet possible due to a lack of available measurement data involving negative tympanic pressures. This could be part of future work.

Comparisons between the middle ear states normal, fluid in the middle ear and static pressure difference between ear canal and middle ear showed characteristic differences in all relevant impedance measures predicted with the model. Furthermore, it was shown that different reference diameters which are used in different measurement devices to compute the absorbance or energy reflectance lead to large differences in these impedance measures. Hence, the results are not comparable and should not be used to define normative data. Instead, quantities that do not require area information should be used, such as the acoustic impedance.

In the future, age-dependent adaptations of the model could be valuable, especially to cover newborns. A further pathological condition to be included might be an oedematous middle ear. Furthermore, a middle ear classifier based on impedance (both magnitude and phase) will be developed.

4.7 Data Availability Statement

An implementation of the complete model is available on GitHub, under the reference https://github.com/tobiassankowsky/acoustic_impedance_infant_ear.

References for Chapter 4

- Blankenship, C. M., Hunter, L. L., Keefe, D. H., Feeney, M. P., Brown, D. K., McCune, A., Fitzpatrick, D. F., and Lin, L. (2018). "Optimizing Clinical Interpretation of Distortion Product Otoacoustic Emissions in Infants". In: *Ear & Hearing* 39.6, pp. 1075–1090. doi: [10.1097/aud.0000000000000562](https://doi.org/10.1097/aud.0000000000000562).
- Blau, M., Sankowsky, T., Roeske, P., Mojallal, H., Teschner, M., and Thiele, C. (2010). "Prediction of the sound pressure at the ear drum in occluded human cadaver ears". In: *Acta Acustica united with Acustica* 96.3, pp. 554–566.
- Dirckx, J. J. J., Marcusohn, Y., and Gaihede, M. L. (2013). "Quasi-static Pressures in the Middle Ear Cleft". In: *The Middle Ear*. Ed. by S. Puria, R. R. Fay, and A. N. Popper. New York: Springer, pp. 93–133. isbn: 978-1-4614-6591-1. doi: [10.1007/978-1-4614-6591-1_5](https://doi.org/10.1007/978-1-4614-6591-1_5).
- Feeney, M. P., Hunter, L. L., Kei, J., Lilly, D. J., Margolis, R. H., Nakajima, H. H., Neely, S. T., Prieve, B. A., Rosowski, J. J., Sanford, C. A., Schairer, K. S., Shahnaz, N., Stenfelt, S., and Voss, S. E. (2013). "Consensus Statement". In: *Ear and Hearing* 34.Supplement 1, 78s–79s. doi: [10.1097/aud.0b013e31829c726b](https://doi.org/10.1097/aud.0b013e31829c726b).
- Gan, R. Z. and Wang, X. (2007). "Multifield coupled finite element analysis for sound transmission in otitis media with effusion". In: *The Journal of the Acoustical Society of America* 122.6, pp. 3527–3538. doi: [10.1121/1.2793699](https://doi.org/10.1121/1.2793699).

- Hoth, S. (2011). "Audiometrie – Die Untersuchung des Gehörs und seine technische Versorgung". In: *Medizintechnik: Verfahren – Systeme – Informationsverarbeitung*. Ed. by R. Kramme. 4th ed. Berlin, Heidelberg: Springer, pp. 217–270. isbn: 978-3-642-16187-2. doi: [10.1007/978-3-642-16187-2_15](https://doi.org/10.1007/978-3-642-16187-2_15).
- Hunter, L. L., Keefe, D. H., Feeney, M. P., Fitzpatrick, D. F., and Lin, L. (2016). "Longitudinal development of wideband reflectance tympanometry in normal and at-risk infants". In: *Hearing Research* 340, pp. 3–14. doi: [10.1016/j.heares.2015.12.014](https://doi.org/10.1016/j.heares.2015.12.014).
- Keefe, D. H., Bulen, J. C., Arehart, K. H., and Burns, E. M. (1993). "Ear-canal impedance and reflection coefficient in human infants and adults." In: *The Journal of the Acoustical Society of America* 94.5, pp. 2617–2638. doi: [10.1121/1.407347](https://doi.org/10.1121/1.407347).
- Keefe, D. H., Hunter, L. L., Patrick Feeney, M., and Fitzpatrick, D. F. (2015). "Procedures for ambient-pressure and tympanometric tests of aural acoustic reflectance and admittance in human infants and adults". In: *The Journal of the Acoustical Society of America* 138.6, pp. 3625–3653. doi: [10.1121/1.4936946](https://doi.org/10.1121/1.4936946).
- Lenk, A. (1977). *Elektromechanische Systeme Band 2. Systeme mit verteilten Parametern*. Berlin: VEB Verlag Technik.
- Marchant, C. D., Shurin, P. A., Turczyk, V. A., Wasikowski, D. E., Tutihasi, M. A., and Kinney, S. E. (1984). "Course and outcome of otitis media in early infancy: A prospective study". In: *The Journal of Pediatrics* 104.6, pp. 826–831. doi: [10.1016/s0022-3476\(84\)80475-8](https://doi.org/10.1016/s0022-3476(84)80475-8).
- Paradise, J. L., Rockette, H. E., Colborn, D. K., Bernard, B. S., Smith, C. G., Kurs-Lasky, M., and Janosky, J. E. (1997). "Otitis Media in 2253 Pittsburgh-Area Infants: Prevalence and Risk Factors During the First Two Years of Life". In: *Pediatrics* 99.3, pp. 318–333. doi: [10.1542/peds.99.3.318](https://doi.org/10.1542/peds.99.3.318).
- Prieve, B. A., Vander Werff, K. R., Preston, J. L., and Georgantas, L. (2013). "Identification of Conductive Hearing Loss in Young Infants Using Tympanometry and Wideband Reflectance". In: *Ear and Hearing* 34.2, pp. 168–178. doi: [10.1097/aud.0b013e31826fe611](https://doi.org/10.1097/aud.0b013e31826fe611).
- Sankowsky-Rothe, T. (2022). *Parametric model of young infants' eardrum and ear canal acoustic input impedances*. Code. Version v1.0. url: https://github.com/tobiassankowsky/acoustic_impedance_infant_ear.
- Sankowsky-Rothe, T., Becker, A., Plotz, K., Schönfeld, R., Radeloff, A., Van de Par, S., and Blau, M. (2019). "Acoustic input impedance of infants with normal and pathological middle ear". In: *Proceedings of the ICA 2019 and EAA Euroregio. 23rd International Congress on Acoustics, integrating 4th EAA Euroregio 2019* (Sept. 2019). Aachen, Germany. isbn: 978-3-939296-15-7.
- Sankowsky-Rothe, T., van de Par, S., and Blau, M. (2022a). "Parametric model of young infants' eardrum and ear canal impedances supporting immittance measurement results. Part I: Development of the model". In: *Acta Acustica* 6, p. 53. doi: [10.1051/aacus/2022047](https://doi.org/10.1051/aacus/2022047).
- Shahnaz, N., Cai, A., and Qi, L. (2014). "Understanding the Developmental Course of the Acoustic Properties of the Human Outer and Middle Ear Over the First 6 Months of Life by Using a Longitudinal Analysis of Power Reflectance at Ambient Pressure". In: *Journal of the American Academy of Audiology* 25.5, pp. 495–511. doi: [10.3766/jaaa.25.5.8](https://doi.org/10.3766/jaaa.25.5.8).
- Silva, V. D. da (2006). *Mechanics and Strength of Materials*. Berlin, Heidelberg: Springer. doi: [10.1007/3-540-30813-x](https://doi.org/10.1007/3-540-30813-x).
- Stirnemann, A., Graf, H., and Meier, H. (2003). "Akustische Impedanzmessungen in der Hörerätetechnik". In: *Fortschritte der Akustik DAGA 2003*. DEGA. Berlin, pp. 496–497.

Wang, X., Keefe, D. H., and Gan, R. Z. (2016). "Predictions of middle-ear and passive cochlear mechanics using a finite element model of the pediatric ear." In: *The Journal of the Acoustical Society of America* 139.4, pp. 1735–1746. doi: [10.1121/1.4944949](https://doi.org/10.1121/1.4944949).

Chapter 5

Acoustic feedback path modeling for hearing aids: Comparison of physical position based and position independent models

This Chapter was published with identical content in:

The Journal of the Acoustical Society of America, vol. 147, no. 1, pp. 85-100,

Sankowsky-Rothe, T., Schepker, H., Doclo, S. and Blau, M. (2020). "Acoustic feedback path modeling for hearing aids: Comparison of physical position based and position independent models", <https://doi.org/10.1121/10.0000509>

Authors' contributions:

- Tobias Sankowsky-Rothe formulated the research question, developed the physical position based modeling approach, developed the one-dimensional electro-acoustic model, interpreted the experimental and modeling data, and wrote the final paper.
- Henning Schepker formulated the research question, implemented the position independent modeling approach, interpreted the experimental and modeling data, and participated in writing the final paper and wrote subsection 5.4.1.
- Simon Docclo formulated the research question, and participated in writing the final paper.
- Matthias Blau formulated the research questions, participated in interpretation of the experimental and modeling data, and participated in writing the final paper.

Hereby I confirm that Tobias Sankowsky-Rothe contributed to the study as stated above.

.....
Date

.....
Steven van de Par (supervisor)

5.1 Abstract

Acoustic feedback in hearing aids occurs due to the coupling between the hearing aid loudspeaker and microphones. In order to reduce acoustic feedback, adaptive filters are often used to estimate the feedback path. To increase the convergence speed and decrease the computational complexity of the adaptive algorithms, it has been proposed to split the acoustic feedback path into a time-invariant fixed part and a time-varying variable part. A key question of this approach is how to determine the fixed part. In this paper, two approaches are investigated: 1) a digital filter design approach that makes use of the signals of at least two hearing aid microphones, and 2) a defined physical location approach using an electro-acoustic model and the signals of one hearing aid microphone and an additional ear canal microphone. An experimental comparison using measured acoustic feedback paths showed that both approaches enable to reduce the number of variable part coefficients. It is shown that individualization of the fixed part increases the performance. Furthermore, the two approaches offer solutions for different requirements on the effort to a specific hearing aid design on the one hand and the effort during the hearing aid fitting on the other hand.

5.2 INTRODUCTION

In recent years the number of hearing-impaired persons supplied with open-fitting hearing aids has been steadily increasing. Open-fitting hearing aids usually comprise a behind-the-ear (BTE) unit with two or three microphones. In this work we additionally consider the availability of an ear-canal microphone as depicted in Figure 5.2(a). While open-fitting hearing aids largely alleviate problems related to the occlusion effect (i.e., the perception of one's own voice), they are especially prone to the problem of acoustic feedback (Blau et al., 2008). This requires the development of fast-acting and robust acoustic feedback cancellation algorithms.

By definition, the term *acoustic feedback path* describes the acoustic path from output of the receiver to input of the microphone. However, it is common practice to use this term with transductions from and to electrical signals included, i.e. the path from electrical receiver input to electrical microphone output. This path is still referred to as acoustic path in order to distinguish it from other feedback paths which may exist, e.g. a mechanical path.

Among several different strategies to reduce the acoustic feedback in hearing aids (see, e.g., Guo et al., 2012; Nakagawa et al., 2015; Schepker et al., 2016; Spriet et al., 2008; Waterschoot and Moonen, 2011), adaptive feedback cancellation (AFC) is the most promising approach. In AFC the impulse response (IR) of the acoustic feedback path between the hearing aid receiver and the microphone is estimated using an adaptive filter, theoretically allowing for perfect cancellation of the feedback signal. In general, the convergence speed and computational complexity of the adaptive filter depend on the number of adaptive parameters (Sayed, 2003). In order to reduce the number of adaptive parameters, it has been proposed to decompose the acoustic feedback path into two filters (Kates, 2000; Ma et al., 2011; Schepker and Doclo, 2014): 1) a time-invariant *fixed part* and 2) a time varying *variable part*. While the fixed part models components that can be assumed, for one individual subject, to be the same in many feedback paths, e.g., intra-individual transducer characteristics and individual ear canal geometries, the time-varying variable part allows to track changes of the acoustic feedback path caused, e.g., by a moving telephone. In this paper we consider modeling of both transducer characteristics and individual ear canal geometries using

the fixed part.

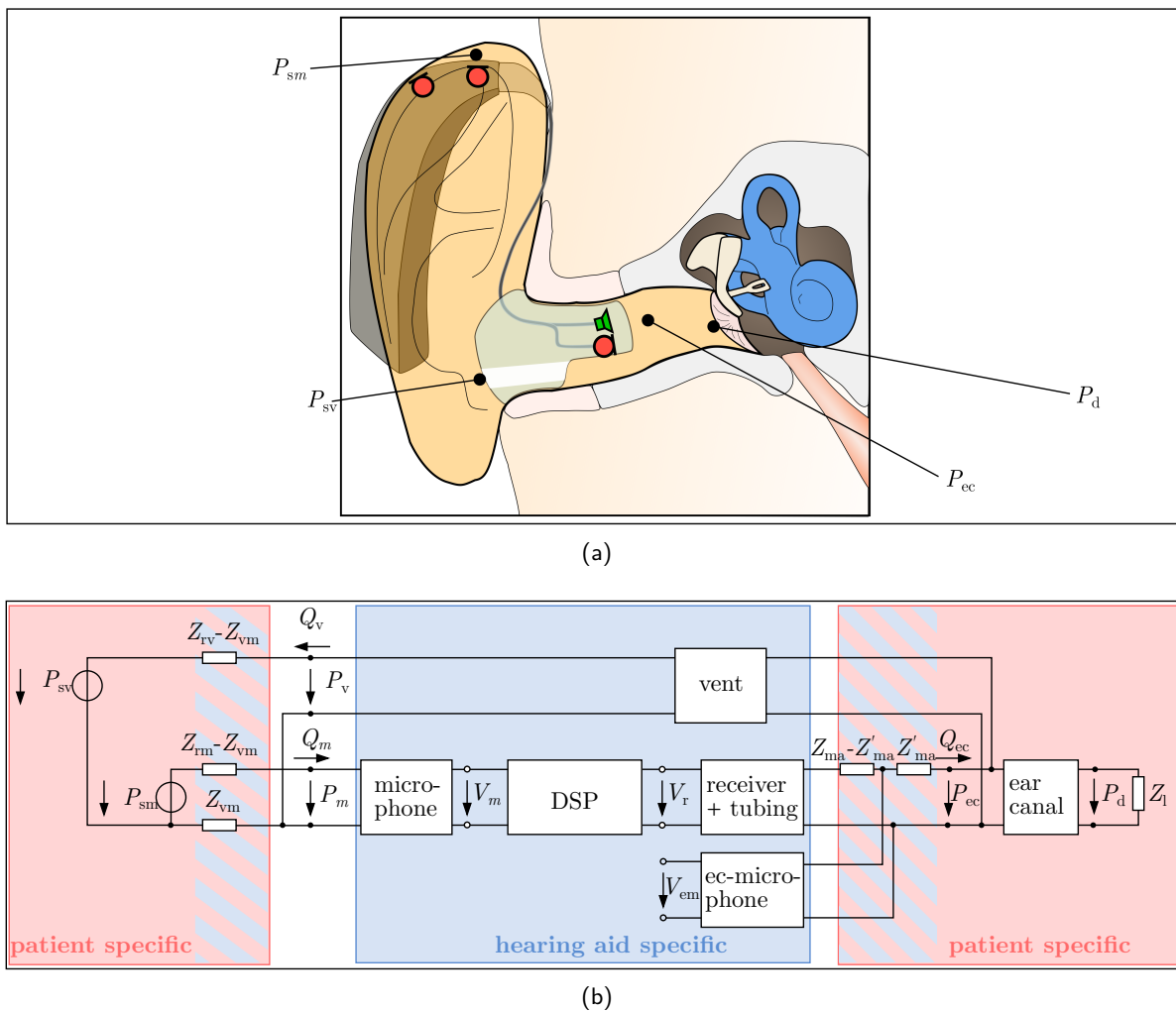


Figure 5.1: (a) Sketch of the scenario with the hearing aid attached to the ear. (b) Electro-acoustic model of the hearing aid at the ear based on the model shown in (Blau et al., 2009).

This decomposition can be achieved by means of different approaches, e.g., using electro-acoustic modeling (Egolf et al., 1989, 1985; Kates, 1988) or using different optimization procedures for digital filter design (Giri and Zhang, 2017; Hashemgeloogherdi and Bocko, 2018; Ma et al., 2011; Schepker and Doclo, 2015, 2016a,b). In electro-acoustic models the different parts of the acoustic feedback path, e.g., the transducer, the tubing, the ear-drum and ear canal as well as the venting are modeled separately. Using two-ports to characterize each of these parts and connecting them in chain they can be used to, e.g., determine the howling frequency components (Egolf et al., 1989). Furthermore, electro-acoustic models can be used to assess the sensitivity of the feedback paths to changes of the ear canal and venting geometries (Kates, 1988). Models based on digital filter design aim at finding a set of common filter coefficients that optimize either the least-squares error (Giri and Zhang, 2017; Hashemgeloogherdi and Bocko, 2018; Ma et al., 2011; Schepker and Doclo, 2016b) or the maximum stable gain of the hearing aid (Schepker and Doclo, 2015, 2016a). While these models do not relate the fixed part to the underlying physical and electro-acoustic properties of the feedback path, they have been shown to be successful in reducing the number of variable part parameters and improving the performance of a state-of-the-art AFC algorithm (Schepker and Doclo, 2016a,b).

Nevertheless, in order to provide a meaningful interpretation of the fixed part it is desirable to specify the physical location up to which the acoustic feedback path can be assumed to be time-invariant. Using electro-acoustic models of the acoustic feedback path allows to separate the complete acoustic feedback path into meaningful units. Such models can be used to specify the physical location between the fixed and the variable feedback path.

In this paper we first briefly review an existing acoustic feedback path model based on digital filter design (Schepker and Doclo, 2016b). Second, in order to define a specific physical location where the fixed part ends, we propose a novel electro-acoustic model of the acoustic feedback path that exploits the availability of an ear canal microphone. Since electro-acoustic analogies are typically not very well suited to model the complex and potentially time-varying sound field outside the ear canal, we also propose to use an all-zero filter to model the variable part. Third, although the ear canal microphone is not placed at the same physical location where the acoustic feedback path is assumed to be split, we propose to directly use the ear canal microphone to measure the fixed part and model it using digital filter optimization. Thus defining the physical location allows to directly control the physical parameters that contribute to the fixed part of the acoustic feedback path and allows in addition to take advantage of the high modeling accuracy of digital filter design and possibilities to track changes.

This paper is organized as follows. In Section 5.3 the generic acoustic feedback cancellation scenario and the acoustic feedback path decomposition is introduced. In Section 5.4 the three different feedback path models, i.e., the feedback path model based on digital filter design, the feedback path model based on electro-acoustic modeling, and a novel combination of these two, are described. In Section 5.5 the three feedback path models are compared using measured acoustic feedback paths from a two-microphone behind-the-ear hearing aid. In Section 5.6 the results are discussed.

5.3 SCENARIO

Consider the single-microphone-single-loudspeaker acoustic feedback cancellation scenario depicted in Figure 5.3(a). The incoming signal in the hearing aid microphone in the frequency-domain is denoted as $S_m(e^{j\Omega})$ at normalized frequency Ω . The microphone signal $Y_m(e^{j\Omega})$ is processed by the hearing aid gain function $G(e^{j\Omega})$, generating the loudspeaker signal $X(e^{j\Omega})$. The loudspeaker and the microphone are coupled by the acoustic feedback path $H_m(e^{j\Omega})$ and the hearing aid gain function $G(e^{j\Omega})$. An (adaptive) filter $\hat{H}_m(e^{j\Omega})$ is used to remove an estimate $\hat{F}_m(e^{j\Omega})$ of the feedback signal $F_m(e^{j\Omega}) = H_m(e^{j\Omega})X(e^{j\Omega})$ from the microphone signal, yielding the error signal $E_m(e^{j\Omega})$. In order to reduce the number of parameters of the filter $\hat{H}_m(e^{j\Omega})$ approximating the acoustic feedback path, the decomposition shown in Figure 5.3(b) can be used, where

$$H_m(e^{j\Omega}) \approx \hat{H}_m(e^{j\Omega}) = \hat{H}^f(e^{j\Omega})\hat{H}_m^v(e^{j\Omega}). \quad (5.1)$$

In this equation, $\hat{H}^f(e^{j\Omega})$ is the time-invariant fixed part independent of $H_m(e^{j\Omega})$ and $\hat{H}_m^v(e^{j\Omega})$ is the variable part that depends on the $H_m(e^{j\Omega})$. In the following we will omit the frequency dependency for conciseness whenever possible.

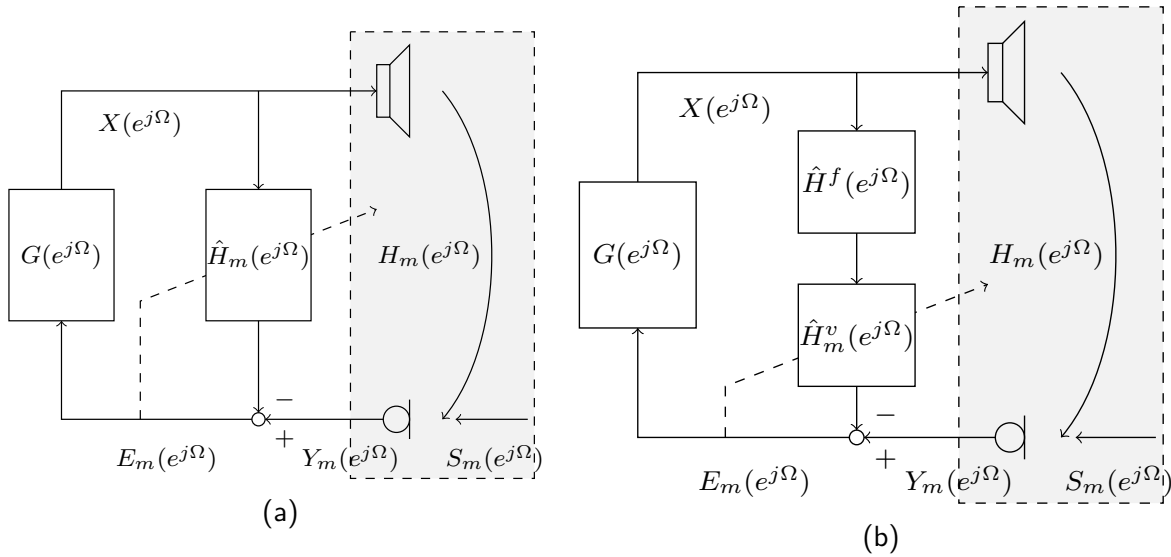


Figure 5.2: Acoustic feedback cancellation frameworks using (a) a conventional adaptive feedback canceller and (b) an adaptive feedback canceller using the proposed feedback path decomposition. The grey box indicates the components included in the acoustic feedback path.

5.4 FEEDBACK PATH MODELS

As mentioned above, the feedback path can be modeled using different approaches that allow for the decomposition of the acoustic feedback path according to (5.1). In the following the acoustic feedback path models based on digital filter design (DFD), the acoustic feedback path model based on electro-acoustic modeling as well as a combination of both will be described. While the feedback path model based on DFD requires the measurement of multiple acoustic feedback paths, e.g., at different microphone locations of the BTE unit, the acoustic feedback path models based on a defined physical location (DPL) for the decomposition (i.e. the electro-acoustic and the combined model) make use of an ear canal microphone to estimate the fixed part of the acoustic feedback path.

5.4.1 Feedback Path Model based on Digital Filter Design

The goal of the feedback path model based on digital filter design (Schepker and Doclo, 2016b) is to decompose a set of M measured acoustic feedback paths $H_m(e^{j\Omega})$ of length N_z^h depicted in Figure 5.4.1(a) into a fixed pole-zero filter $\hat{H}^f(e^{j\Omega})$ with N_p^f poles and N_z^f zeros and M variable all-zero filters $\hat{H}_m^v(e^{j\Omega})$ with N_z^v zeros each depicted in Figure 5.4.1(b), i.e.,

$$\hat{H}^f(e^{j\Omega}) = \frac{B^f(e^{j\Omega})}{A^f(e^{j\Omega})} = \frac{\sum_{i=0}^{N_z^f} b^f[i]e^{-ji\Omega}}{1 + \sum_{i=1}^{N_p^f} a^f[i]e^{-ji\Omega}}, \quad (5.2)$$

$$\hat{H}_m^v(e^{j\Omega}) = B_m^v(e^{j\Omega}) = \sum_{i=0}^{N_z^v} b_m^v[i]e^{-ji\Omega}, \quad (5.3)$$

where $b^f[i]$, $a^f[i]$ and $b_m^v[i]$ are the coefficients of the polynomials representing the fixed zeros, fixed poles and variable zeros, respectively. Note that $A^f(e^{j\Omega})$ is assumed to be based on a monic polynomial, i.e., $a^f[0] = 1$. Note that the feedback path model based on digital filter design does

not make any assumptions on the specific components of the acoustic feedback path that are part of the fixed part but aims at including all components that are common across multiple feedback paths. In order to estimate all the coefficients of the fixed part and the variable parts, the aim is to minimize the least-squares cost function

$$J_{OE}(\mathbf{a}^f, \mathbf{b}^f, \mathbf{b}^v) = \sum_{m=1}^M \int_0^\pi |\tilde{E}_m(e^{j\Omega})|^2 d\Omega, \quad (5.4)$$

with $\tilde{E}_m(e^{j\Omega})$ the so-called output-error

$$\tilde{E}_m = H_m - \frac{B^f}{A^f} B_m^v, \quad (5.5)$$

and $\mathbf{a}^f = [a^f[1] \ a^f[2] \ \dots \ a^f[N_p^f]]^T$, $\mathbf{b}^f = [b^c[0] \ b^f[1] \ \dots \ b^f[N_z^f]]^T$, $\mathbf{b}^v = [(\mathbf{b}_1^v)^T \ (\mathbf{b}_2^v)^T \ \dots \ (\mathbf{b}_M^v)^T]^T$ and $\mathbf{b}_m^v = [b_m^v[0] \ b_m^v[1] \ \dots \ b_m^v[N_z^v]]^T$ the coefficient vectors of the fixed poles, fixed zeros, the stacked variable zeros, and the microphone dependent variable zeros, respectively. $[\cdot]^T$ denotes the transpose operation.

The output-error in (5.5) is non-linear in A^f , B^f and B_m^v and hence minimization of the cost function in (5.4) is not straightforward. In order to circumvent this difficulty, (Schepker and Doclo, 2016b) proposed to minimize the so-called equation-error instead, i.e. to minimize the least-squares cost function

$$J_{EE}(\mathbf{a}^f, \mathbf{b}^f, \mathbf{b}^v) = \sum_{m=1}^M \int_0^\pi |E_m(e^{j\Omega})|^2 d\Omega, \quad (5.6)$$

with E_m the equation-error

$$E_m = A^f H_m - B^f B_m^v. \quad (5.7)$$

The equation-error is only non-linear in B^f and B_m^v and can be optimized using a two-step alternating least-squares procedure (Schepker and Doclo, 2016b). Assuming the coefficient vectors of the fixed part fixed, in the first step the variable part coefficient vector minimizing (5.6) is computed. Assuming the coefficient vector of the variable part fixed, in the second step the fixed part coefficient vectors minimizing (5.6) are computed. These two steps are alternated until a convergence criterion is fulfilled. For a more detailed description of the optimization procedure the reader is referred to Schepker and Doclo, 2016b. Note that the fixed pole-zero filter estimated by minimizing the equation-error is in general stable (Schepker and Doclo, 2016b). However, minimizing the equation-error cost function in (5.6) leads to an undesired weighting of the output-error in (5.5), i.e., $E_m = A^f \tilde{E}_m$, which may lead to poor modeling accuracy in the vicinity of large spectral resonances (Schepker and Doclo, 2016b). To counteract this inherent weighting, the so-called weighted equation-error can be iteratively minimized, i.e., at each iteration i the least-squares cost function

$$J_{WEE}(\mathbf{a}_i^f, \mathbf{b}_i^f, \mathbf{b}_i^v) = \sum_{m=1}^M \int_0^\pi \left| \frac{1}{A_{i-1}^f(e^{j\Omega})} E_{m,i}(e^{j\Omega}) \right|^2 d\Omega \quad (5.8)$$

is minimized (Schepker and Doclo, 2016b).

From (5.8) it can be observed that if $A_{i-1}^f \approx A_i^f$, then $\frac{1}{A_{i-1}^f} E_{m,i} \approx \tilde{E}_m$, hence approximating the desired output-error minimization in (5.4). However, note that the minimization in (5.8) does not guarantee stability of the estimated all-pole filter component $\frac{1}{A^f(z)}$, thus requiring a constraint on

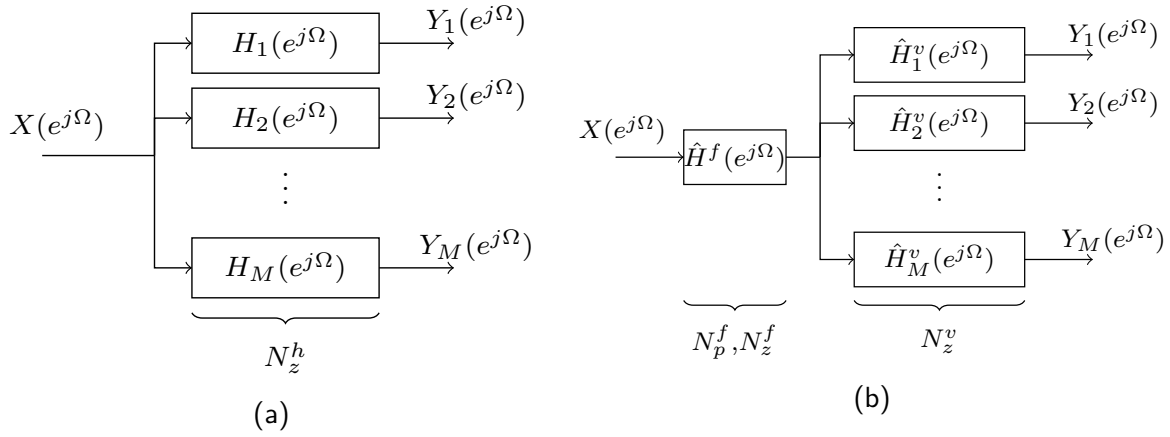


Figure 5.3: System models for the digital filter design based feedback path model: (a) general SIMO system and (b) approximation of the SIMO system using a fixed part

the pole location. Here we use a constraint based on the positive realness of the frequency response $A^f(e^{j\Omega})$ as proposed in Schepker and Doclo, 2016b, i.e.,

$$\Re\{A_i^f(e^{j\Omega})\} \geq \delta \quad \forall \Omega, \quad (5.9)$$

where $\Re\{\cdot\}$ denotes the real part and δ is a small positive constant to control the stability constraint. Similar to minimizing (5.6), (5.8) subject to the constraint in (5.9) can be minimized using a two-step alternating least-squares procedure (Schepker and Doclo, 2016b).

5.4.2 Feedback Path Model based on Electro-Acoustic Modeling

The electro-acoustic model of the hearing aid attached to the ear is depicted in Figure 5.2(b). Based on that model, the components can be divided into three parts:

1. Patient-specific parts, i.e., the sound field at the outer ear, the ear canal, and the load impedance Z_l including the eardrum with the attached middle ear;
2. Hearing aid-specific parts, i.e., microphones, receiver with tubing, and the venting;
3. Patient-specific and hearing aid-specific, i.e., the radiation impedances of the vent Z_{rv} and the microphone Z_{rm} as well as the transfer impedance Z_{vm} between the lateral end of the vent and the microphone, and the cross-sectional change between the receiver tubing and the ear canal represented by the impedance Z_{ma} .

Using this model, the acoustic feedback path is defined by

$$H_m = \frac{V_m}{V_r}, \quad (5.10)$$

where V_m is the voltage at the microphone and V_r is the voltage at the receiver. In the original model depicted in Figure 5.1, P_{sv} and P_{sm} are sound pressures from an external source at the rigidly terminated vent and at the rigidly terminated hearing aid microphone. In order to model the acoustic feedback path only, the model in Figure 5.2(b) can be simplified by omitting the sound sources P_{sv} and P_{sm} outside the ear (i.e. $P_{sv} = P_{sm} = 0$), reducing the two-port representing the ear canal and

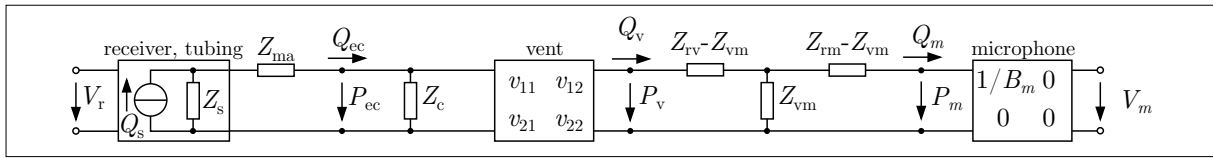


Figure 5.4: Equivalent circuit of the feedback path.

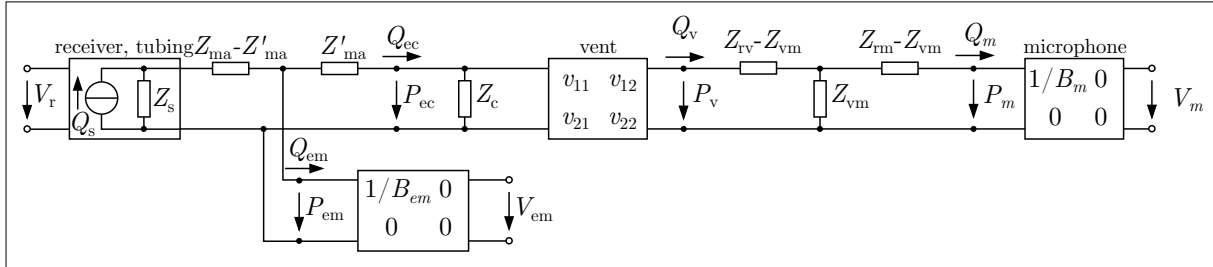


Figure 5.5: Equivalent circuit of the feedback path with incorporation of an ear canal microphone.

the load impedance to a lumped element Z_c , and by omitting the two-port representing the DSP resulting in an open loop structure as depicted in Figure 5.4. Assuming the input impedance of the microphone to be high compared to the impedance of the sound field, i.e., assuming the volume velocity at the microphone Q_m and the lower row of the transfer matrix parameters to be zero, the only parameter used to characterize the microphone equals $\frac{1}{B_m}$, i.e., the reciprocal of the microphone sensitivity B_m . Note that due to the open loop structure the upper right transfer matrix parameter equals zero. Based on these assumptions the feedback path estimate is calculated as

$$\hat{H}_m = \frac{Q_s}{V_r} \frac{Z_s Z_{ec}}{Z_s + Z_{ec} + Z_{ma}} Y_{tv} Z_{vm} B_m, \quad (5.11)$$

with volume velocity Q_s and impedance Z_s the parameters of the Norton-equivalent source, representing the receiver and tubing, Z_{ec} the ear canal impedance resulting from Z_c and the vent input impedance acting in parallel, and Y_{tv} the transfer admittance of the vent. Y_{tv} is defined as the ratio of the volume velocity at the output of the vent Q_v divided by the sound pressure at the input of the vent P_{ec} , i.e.,

$$Y_{tv} = \frac{1}{v_{11} Z_{rv} + v_{12}}, \quad (5.12)$$

with v_{11} and v_{12} the transfer matrix parameters which may be calculated based on a model of an acoustic duct (cf. Section 5.4.2.2).

If the sound pressure in the ear canal P_{ec} is known, the parameters of the Norton-equivalent source Q_s and Z_s as well as the input impedance of the ear canal Z_{ec} are not required and (5.11) can be reformulated as

$$\hat{H}_m = \frac{P_{ec}}{V_r} Y_{tv} Z_{vm} B_m. \quad (5.13)$$

In order to sense the sound pressure in the ear canal, we make use of an ear canal microphone which is located at the medial end of the hearing aid earmold. Unfortunately, this position is located at a cross-sectional change which is known to be influenced by near-field effects (see, e.g., Stinson and Daigle, 2007).

On the other hand, the geometry of this setup, including the position of the microphone, can

be assumed to remain unchanged over time, and hence a simple way of accounting for near-field effects is to split Z_{ma} into two parts, $(Z_{ma} - Z'_{ma})$ and Z'_{ma} , see Figures 5.5 and 5.2(b). Consequently, the sound pressure in the ear canal, P_{ec} , is related to the voltage at the ear canal microphone V_{em} by

$$P_{ec} = \frac{V_{em}}{B_{em}} H_{nf}, \quad (5.14)$$

with B_{em} the sensitivity of the ear canal microphone and

$$H_{nf} = \left(\frac{Z'_{ma}}{Z_{ec}} + 1 \right)^{-1}, \quad (5.15)$$

the transfer function accounting for the near-field effects.

5.4.2.1 Decomposition of the feedback path model based on electro-acoustic modeling

Different factors influence the acoustic feedback path of a hearing aid. For example, variations of the acoustics outside the ear (Hellgren et al., 1999) and ear-canal geometries (Sankowsky-Rothe et al., 2015b) both have a large influence, while different jaw positions have only minor effects (Hellgren et al., 1999; Sankowsky-Rothe and Blau, 2017). Motivated by these results, we propose to decompose the acoustic feedback path based on the different parts used in the model.

For an individually fitted hearing aid the size of the vent will not change and the dimensions of the ear canal undergo only small changes due to jaw movements. Therefore, it is reasonable to incorporate the characteristics of the receiver, the microphones, the ear canal and the vent into the highly individual but (mostly) time-invariant fixed part, i.e., decompose the acoustic feedback paths in (5.13) using (5.14) into a fixed part

$$\hat{H}^f = \frac{V_{em}}{V_r} H_{nf} Y_{tv} \frac{B_m}{B_{em}}, \quad (5.16)$$

and variable parts

$$\hat{H}_m^v = Z_{vm} = \frac{P_m}{Q_v}, \quad (5.17)$$

where the variable parts consider the acoustics of the outer sound field represented by the transfer impedance Z_{vm} , i.e., the sound pressure at the microphone relative to the volume velocity out of the lateral end of the vent.

Strictly speaking, every variation in the feedback path, including variations in the variable part, effects the fixed part as defined above, because the load impedance seen by the source varies. This includes variations in the acoustics of the outer sound field, and variations which are not explicitly included in the model, e.g. additional leakage due to a loose fit. For open fittings, which are addressed here, the effect on the load impedance is supposed to be small. In principle, any variation of the feedback path has to be compensated by the variable part.

5.4.2.2 Parameters of the feedback path model based on electro-acoustic modeling

The fixed part of the feedback path model according to (5.16) consists on the one hand of components being well suited for parametric electro-acoustic modeling, e.g., the near-field effects H_{nf} and the transfer admittance of the vent Y_{tv} . Other components can not easily be modeled parametrically and are therefore measured, e.g., the transfer function of the voltage at the ear canal microphone

relative to the voltage driving the receiver V_{em}/V_r , and the transfer function of the microphone sensitivities B_m/B_{em} . In the following, the computation of H_{nf} and Y_{tv} is described.

The near-field effects are characterized by a shift of the minima in the measured sound pressure (Sankowsky-Rothe et al., 2015a). If near-field effects have a significant influence, the level of the transfer function V_{em}/V_m will show a characteristic notch followed by a peak and the phase shows an increase followed by a decrease, since the minimum is shifted only in V_{em} but not in V_m . This could potentially be used to estimate the transfer function Z'_{ma}/Z_{ec} used to compute the transfer function H_{nf} accounting for the near-field effects. This transfer function can be described by four parameters: an acoustic mass M_{ma} representing the impedance Z_{ma} , and an acoustic mass M_{ec} , an acoustic compliance C_{ec} , and a resistance R_{ec} representing the impedance Z_{ec} .

Alternatively, the function used to compensate the near-field effects can be approximated by a pole-zero filter using a pair of complex conjugated poles and a pair of complex conjugated zeros. Since the absolute value of both the poles and the zeros can be assumed to be the same, only three parameters need to be estimated: the absolute value r , the phase angle of the poles φ_p , and the phase angle of the zeros φ_z . The transfer function H_{nf} is then given by

$$H_{nf}(r, \varphi_p, \varphi_z) = \frac{1 - 2r \cos(\varphi_z) e^{-j\Omega} + r^2 e^{-j2\Omega}}{1 - 2r \cos(\varphi_p) e^{-j\Omega} + r^2 e^{-j2\Omega}}. \quad (5.18)$$

The three parameters were estimated as follows: In order to determine the phase angles of the poles and zeros, the frequencies at which the derivative of the unwrapped phase of the transfer function V_{em}/V_m had a minimum and a maximum, respectively, were identified, see Figure 5.4.2.2(a). It should be noted that the acoustic feedback path as well as the sound pressure in the ear canal typically show a minimum between 4 kHz and 10 kHz, which is in first approximation caused by a quarter wavelength resonance of the residual ear canal. Hence, in the identification only frequencies larger than 3 kHz were considered. The phase angles of the poles and zeros are given by the normalized frequencies $\varphi_p = \Omega_p$ and $\varphi_z = \Omega_z$, computed as

$$\Omega_p = \operatorname{argmax} \left(\frac{d \operatorname{arg}_u \{V_{em}/V_m\}}{d\Omega} \right), \quad (5.19)$$

$$\Omega_z = \operatorname{argmin} \left(\frac{d \operatorname{arg}_u \{V_{em}/V_m\}}{d\Omega} \right), \quad (5.20)$$

with $\operatorname{arg}_u \{\cdot\}$ the unwrapped phase.

The transfer function H_{nf} used to compensate for the near-field effects is specified to have unity gain, i.e. the first polynomial coefficient representing the zeros $b[0] = 1$. Thus the value of the transfer function at the frequency of the pole location is given by

$$H_{nf}(\Omega_p) = H_0 = \begin{cases} \sqrt{\left| \frac{V_{em}(\Omega_z)/V_m(\Omega_z)}{V_{em}(\Omega_p)/V_m(\Omega_p)} \right|} e^{-j\pi/4} & \text{if } \varphi_z > \varphi_p \\ \sqrt{\left| \frac{V_{em}(\Omega_z)/V_m(\Omega_z)}{V_{em}(\Omega_p)/V_m(\Omega_p)} \right|} e^{j\pi/4} & \text{if } \varphi_z < \varphi_p \end{cases}, \quad (5.21)$$

with the magnitude determined as depicted in Figure 5.4.2.2(b). Using (5.18) the absolute value

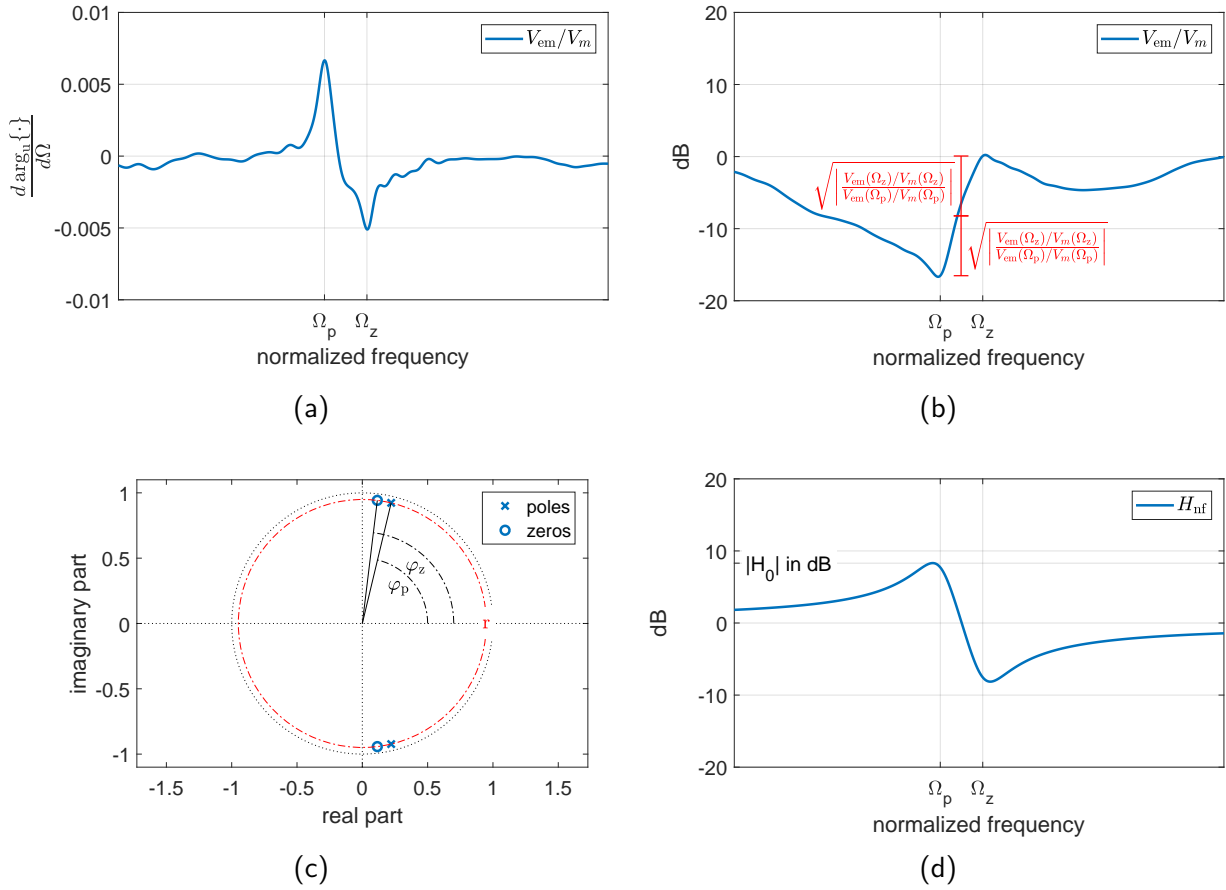


Figure 5.6: Parameter estimation of the transfer function H_{nf} used to compensate nearfield effects. (a) phase angles φ_p and φ_z of the poles and zeros are derived from the derivative of the unwrapped phase of the transfer function V_{em}/V_m . (b) the magnitude $|H_{nf}(\Omega_p)|$ is determined from the transfer function V_{em}/V_m at frequencies Ω_p and Ω_z . (c) poles and zeros in the z-plane. (d) magnitude in dB of the resulting transfer function H_{nf} .

of the poles and zeros (see Figure 5.4.2.2(c)) can than be calculated by

$$r = \left| \sqrt{-e^{j2\varphi_p} + \left((\cos \varphi_z - \cos \varphi_p H_0) \frac{e^{j\varphi_p}}{H_0 - 1} \right)^2} - (\cos \varphi_z - \cos \varphi_p H_0) \frac{e^{j\varphi_p}}{H_0 - 1} \right|. \quad (5.22)$$

The calculation of the transfer admittance Y_{tv} of the vent using (5.12) requires the transfer matrix parameters v_{11} , v_{12} and the radiation impedance Z_{rv} of the vent. The vent was modeled as an acoustical duct considering visco-thermal losses, according to Benade, 1968. This model requires the length l_v and the radius a_v of the vent and additionally we consider a frequency-independent scalar damping factor g_v with which the real part of the propagation constant is multiplied. In previous tests, the coupling of the damping factor g_v to the radius using $g_v = 7 \text{ mm}/a_v$ turned out to be suitable.

The radiation impedance Z_{rv} was modeled as a piston in an infinite baffle with the following approximation (Strutt (Lord Rayleigh), 1896, §§ 302)

$$Z_{rv}(k, a_v) = \frac{\rho c}{\pi a_v^2} \left(\frac{(ka_v)^2}{2} + j \frac{8ka_v}{3\pi} \right), \quad (5.23)$$

with $k = 2\pi\Omega/c$ the wave number, ρ the density of air, and c the speed of sound.

For the transfer impedance Z_{vm} between the lateral end of the vent and the microphone free-field propagation is assumed, i.e., no additional obstructions are in proximity to the ear. Thus the distance-dependent transfer impedance was modeled as a point source on a baffle, i.e.,

$$Z_{vm}(d_{vm}) = e^{-jk d_{vm}} \frac{j\Omega\rho}{2\pi d_{vm}}, \quad (5.24)$$

with d_{vm} being the distance between the vent and the microphone.

The vent parameters and the distance between vent and microphone were estimated using a two-step procedure. In the first step, a desired transfer admittance \tilde{Y}_{tv} was computed from the measured transfer functions V_m/V_{em} and B_{em}/B_m , the correction for the near-field effects $H_{nf}(r, \varphi_p, \varphi_z)$, and the transfer impedance $Z_{vm}(d_{vm})$ with an initial value for the distance d_{vm} , using

$$\tilde{Y}_{tv} = \frac{V_m}{V_{em}} \frac{B_{em}}{B_m} \frac{1}{H_{nf} Z_{vm}}. \quad (5.25)$$

The initial value of d_{vm} was assumed to be 3.8 cm, determined by a measurement of the distance at one ear. In order to obtain the parameters a_v , l_v and g_v used to compute the transfer admittance Y_{tv} in (5.12), the cost function

$$J(a_v, l_v, g_v) = \sum_n \left(\left(20 \log_{10} \left| \frac{Y_{tv}(\Omega_n)}{\tilde{Y}_{tv}(\Omega_n)} \right| \right)^2 \left(1 + \frac{\arg_u(Y_{tv}(\Omega_n)) - \arg_u(\tilde{Y}_{tv}(\Omega_n))}{2\pi} \right)^2 \right) \quad (5.26)$$

was minimized, using logarithmically spaced frequencies Ω_n from 0.0131 to 1.309 (corresponding to 100 Hz to 10 kHz at a sampling frequency of 48 kHz). Minimization of (5.26) is performed using a simplex-fitting procedure (fminsearch from Matlab).

In the second step, the distance d_{vm} was estimated by minimizing the least-squares cost function

$$J(d_{vm}) = \sum_n \left(\frac{\arg_u \left(\frac{V_m}{V_{em}} \frac{B_{em}}{B_m} \frac{1}{H_{nf}} \right) - \arg_u(Y_{tv} Z_{vm})}{2\pi} \right)^2. \quad (5.27)$$

In order to avoid erroneous fitting using unreliable measurements, in both fitting procedures, only those frequency bins were considered where the magnitude squared coherence of V_{em} and V_r was at least 0.8.

The variable part in this modeling approach represents the acoustics outside the ear. A first approximation assuming free-field propagation for a static case is given by (5.24). A possible extension in order to consider reflecting obstructions near the ear would be to incorporate one or more image sources into the model. However, this kind of modeling is expected to lack sufficient precision required for acoustic feedback cancellation. Therefore, in Section 5.4.3 we additionally propose to combine the fixed part as obtained from (5.16) with a variable part obtained using digital filter design.

5.4.2.3 Parameter reduction of measured transfer functions and model variants of the fixed part model based on electro-acoustic modeling

In the modeling approach presented above many components are modeled using electro-acoustic parametrization. However, the transfer functions V_{em}/V_r and B_m/B_{em} are less suited for this kind of parametrization and measurements are usually required. Although this allows for a precise modeling, parametric modeling allows for a low number of parameters to describe these transfer functions efficiently. One way to reduce the number of parameters of the model components characterized by measured transfer functions is to represent the latter by pole-zero filters.

Two different variants to obtain a pole-zero filter for the fixed part, based on electro-acoustic modeling, are proposed:

- (A) the product of the transfer functions V_{em}/V_r and B_m/B_{em} is modeled using a pole-zero filter, i.e. the number of parameters $N^{f,A}$ is given by the sum of N_p^A poles, N_z^A zeros and the 6 parameters ($a_v, l_v, g_v, r, \varphi_p, \varphi_z$) of the electro-acoustic parametrization, resulting in

$$\hat{H}^{f,A} = H_{nf} Y_{tv} \frac{\sum_{i=0}^{N_z^{f,A}} b^A[i] e^{-ij\Omega}}{1 + \sum_{i=1}^{N_p^{f,A}} a^A[i] e^{-ij\Omega}}, \quad (5.28)$$

with $b^A[i]$ and $a^A[i]$ the coefficients of the zeros and poles, respectively. Variant A results in a total number of $N^{f,A} = N_p^{f,A} + N_z^{f,A} + 6$ parameters.

- (B) the complete fixed part obtained from (5.16) is modeled using a pole-zero filter, i.e.,

$$\hat{H}^{f,B} = \frac{\sum_{i=0}^{N_z^{f,B}} b^B[i] e^{-ij\Omega}}{1 + \sum_{i=1}^{N_p^{f,B}} a^B[i] e^{-ij\Omega}}, \quad (5.29)$$

with $b^B[i]$ and $a^B[i]$ the coefficients of the zeros and poles, respectively. Variant B results in a total number of $N^{f,B} = N_p^{f,B} + N_z^{f,B}$ parameters.

5.4.3 Combined Feedback Path Model

5.4.3.1 Combined models using electro-acoustic modeling to derive the fixed part

In order to exploit the high robustness and generalization of electro-acoustic modeling as well as the high flexibility and fast adaptation of digital filter design, in this section both approaches are combined. The combined models using electro-acoustic modeling to derive the fixed part comprises the parametrized variants A or B of the fixed part presented in 5.4.2.3 and a variable part modeled as an FIR-filter, i.e.,

$$\hat{H}^v(z) = B^v(z) = \sum_{i=0}^{N_z^v} b^v[i] z^{-i}, \quad (5.30)$$

with N_z^v filter coefficients. The filter coefficients were estimated by minimizing the following least-squares cost function of the Wiener-Filter

$$J(\mathbf{b}^v) = \int_0^\pi |H(e^{j\Omega}) - B^v(e^{j\Omega}) \hat{H}^{f,x}(e^{j\Omega})|^2 d\Omega, \quad (5.31)$$

with $\hat{H}^{f,x}$ being either $\hat{H}^{f,A}$ or $\hat{H}^{f,B}$.

5.4.3.2 Combined model using a measured transfer function as the fixed part

While the fixed part can be modeled using electro-acoustic modeling as presented in the previous section, it could also be measured using a microphone placed at a position where the acoustic feedback path is time-invariant or only slowly time-varying. This can be assumed for the ear canal microphone, which could hence be exploited also to measure the fixed part of the acoustic feedback paths. Therefore, we propose a combined model $\hat{H}^{f,C}$ in which the product of the transfer functions V_{em}/V_r and B_m/B_{em} is represented by a pole-zero filter with $N_p^{f,C}$ poles and $N_z^{f,C}$ zeros for the fixed part referred to variant C. The variable part was again modeled by a FIR-filter whose coefficients are obtained by minimizing eq. (5.31) using $\hat{H}^{f,C}$.

5.5 EXPERIMENTAL COMPARISON

5.5.1 Acoustic setup and performance measures

In this Section, the different feedback path models, i.e., the model based on digital filter design (cf. Section 5.4.1), and the model based on a defined physical location (cf. Sections 5.4.2 and 5.4.3) including their different variants are compared using measured acoustic feedback paths. The measurements (published in Sankowsky-Rothe et al., 2015b) were performed using a two-microphone BTE hearing aid attached to a dummy head with variable ear canals similar to Hiipakka et al., 2010. Different conditions for the acoustics outside the ear, the ear-canal geometries, and the venting were used. More specifically, three different conditions for the acoustics outside the ear were considered: 1) a free-field condition, i.e., without any obstruction in vicinity of the ear, 2) a wall condition, where the dummy head was placed with its shoulder at a wall, and 3) a telephone condition, where a telephone receiver was placed close to the ear. Furthermore, two different ear canal sizes were used, 1) a small ear canal of 6 mm diameter and 15 mm length, and 2) a large ear canal of 7 mm diameter and 20 mm length. In all measurements custom made open-fitting ear molds were used. The measurements were performed at a sampling rate of 48 kHz and provided as transfer functions computed using a discrete fourier transform with 2^{14} frequency points. The measured feedback paths for the different conditions and ear canal sizes used in the experimental evaluation are depicted in fig. 5.5.1(a). For comparison V_{em}/V_r , which is the voltage at the ear canal microphone relative to the voltage at the receiver, is shown in fig. 5.5.1(b).

The performance of the models is assessed using the added stable gain (ASG), which is defined as (Kates, 2001)

$$ASG = MSG - 20 \log_{10} \left(\min_{\Omega} \frac{1}{|H(e^{j\Omega})|} \right), \quad (5.32)$$

where MSG denotes the maximum stable gain defined as

$$MSG = 20 \log_{10} \left(\min_{\Omega} \frac{1}{|H(e^{j\Omega}) - \hat{H}(e^{j\Omega})|} \right). \quad (5.33)$$

5.5.2 Algorithmic parameters

The algorithmic parameters used in the experimental evaluation will be described in the following sections. First, the general parameters are considered followed by the parameters of the feedback path models based on digital filter design and the parameters of the feedback path models based on a defined physical location for the decomposition.

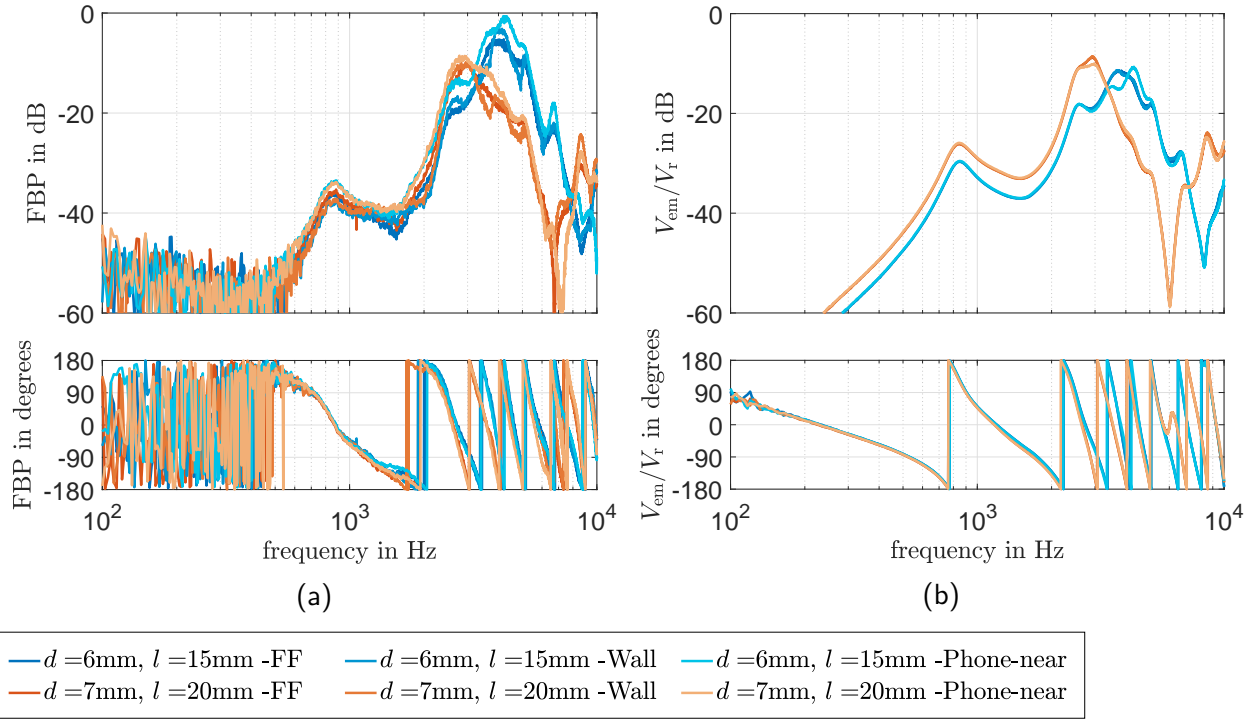


Figure 5.7: (a) acoustic feedback paths (defined as V_m/V_r) and (b) transfer function of the ear canal microphone relative to the receiver voltage V_{em}/V_r measured using a BTE hearing aid on a dummy head with variable ear canals for different sound field conditions and ear canal geometries.

5.5.2.1 General parameters

All impulse responses were computed from the transfer functions as provided in Sankowsky-Rothe et al., 2015b, resampled to 16 kHz, and truncated to a length of 100 samples.

5.5.2.2 Parameters of the feedback path model based on digital filter design

The feedback path model based on digital filter design obtained by minimizing the equation-error (ee) cost functions in (5.6) and the weighted equation-error (wee) cost function in (5.8) was computed for the following set of fixed poles, fixed zeros and variable zeros: $N_p^c, N_z^c \in [0, 1, 2, \dots, 30]$, $N_z^v \in [0, 2, 4, \dots, 50]$. The frequency response $A_i^f(e^{j\Omega})$ in (5.9) of the poles of the fixed part used in the constraint when minimizing the weighted equation-error in (5.8) was computed using a 2048-point discrete Fourier transform. Convergence of the alternating least-squares procedures was assumed when the normalized sum of the difference between successive common part coefficient vectors and successive variable part coefficients vectors was smaller than a predefined constant ϵ , i.e.,

$$\frac{\|\mathbf{p}_{i-1}^c - \mathbf{p}_i^c\|_2}{\|\mathbf{p}_{i-1}^c\|_2} + \frac{\|\mathbf{b}_{i-1}^v - \mathbf{b}_i^v\|_2}{\|\mathbf{b}_{i-1}^v\|_2} \leq \epsilon \quad (5.34)$$

with $\mathbf{p}_i^c = [(\mathbf{a}_i^c)^T \ (\mathbf{b}_i^c)^T]^T$ and $\epsilon = 10^{-4}$. Furthermore, for the minimization of the weighted equation error minimization $\delta = 10^{-4}$ was chosen in (5.9). Two different sets of acoustic feedback paths were considered to compute the fixed pole-zero filter: 1) only the acoustic feedback paths measured in the free-field ($M = 2$) condition were used (DFD ee and DFD wee), 2) all acoustic feedback paths ($M = 6$), i.e., free-field, wall, and telephone, where used (DFD ee full and DFD wee full).

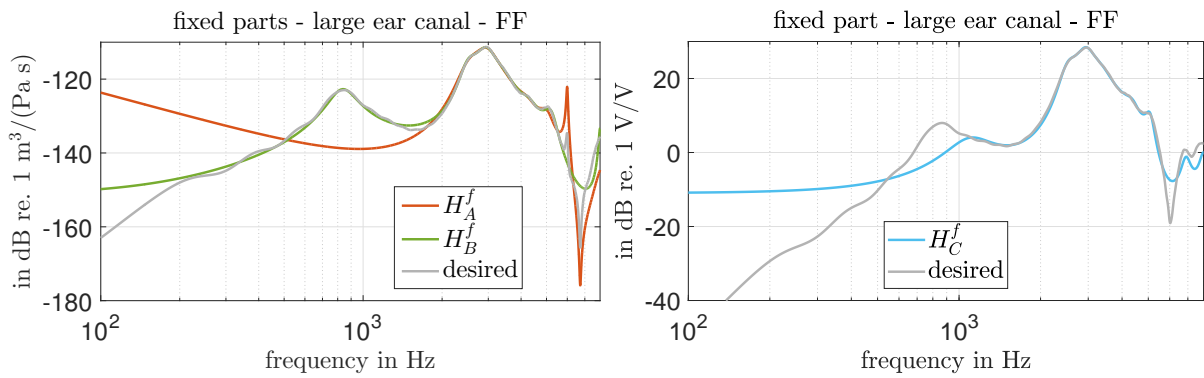


Figure 5.8: Example of the different fixed part variants ($N^f = 20$) for the large ear canal and the free-field condition.

5.5.2.3 Parameters of the feedback path model based on a defined physical location for the decomposition

The filter coefficients in (5.28) and (5.29) of the fixed part variants A and B respectively as well as the coefficients of variant C for the fixed part (cf. section 5.4.3) were derived using the iterative procedure according to Steiglitz and McBride, 1965, using 5 iterations. For all three variants (A, B, and C), the coefficients were computed for $N_p, N_z \in [0, 1, 2, \dots, 30]$.

5.5.3 Comparison of the fixed part variants based on a defined physical location for the decomposition

The fixed parts according to the variants A and B estimate $Q_v B_m / V_r$, i.e., the volume velocity out of the vent multiplied by the sensitivity of the hearing aid microphone divided by the voltage driving the receiver. The fixed part in variant C estimates V_{em} / V_r , i.e., the voltage at the ear canal microphone relative to the receiver voltage. Thus, the three variants cannot be compared directly. The volume velocity cannot be measured without causing additional errors. This means the true fixed part for the variants A and B is in principle unknown. However, the parametrization of the transfer functions can be compared in variants A and B, i.e., comparing the desired fixed part given by (5.16) with H_A^f and H_B^f given by (5.28) and (5.29).

In the left panel of Figure 5.8 the fixed parts according to the variants A and B can be seen for the feedback path measured on the large ear canal under free-field condition using $N^f = 20$ parameters. Additionally, the desired transfer function of the fixed part is shown which results from the non-parameterized feedback path according to (5.16). For both variants the highest accuracy is reached in the frequency range where the transfer function has its maximum. This is a characteristic of the fitting procedure according to Steiglitz and McBride, 1965, which is a desired effect here. Variant A shows much larger deviations to the desired transfer function of the fixed part for frequencies below 1.5 kHz compared to variant B. This is due to the fact that in variant A only 14 parameters of the $N^f = 20$ parameters are used for the pole-zero filter of the fixed part, while in variant B all 20 parameters are used for the pole-zero filter. On the other hand variant A shows a better agreement than variant B at high frequencies where the desired transfer function has its minimum.

The desired (V_{em} / V_r) and the parametrized transfer function of the fixed part of variant C are shown in the right panel of Figure 5.8. Similarly to the other variants, a very good agreement can be seen in a broad frequency range around the maximum of the transfer function. For frequencies

below 1 kHz and at the minimum at about 8 kHz large deviations can be seen.

5.5.4 Comparison of feedback path models

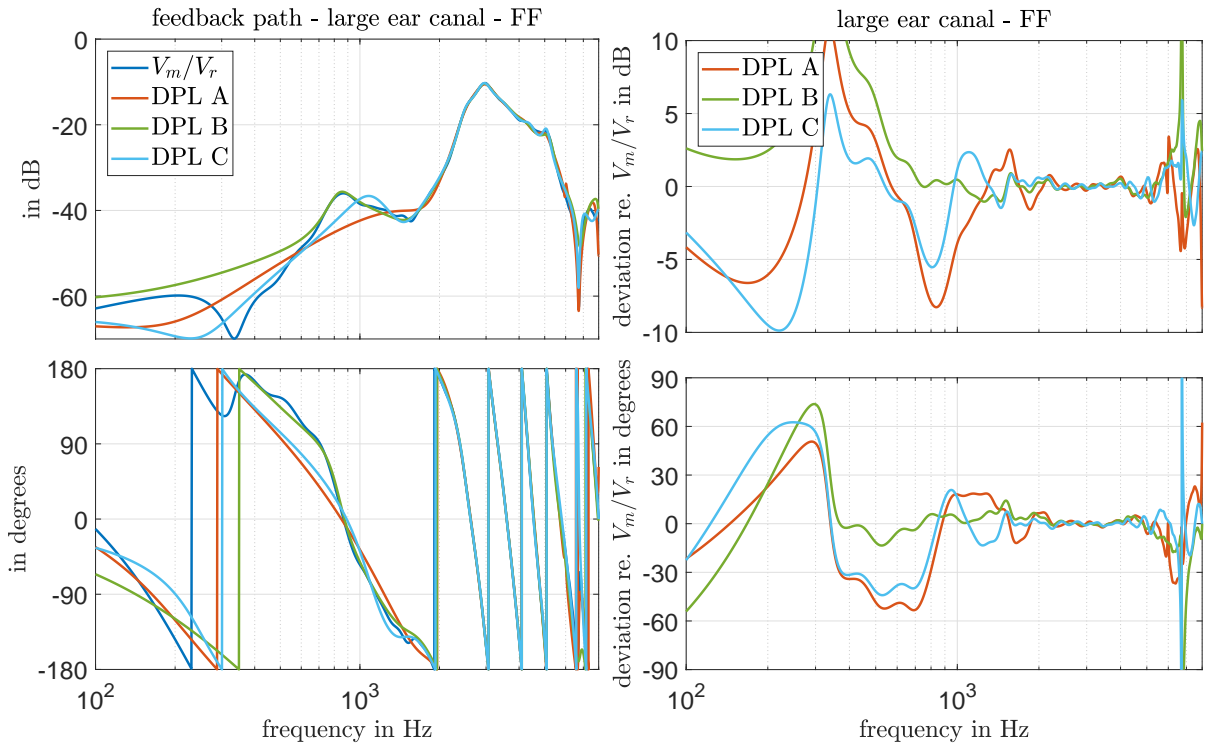


Figure 5.9: Left: Feedback paths for the large ear canal and the free-field condition, measurement and estimations with the combined feedback path models using the different fixed part variants ($N^f = 20$, $N^v = 20$). Right: Deviation of the estimated relative to the measured feedback path.

Figure 5.9 shows in the left column the measured and the estimated complete feedback path using the 3 variants based on a defined physical location (DPL A, DPL B, DPL C) for the large ear canal and the free-field condition. The right column shows the deviations of the estimated to the measured feedback path. The estimations of all variants show a very good agreement with the measurement for the important frequency range around the maximum of the feedback path. At lower and at higher frequencies larger deviations from the measured feedback path as well as differences between the variants can be observed. However, it can be assumed that these deviations don't affect feedback cancellation due to the limited maximum output of the speaker at these frequencies.

While it is difficult to assess the performance of the different variants based on Figure 5.9, in this section all feedback path models are compared in terms of the added stable gain. In all models described in the previous sections the achieved ASG depends on both, the number of parameters of the fixed part and that of the variable part. In order to compare the different models an exemplary number of fixed part parameters $N^f = 20$ was chosen. Note that for the DFD models, different combinations of poles and zeros can result in the same number of fixed parameters, we show the results of those combinations that resulted in the largest ASG, which may be different for different N^v . Figure 5.10 shows the ASG for the free-field condition and the large ear canal for each model as a function of N^v . For values of $N^v \leq 10$ a large increase of the ASG with N^v can be observed for all models. From about $N^v = 10$ this increase is slightly smaller and from about $N^v = 30$ is very small.

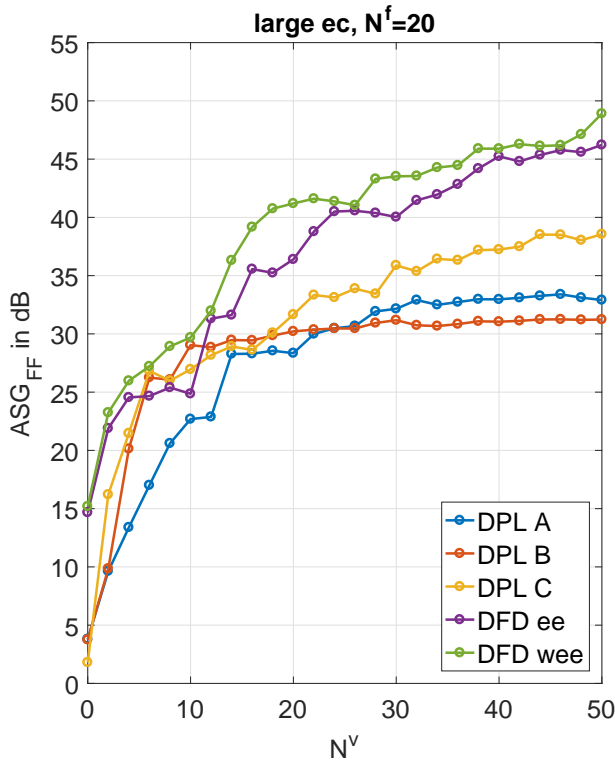


Figure 5.10: Added stable gain as a function of N^v with $N^f = 20$ for the large ear canal and the free-field condition for all models.

The largest ASGs were achieved by the DFD wee model followed by the DFD ee model which are both based on digital filter design. The models based on a defined physical location achieve significantly smaller values of ASG for $N^v > 10$. For $N^v \geq 20$ the variant C outperforms the variants A and B. While these results show the potential of the different models, they do not allow to draw conclusions about the generalizability and robustness, see discussion in Sections 5.6.1 and 5.6.2.

In order to compare the performance of all models for both ear canals and all environmental condition, Figure 5.11 shows the median and quartiles of the ASG values in the range of $10 \leq N^v \leq 30$ for each combination of model, ear canal and environmental condition. The left panel of Figure 5.11 shows the results for the free-field condition. As can be observed the digital filter design based models using only the free-field measurement for optimization (DFD ee and DFD wee) achieve the largest ASG values for the smaller ear canal as well as for the larger ear canal. As can be expected when increasing the set of acoustic feedback paths included in the optimization, the ASG values for the DFD ee full and DFD wee full models are generally lower in the free-field condition. For the other environmental conditions the performance of the different approaches changes. For both, the wall (middle panel of Figure 5.11) and the telephone condition (Figure 5.11) the models based on a defined physical location achieve significantly better ASG values compared to the models based on digital filter design that used only the free-field measurements for optimization (DFD ee and DFD wee). When using all measurements for optimization, however, the performance of the models based on digital filter design is comparable to the performance of the models based on a defined physical location. Generally, among the models based on a defined physical location there is no clear difference between the variants. However, note that for the small ear canal a trend of better ASG values with variant C compared to variants A and B can be observed. Comparing the models based on digital filter design the DFD wee and DFD wee full models achieve better values

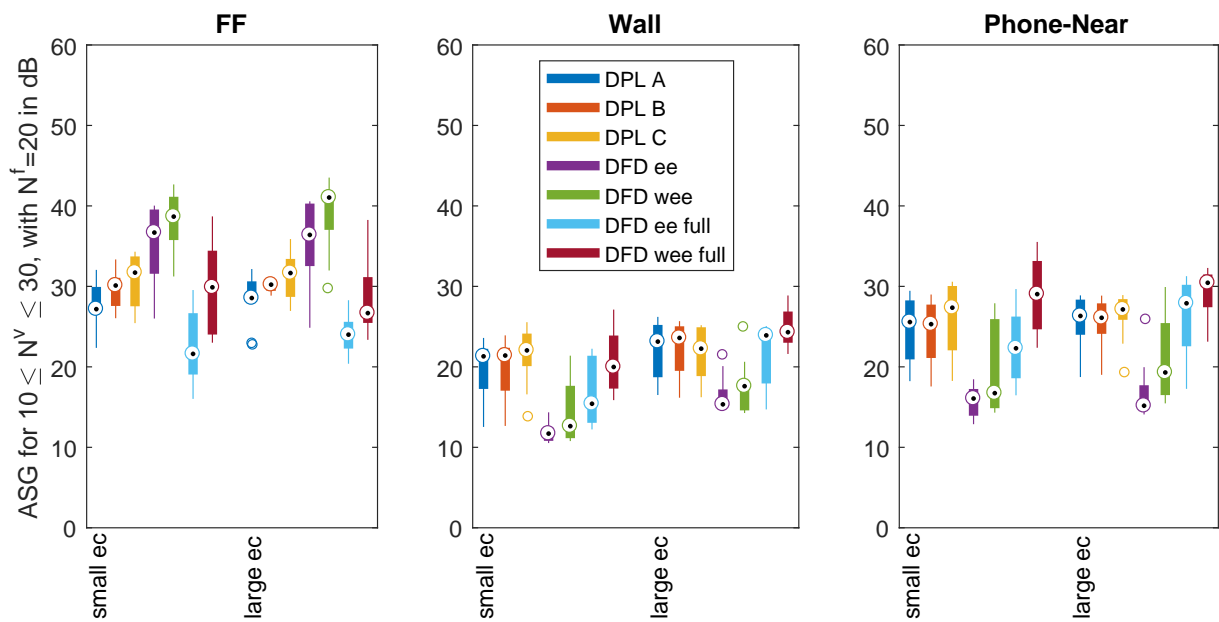


Figure 5.11: Results of the added stable gain for $10 \leq N^v \leq 30$ with $N^f = 20$ for each model and each ear canal. Results are shown on the left for the free-field condition, in the middle for the condition next to a wall, and on the right for the telephone condition.

of the ASG than the DFD ee and DFD ee full models.

5.6 DISCUSSION

5.6.1 Practical considerations and robustness

Two different approaches have been presented to decompose the acoustic feedback path(s) into a time-invariant fixed part and time-varying variable part(s) either using a model based on a defined physical location or based on digital filter design. Both of these modeling approaches provide (mostly) complementary advantages and disadvantages.

On the one hand, the model based on a defined physical location for the decomposition requires an additional microphone in the ear canal and knowledge of the microphone sensitivities. Using the additional microphone, the effort to fit the acoustic feedback path model can be kept small, requiring only a single measurement on the subject, which is similar to fitting procedures of feedback cancellation system of commercially available hearing aids. Furthermore, the model based on a defined physical location is able to provide a fixed part that generalizes well across different acoustic feedback paths.

On the other hand, the model based on digital filter design does not require an additional microphone and can thus be applied to any hearing aid, e.g., in this study a BTE hearing aid with two microphones, which is the case for most commercially available hearing aids. While the measurement of the acoustic feedback paths can be performed in a comparable amount of time that is used to fit acoustic feedback cancellation system in commercially available hearing aids, the fixed part obtained using a single measurement is not as robust to changes in the acoustic feedback paths as the fixed part obtained from the model based on a defined physical location for the decomposition. However, the robustness of the fixed part obtained by using digital filter optimization to variations

can be significantly increased by using multiple feedback path measurements in the optimization (e.g., when the acoustic feedback path is measured in different acoustic conditions as used in the ee full and wee full models). Nevertheless, this requires a careful choice of the acoustic conditions included in the different feedback path measurements. Note that in this study, we have included a free-field, a wall and a telephone condition which covered a broad variability, hence, even though evaluations were carried out using the same measurements, it is expected, that the robustness to unknown feedback paths is similar.

In conclusion, both modeling approaches provide a trade-off between suitability to a specific hearing aid design combined with robustness to variations and the independence of the hearing aid design combined with an increased effort during fitting to achieve robustness.

5.6.2 Number of parameters

In all considered approaches the feedback path is modeled with a fixed part and a variable part. In order to ensure a fast adaptation of the feedback canceler to a changing feedback path, the number of parameters of the variable part should be small. However, if the number of parameters of the variable part is too small, variations of the feedback path cannot be captured, i.e., the ASG decreases. Furthermore, the number of parameters of the fixed part should not be too large in order to avoid overfitting.

A detailed evaluation addressing the optimal order of the models is beyond the scope of this paper, however, Figure 5.12 shows the ASG as a function of the number of fixed parameters for a constant number of both, fixed part and variable part parameters of $N = 40$.

A desired property of the modeling of the fixed part is to reduce the number of variable part parameters while maintaining a high ASG, i.e., having results that are in the top right corner in Figure 5.12. As can be seen for a number of up to 20 parameters for the fixed part (N^f), the performance of the two different models is very similar. For the small ear canal the ASG is in the range of 20 dB to 35 dB and for the large ear canal the ASG is in the range of 22 dB to 37 dB. If N^f is increased further (i.e. the numbers of parameters of the variable part N^v is decreased), the ASG decreases for the combined model with variant C of the fixed part. With the DFD wee full model based on digital filter design the ASG only slightly decreases or even remains constant for N^f between 20 and 30. Hence, when aiming to reduce the number of variable part parameters, the DFD wee model leads to the best results. However, note that especially for larger $N_f > 20$, the presented results need to be interpreted with care since in contrast to the DPL model all feedback paths were known during the optimization. While the DFD model is expected to result in slightly lower ASG values for unknown feedback paths compared to the known feedback paths, results in Schepker and Doclo, 2016b suggest that the performance can still be considered similar. In conclusion, both models are able to reduce the number of variable part parameters, which in a practical implementation may lead to an increased convergence speed of an adaptive filter as has been shown in Schepker and Doclo, 2016a,b.

5.6.3 Difference in model structure to Ma et al., 2011

The decomposition of the acoustic feedback path in hearing aids into a fixed part and a variable part was first proposed by Kates, 2000 and recently extended in Ma et al., 2011, and Schepker and Doclo, 2014. Ma et al., 2011 argued that, in contrast to models based on digital filter design, pure

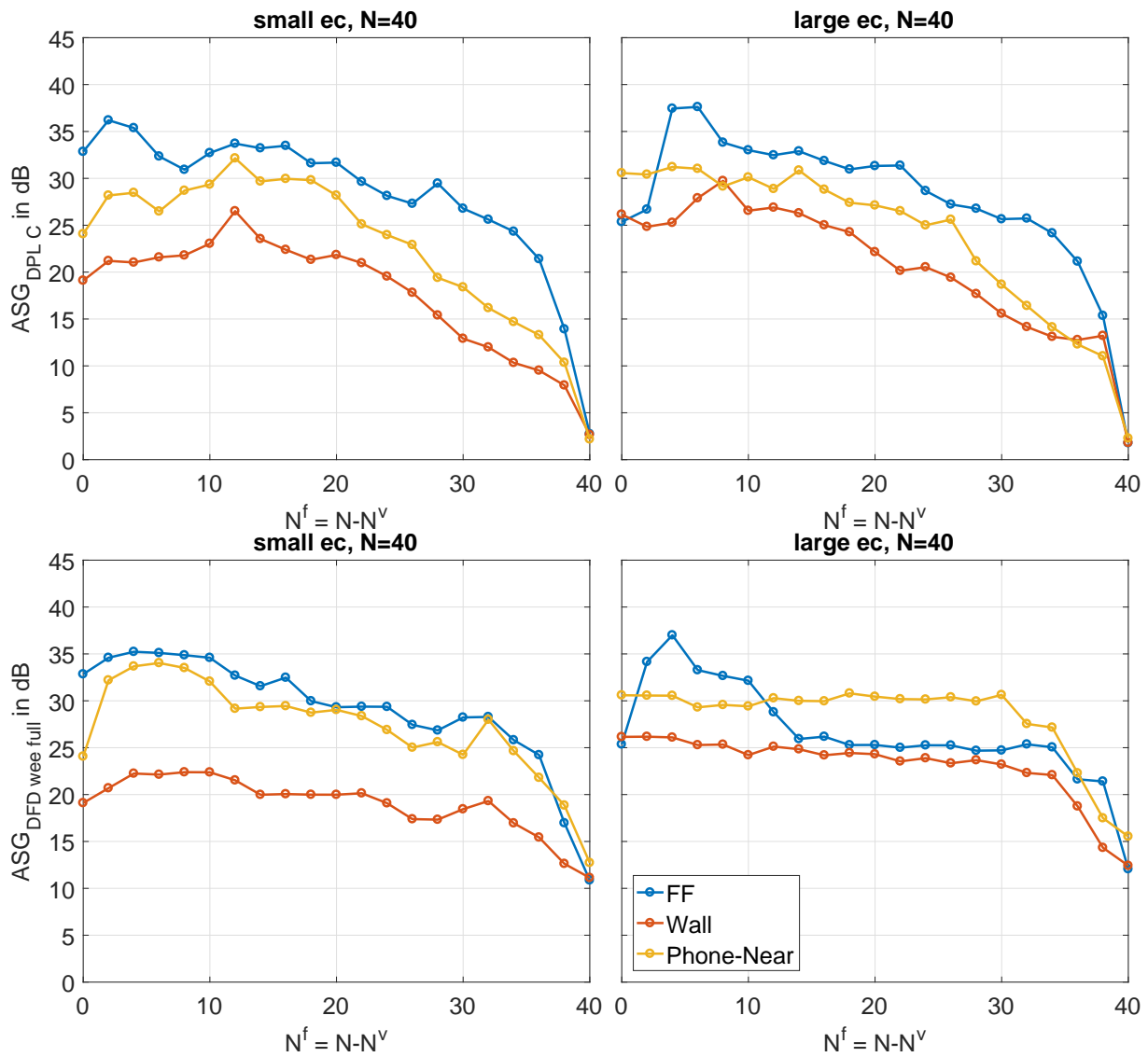


Figure 5.12: Results of the added stable gain for a constant $N = 40$ for the combined model with variant C (top) and for the model wee full (bottom). The left column shows results for the small ear canal and the right column results of the large ear canal. The different colors indicate the different environmental conditions.

electro-acoustic models of the acoustic feedback could not provide the necessary modeling accuracy. However, as shown in this study, models based on a defined physical location for the decomposition, including electro-acoustic models, can be used to obtain a good estimate of the fixed part which can provide a significant increase in the robustness of the estimated acoustic feedback path towards unknown variants that may occur in everyday use.

Furthermore, Ma et al., 2011 assumed that the fixed part models only hearing aid specific parts. This is in contrast to the present study, where patient specific characteristics, i.e., properties of the acoustic feedback path due to the individual anatomy of the patients' ears, are included in the fixed part of the acoustic feedback path model. When using the model based on a defined physical location for the decomposition, these patient specific characteristics are explicitly included, while for the model based on digital filter optimization these are included by the choice of the set of measurements that is used to optimize the fixed and variable parts.

In order to compare the effects of a patient specific fixed filter and a hearing aid specific filter,

Figure 5.13 shows the results for the model based on digital filter optimization when different sets of acoustic feedback paths are used in the optimization. In addition to the previously compared models we also include the following models:

1. DFD non-ind. ee and the DFD non-ind. wee model, where we used the free-field measurements of both ear canal configurations, i.e., a total of $M = 4$ measurements, to obtain a patient independent and hearing aid specific fixed part. Note that by the choice of the measurements, these models can be considered to provide average models across two ear canal geometries.
2. DFD ee half and DFD wee half, where for each ear canal setting we used the free-field and phone-near measurements, i.e., a total of $M = 4$ measurements, to obtain patient-specific fixed parts.

These models allow to compare the effects of a patient-specific fixed filter and a hearing aid specific fixed filter using the same number of measurements used in the optimization of the fixed filter. Note that for both settings the wall condition was not included in the optimization and thus provides insights into the robustness of the fixed part. In general, for the free-field and phone-near conditions the assumptions of an patient-specific fixed filter leads to larger ASG. For the wall condition, the results indicate that depending on the used optimization procedure a similar or better median performance is obtained for the patient-specific fixed part compared to a hearing aid-specific fixed part.

In practice, generally the lowest ASG across different acoustic conditions determines the amount of amplification that can be applied in a hearing aid. For the results in Figure 5.13 the lowest median ASGs for the different models are 12 dB (DFD non-ind. ee), 13 dB (DFD non-ind. wee), 12 dB (DFD ee half), and 14 dB (DFD wee half) for the smaller ear canal, as well as 15 dB (DFD non-ind. ee), 23 dB (DFD non-ind. wee), 20 dB (DFD ee half), and 22 dB (DFD wee half) for the large ear canal. Again, this analysis shows that depending on the used optimization procedure, the patient-specific fixed part performs better or at least as well as the hearing aid specific fixed part.

5.7 CONCLUSION

In this paper, acoustic feedback path models were investigated where the acoustic feedback path was decomposed into two different filters: 1) a time-invariant *fixed part* and 2) a time varying *variable part*. Two different approaches used to model the fixed part were compared, both using signals from at least two microphones: 1) a digital filter design approach using an existing acoustic feedback path model which makes use of at least two measurements, e.g., from the two microphones in a two-microphone hearing aid and 2) a defined physical location approach that exploits a novel electro-acoustic model of a hearing aid as well as the signals of one hearing aid microphone and an additional ear canal microphone. The performance of both approaches was investigated using measured feedback paths from a two-microphone behind-the-ear hearing aid with an additional ear canal microphone.

It was shown that both approaches yield comparable results in terms of the average ASG. In order to compute a fixed part model that allows for a robust performance with different unknown acoustic feedback paths, both approaches provide a trade-off between the requirement of an ear

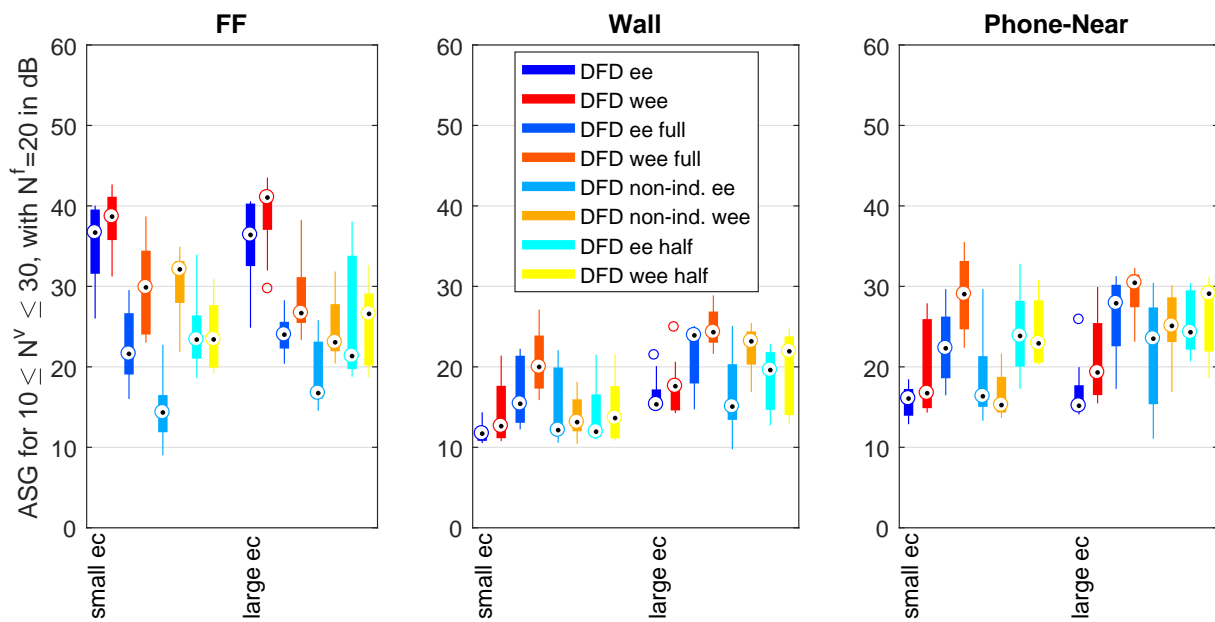


Figure 5.13: Results of the added stable gain for $10 \leq N^v \leq 30$ with $N^f = 20$ for the DFD-models with and without individualization for each ear canal. Results are shown for the free-field condition (left), for the condition next to a wall (center), and for the telephone condition (right).

canal microphone and a minimal effort during hearing aid fitting for the physical-location-based model on the one hand, and the independence of the hearing aid design and an increased effort during fitting for the digital filter-design-based model on the other hand. A comparison of the performance for a constant total number of parameters ($N = 40$) using the best variants of both approaches showed that both models are able to reduce the number of variable part parameters while maintaining a high ASG and therefore potentially allow for an increased convergence speed of an adaptive filter, as has been shown in Schepker and Doclo, 2016a,b. Furthermore, a comparison between a hearing aid-specific fixed part and the proposed patient-specific fixed part showed the potential of using a patient-specific fixed part.

Acknowledgments

This work was funded by the Deutsche Forschungsgemeinschaft (DFG, German Research Foundation) – project number 352015383 – SFB 1330 C1, the Research Unit FOR 1732 "Individualized Hearing Acoustics", and the Cluster of Excellence 1077 "Hearing4All".

References for Chapter 5

- Benade, A. H. (1968). "On the Propagation of Sound Waves in a Cylindrical Conduit". In: *The Journal of The Acoustical Society of America* 44.2, pp. 616–623. doi: [10.1121/1.1911130](https://doi.org/10.1121/1.1911130).
- Blau, M., Sankowsky, T., Stirnemann, A., Oberdanner, H., and Schmidt, N. (2008). "Acoustics of Open Fittings". In: *Proceedings of Acoustics '08 Paris*, pp. 711–716.
- Blau, M., Sankowsky, T., Roeske, P., and Fischer, S. (2009). "Predicting the acoustics of individual ears for hearing aid and audio applications - model framework and future work". In: *Proceedings of NAG/DAGA 2009 in Rotterdam (the Netherlands)*, pp. 1266–1268.

- Egolf, D. P., Haley, B. T., Howell, H. C., Legowski, S., and Larson, V. D. (1989). "Simulating the open-loop transfer function as a means for understanding acoustic feedback in hearing aids". In: *The Journal of the Acoustical Society of America* 85.1, pp. 454–467. doi: [10.1121/1.397697](https://doi.org/10.1121/1.397697).
- Egolf, D. P., Howell, H. C., Weaver, K. A., and Barker, D. S. (1985). "The hearing aid feedback path: Mathematical simulations and experimental verification". In: *The Journal of the Acoustical Society of America* 78.5, pp. 1578–1587. doi: [10.1121/1.392795](https://doi.org/10.1121/1.392795).
- Giri, R. and Zhang, T. (2017). "Bayesian Blind Deconvolution with application to acoustic Feedback Path modeling". In: New Orleans, LA, USA. New Orleans, LA, USA: IEEE, pp. 601–605. isbn: 978-1-5090-4118-3. doi: [10.1109/ICASSP.2017.7952226](https://doi.org/10.1109/ICASSP.2017.7952226).
- Guo, M., Jensen, S. H., and Jensen, J. (2012). "Novel Acoustic Feedback Cancellation Approaches in Hearing Aid Applications Using Probe Noise and Probe Noise Enhancement". In: *IEEE Transactions on Audio, Speech, and Language Processing* 20 (9), pp. 2549–2563. doi: [10.1109/TASL.2012.2206025](https://doi.org/10.1109/TASL.2012.2206025).
- Hashemgeloogardi, S. and Bocko, M. F. (2018). "Inherently Stable Weighted Least-Squares Estimation of Common Acoustical Poles With the Application in Feedback Path Modeling Utilizing a Kautz Filter". In: *IEEE Signal Processing Letters* 25 (3), pp. 368–372. doi: [10.1109/LSP.2017.2785355](https://doi.org/10.1109/LSP.2017.2785355).
- Hellgren, J., Lunner, T., and Arlinger, S. (1999). "Variations in the feedback of hearing aids." In: *The Journal of the Acoustical Society of America* 106.5, pp. 2821–2833. doi: [10.1121/1.428107](https://doi.org/10.1121/1.428107).
- Hiipakka, M., Tikander, M., and Karjalainen, M. (2010). "Modeling the External Ear Acoustics for Insert Headphone Usage". In: *J. Audio Eng. Soc.* 58.4, pp. 269–281.
- Kates, J. M. (2001). "Room reverberation effects in hearing aid feedback cancellation." In: *The Journal of the Acoustical Society of America* 109.1, pp. 367–378. doi: [10.1121/1.1332379](https://doi.org/10.1121/1.1332379).
- Kates, J. M. (1988). "A computer simulation of hearing aid response and the effects of ear canal size". In: *The Journal of the Acoustical Society of America* 83.5, pp. 1952–1963. doi: [10.1121/1.396481](https://doi.org/10.1121/1.396481).
- Kates, J. M. (2000). "Feedback cancellation apparatus and methods". 6,072,884.
- Ma, G., Gran, F., Jacobsen, F., and Agerkvist, F. (2011). "Extracting the invariant model from the feedback paths of digital hearing aids." In: *The Journal of the Acoustical Society of America* 130.1, pp. 350–363. doi: [10.1121/1.3592240](https://doi.org/10.1121/1.3592240).
- Nakagawa, C., Nordholm, S., and Yan, W.-Y. (2015). "Analysis of Two Microphone Method for Feedback Cancellation". In: *IEEE Signal Processing Letters* 22.1, pp. 35–39. doi: [10.1109/LSP.2014.2345571](https://doi.org/10.1109/LSP.2014.2345571).
- Sankowsky-Rothe, T., Blau, M., Köhler, S., and Stirnemann, A. (2015a). "Individual Equalization of Hearing Aids with Integrated Ear Canal Microphones". In: *Acta Acustica united with Acustica* 101.3, pp. 552–566. doi: [10.3813/AAA.918852](https://doi.org/10.3813/AAA.918852).
- Sankowsky-Rothe, T. and Blau, M. (2017). "Static and dynamic measurements of the acoustic feedback path of hearing aids on human subjects". In: *Proceedings of Meetings on Acoustics*. Vol. 30. 1. Boston, p. 050008. doi: [10.1121/2.0000618](https://doi.org/10.1121/2.0000618).
- Sankowsky-Rothe, T., Schepker, H., and Blau, M. (2015b). "Reziproke Messung des akustischen Feedbackpfades bei Hörgeräten". In: *Fortschritte der Akustik DAGA 2015*. Nürnberg.
- Sayed, A. (2003). *Fundamentals of Adaptive Filtering*. John Wiley & Sons, Hoboken, NJ.
- Schepker, H. and Doclo, S. (2014). "Modeling the common part of acoustic feedback paths in hearing aids using a pole-zero model". In: *IEEE International Conference on Acoustics, Speech*

- and *Signal Processing (ICASSP)*. Florence, Italy, pp. 3693–3697. doi: [10.1109/icassp.2014.6854285](https://doi.org/10.1109/icassp.2014.6854285).
- Schepker, H. and Doclo, S. (2015). “Common part estimation of acoustic feedback path in hearing aids optimizing maximum stable gain”. In: *IEEE International Conference on Acoustics, Speech and Signal Processing (ICASSP)*. Brisbane, Australia. doi: [10.1109/icassp.2015.7178049](https://doi.org/10.1109/icassp.2015.7178049).
- Schepker, H. and Doclo, S. (2016a). “A Semidefinite Programming Approach to Min-max Estimation of the Common Part of Acoustic Feedback Paths in Hearing Aids”. In: *IEEE/ACM Transactions on Audio, Speech, and Language Processing* 24.2, pp. 366–377. doi: [10.1109/taslp.2015.2507940](https://doi.org/10.1109/taslp.2015.2507940).
- Schepker, H. and Doclo, S. (2016b). “Least-Squares Estimation of the Common Pole-Zero Filter of Acoustic Feedback Paths in Hearing Aids”. In: *IEEE/ACM Transactions on Audio, Speech, and Language Processing* 24.8, pp. 1334–1347. doi: [10.1109/taslp.2016.2554288](https://doi.org/10.1109/taslp.2016.2554288).
- Schepker, H., Tran, L. T. T., Nordholm, S., and Doclo, S. (2016). “Improving adaptive feedback cancellation in hearing aids using an affine combination of filters”. In: Shanghai, China. Shanghai, China: IEEE, pp. 231–235. isbn: 978-1-4799-9987-3. doi: [10.1109/ICASSP.2016.7471671](https://doi.org/10.1109/ICASSP.2016.7471671).
- Spriet, A., Doclo, S., Moonen, M., and Wouters, J. (2008). “Springer Handbook of Speech Processing”. In: *Springer Handbook of Speech Processing*. Ed. by J. Benesty, M. Sondhi, and Y. Huang. Springer Berlin Heidelberg. Chap. Feedback Control in Hearing Aids, pp. 979–1000. isbn: 978-3-540-49125-5. doi: [10.1007/978-3-540-49127-9_48](https://doi.org/10.1007/978-3-540-49127-9_48).
- Steiglitz, K. and McBride, L. (1965). “A technique for the identification of linear systems”. In: *IEEE Transactions on Automatic Control* 10.4, pp. 461–464. doi: [10.1109/TAC.1965.1098181](https://doi.org/10.1109/TAC.1965.1098181).
- Stinson, M. R. and Daigle, G. A. (2007). “Transverse pressure distributions in a simple model ear canal occluded by a hearing aid test fixture.” In: *The Journal of the Acoustical Society of America* 121.6, pp. 3689–3702. doi: [10.1121/1.2722214](https://doi.org/10.1121/1.2722214).
- Strutt (Lord Rayleigh), J. W. (1896). *The Theory of Sound. Volume 2*. London: Macmillan.
- Waterschoot, T. van and Moonen, M. (2011). “Fifty Years of Acoustic Feedback Control: State of the Art and Future Challenges”. In: *Proceedings of the IEEE* 99.2, pp. 288–327. doi: [10.1109/JPROC.2010.2090998](https://doi.org/10.1109/JPROC.2010.2090998).

Chapter 6

General discussion

The main objective of this thesis was the improvement of existing diagnostic and rehabilitative applications addressing hearing impairment or to gain a better understanding of them. This should be achieved by improving one-dimensional electro-acoustic models. In the diagnostic field, the application to be improved was the middle ear screening based on WAI, while in the rehabilitative field, the application was feedback cancellation in hearing aids.

6.1 Main findings of the thesis

In chapter 2, measurements of the acoustic input impedance of young infant's ears were presented. The infants' age was between 2 weeks and 5 months. The measurements were made on subjects assessed to have either a normal or a pathological middle ear. In all pathological ears fluid was present in the middle ear. A custom-made impedance probe with a pressure equalizing duct was used in order to avoid overpressure caused by insertion. It was found that the measurement of the acoustic input impedance in young infants' ear canals using the custom made probe was possible, however, especially with young infants a successful measurement of the acoustic impedance in the ear canal is a special challenge, which can be overcome only partly by technical measures and examination skills. At low frequencies, up to about 1 kHz, many measurements suffer from a bad SNR. Furthermore, a high variability in the sealing of the ear canal was observed in the measurements. A general difference between normal and pathological ears could be observed in the frequency range from 1 kHz to 5 kHz, in both, magnitude and phase of the measured impedances. At high frequencies, a high variability was observed which was supposed to be due to inter-individual differences in the middle ear and the ear canal.

In chapter 3, an existing one-dimensional electro-acoustic model for the adult ear canal and middle ear was adapted to the young infant ear. Further adaptations comprised modifications in order to improve the link to physiological properties and to reduce the overall number of model parameters. Based on physiological differences between young infants and adults, model parameters of the ear canal, the eardrum and the middle ear cavities were modified. The length and the radius of the ear canal were decreased and additionally the effect of the soft and flexible ear canal walls of young infant was taken into account. The increased thickness of the young infants' eardrum was implemented by an increase of the acoustical and mechanical mass and a decreased acoustical compliance. Furthermore, the eardrum acoustical resistance was decreased and parameter values modeling the effective eardrum area, namely the quality factor and the low-pass resonant frequency,

were modified. In the middle ear cavity part of the model, the mastoid air cells were omitted and the volumes of tympanic cavity and the antrum were decreased. In order to improve the relation to the physiology, a model of a stretched circular membrane was used for the eardrum. Simplifications of the model were made for some correction factors of the originally proposed adult model affecting the eardrum acoustic shunt impedance and the effective eardrum area. Finally, the effect of the aditus ad antrum (acting as an acoustical mass) was neglected.

The acoustic input impedance of the ear predicted by the model agreed well with the measurements on normal ears from chapter 2. Based on model simulations, it was found that the soft and flexible ear canal walls of young infants influence the acoustic input impedance of the ear up to about 1.5 kHz. The medium frequency range of the acoustic input impedance of the ear between about 1 kHz to 3 kHz was found to be dominated by the eardrum impedance and thus was deemed to be optimal in order to sense different middle ear properties.

The model was then extended in chapter 4 in order to account for the pathological middle ear conditions of fluid in the middle ear and of a negative static air pressure difference between the ear canal and the middle ear cavities. Both, the fluid condition and the pressure difference condition were implemented by one additional parameter each. The effect of fluid in the middle ear was modeled by decreasing the area of the eardrum and the volume of the tympanic cavity. The general effects of fluid in the middle ear on the acoustic input impedance of the ear which were observed in the measurements from chapter 2 could be reproduced well with the model. A modeling approach for the pathological condition of a negative static air pressure difference between the ear canal and the middle ear cavities was proposed by introducing a model parameter for the pressure difference. However, a validation was not yet possible because too few measurements were available. Using the extended model, the WAI quantities input impedance of the ear, complex reflectance, energy reflectance and energy absorbance were predicted for the different middle ear conditions. An effect caused by the implemented pathological middle ear conditions was found for all WAI measures. Finally, the model was used to predict the effect of different assumptions of the ear canal cross-sectional area at the measurement position on the resulting acoustic absorbance. For this purpose, values of the cross-sectional area were used which had been chosen in other studies. It was shown that the energy absorbance is strongly sensitive to the choice of the assumed ear canal cross-sectional area at the measurement position. Consequently, results from different studies are not comparable and the energy absorbance should not be used to define normative data unless the cross-sectional area at the measurement position is specified.

In chapter 5, the problem of acoustic feedback in hearing aids was investigated in order to improve adaptive feedback cancellation. Two different approaches, namely a position independent approach and an approach based on a defined physical location, used to derive a time-invariant fixed part of the acoustic feedback path of a hearing aid, were compared. The position independent approach was based purely on digital filter design techniques and represented the current state of the art. For the defined physical location approach, a one-dimensional electro-acoustic model was proposed. It was used to define components behaving in a time-invariant manner. The comparison was made in order to quantify the performance in adaptive feedback cancellation by means of the added stable gain. The two approaches, the position independent and the defined physical location approach investigated here, were based on different requirements. The position independent approach, which was based purely on digital filter design techniques, required a set of at least two measured acoustic feedback paths, e.g. at different microphone locations of the hearing aid. The

defined physical location approach required an ear canal microphone.

With the one-dimensional electro-acoustic model, the receiver, the residual ear canal including the acoustic input impedance of the eardrum, the vent of the hearing aid and the microphone were identified to behave in a time-invariant manner. In a first step, different variants of time-invariant fixed parts according to the physical position based approach were compared. It was found that the fixed part directly derived from the transfer function between the receiver signal and the signal of the ear canal microphone slightly outperforms fixed parts which additionally include the sound propagation through the vent of the hearing aid. The variant in which the vent of the hearing aid was excluded from the fixed part, although it is a time-invariant component, might be interpreted to be a combination of the two approaches. In a next step, it was shown that the performance of the position independent digital filter design approach highly depends on the selection of measured feedback paths used to derive the time-invariant fixed part. Eventually, a comparison of the performance between the two approaches showed comparable results.

Besides the different requirements of the two approaches, different advantages were identified. The defined physical location approach, on the one hand, showed a robust performance while only a single measurement in the process of hearing aid fitting was required. The position independent approach, on the other hand, can be used with a standard hearing aid, i.e. there is no need for an ear canal microphone.

6.2 Conclusions

In this section, concise answers to the questions raised in this thesis are given.

6.2.1 Middle ear screening for young infants based on WAI

- How can the general differences between the adult's and the young infant's ear canal and middle ear be considered in a one-dimensional electro-acoustic model?
 - In a one-dimensional electro-acoustic model, which has a close relation to the physiological properties, differences in size and mass can easily be considered by modified parameter values. An extended model structure is required in order to consider the effects of the soft and flexible ear canal wall of young infants. A simplification of the model is possible in the middle ear cavity part due to the fact that the pneumatisation of the mastoid is very weak at that age.
- To what extent is the acoustic input impedance influenced by the soft and flexible ear canal wall?
 - The acoustic input impedance is significantly decreased in magnitude and increased in phase at frequencies below about 1.5 kHz.
- Does an optimal frequency range of the acoustic impedance exist, which is sensitive to middle ear properties, without being too much affected by ear canal properties?
 - Yes, the medium frequency range between about 1 kHz to 3 kHz appears to be best suited to sense middle ear properties.

- How can frequent pathological middle ear conditions be considered in the one-dimensional electro-acoustic model?
 - The most frequent pathological middle ear condition in young infants, fluid in the middle ear, can be considered by introducing a single additional model parameter which reduces the effective area of the eardrum. Furthermore, it was proposed to consider the condition of a negative static air pressure difference between the middle ear cavities and the ear canal by an additional model parameter.
- How do different middle ear conditions influence different WAI-measures?
 - For the middle ear conditions investigated (fluid in the middle ear and static air pressure difference between middle ear cavities and ear canal), all relevant WAI-measures show significant and characteristic effects at frequencies between about 700 Hz and 5 kHz. In the complex-valued WAI quantities, these effects can be observed in both, magnitude and phase.
- How do different assumptions of the ear canal cross-sectional area affect the acoustic absorbance?
 - The acoustic absorbance, as would be measured in the ear canals of young infants, is highly sensitive to the choice of the assumed cross-sectional area of the ear canal at the measurement position. Model predictions for the frequency range from 100 Hz to 10 kHz show significant effects at all frequencies.
- Is it possible to trace general differences in the measured impedance caused by pathological conditions?
 - Clear characteristic differences caused by fluid in the middle ear can be observed in measurements of the acoustic input impedance in young infants.
- Is it possible to distinguish such general differences from variations caused by inter-individual differences?
 - A distinction between differences caused by fluid in the middle and inter-individual differences in measurements is possible. A characteristic effect caused by fluid in the middle ear can be observed in the medium frequency range of the measured acoustic input impedance. Only at high frequencies, this effect is superimposed by effects caused by inter-individual differences.

6.2.2 Adaptive feedback cancellation in hearing aids

- How to determine an optimal time-invariant part so that the time varying part can be adapted as fast as possible?
 - Different approaches to determine a time-invariant fixed part of the acoustic feedback path, each with different requirements and advantages, allow a comparable performance in adaptive feedback cancellation, i.e. similar added stable gain while only a small number of filter coefficients is required for the time varying part. Either, a position independent approach which is based purely on digital filter design techniques, or a physical position

based approach which can be represented by a one-dimensional electro-acoustic model can be used.

- Which model components of the one-dimensional electro-acoustic model behave in a time-invariant manner?
 - The hearing aid receiver, the residual ear canal including the acoustic input impedance of the eardrum, the vent of the hearing aid and the microphone were identified to behave in a time-invariant manner.
- What are advantages and disadvantages of the physical position based approach compared to traditional approaches in adaptive feedback cancellation?
 - Compared to the position independent approach, an advantage of the physical position based approach is that only a single measurement is required in the process of hearing aid fitting to determine the time-invariant fixed part. However, a disadvantage is that the hearing aid has to be equipped with an ear canal microphone.
- Is there a benefit from combining the physical position based approach with a traditional approach?
 - The vent of the hearing aid was identified to be a component which behaves in a time-invariant manner. However, it turned out that it is advantageous to exclude the vent from the time-invariant fixed part which can be interpreted as a combination of the physical position based approach with the position independent approach.

6.3 Further implications and outlook

6.3.1 Middle ear screening

The detection of pathological middle ear conditions in young infants is of particular interest not only in order to get information of a subject's state of health. Furthermore, it is of interest in order to assess the consequences regarding the results of other tests. Screening tests which are primarily intended to detect sensorineural hearing loss like tests using otoacoustic emissions or auditory brainstem response typically fail if middle ear sound conduction is impaired. WAI measurements have the potential to detect pathological middle ear conditions. This was confirmed for young infants by this thesis.

A further improvement of the one-dimensional electro-acoustic model should be an evaluation of the proposed modeling approach for the pathological condition of static air pressure difference between the ear canal and the middle ear. This can be achieved by collecting more measurement data of young infants. Another improvement pertains to the age dependency. There are two different aspects to consider here. The acoustic input impedance of the ear predicted by the model was compared to measurements on infant ears aged between 2 weeks to 5 months and it can be expected that there is a developmental change at this age range. In Keefe et al. (1993), it was found that the acoustic input impedance decreases with increasing age in both, the magnitude at frequencies between 400 Hz and 7 kHz and the phase at frequencies between 200 Hz and 4 kHz. This decrease can mostly be explained by ear canal growth. However, another important contribution to the age-dependent differences is the vibration of the soft and flexible ear canal walls which decreases

with increasing age. The model could be improved further by consideration of the age dependency of the decreasing effect caused by the soft end flexible ear canal walls. The second aspect concerning age dependency addresses the group of newborns or neonates. This group, which refers to the age range from birth up to 4 weeks, was barely represented in the measurements in chapter 2. Hunter et al. (2016) published mean acoustic absorbance data for different age groups including newborns and one month old infants. They found lower mean absorbance values for the newborn group compared to the one month group. They explained this effect with remnants of amniotic fluid that resorbs by one month of age. A similar age-dependent difference of group mean values was reported in Merchant et al. (2010), however, the difference was not statistically significant. An extension of the one-dimensional electro-acoustic model in order to predict WAI measures for newborns could provide valuable knowledge for the application of a middle ear screening in conjunction with the universal newborn hearing screening which is typically made in the first days of life.

Normative data are currently lacking for an application of middle ear screening for young infants based on WAI. Therefore, the definition of a suitable measure is necessary. This means that measurement results must not depend on the measurement devices used. The model presented in this thesis could be used to investigate WAI measures based on simulations in which parameter values are varied in order to cover a realistic range. Another necessary stage will be the development of a technical standard for WAI measurement devices. This was pointed out recently in Nørgaard (2022) and is encouraged here. However, concerning the presumption on infant-screening in Nørgaard (2022), that *"the assumption of a fixed characteristic impedance ... may be an adequate and the only feasible measurement method to evaluate the status of the middle ear"* is disagreed. A fixed characteristic impedance means the assumption of a fixed cross-sectional area of the ear canal and the choice of a reflectance quantity like the energy absorbance as a metric. As was shown in this thesis, the acoustic input impedance of the ear is sensitive to pathological middle ear conditions. For this quantity, no assumption about the cross-sectional area of the ear canal has to be made, which eliminates a source of error compared to reflectance quantities. Furthermore, the feasibility of the measurement in young infant's ears was shown.

6.3.2 Ear canal microphones in hearing aids

The use of adaptive feedback cancellation in hearing aids requires the measurement of the acoustic feedback path during the fitting process while the hearing aid is inserted in the subject's ear. In order to obtain a time-invariant fixed part using the position independent approach that achieves high performance while providing robustness to unknown variations of the feedback path, multiple measurements must be made in the fitting process. Between these measurements, the feedback path has to be varied where possible. The defined physical location approach requires only a single measurement at the subjects' ear, in which the transfer function between the signals at the hearing aid receiver and the ear canal microphone is measured. The requirement of an ear canal microphone might appear to be excessive. However, there are a number of other applications that are made possible by an ear canal microphone.

One of these applications is active occlusion control. It is supposed to reduce the annoying acoustic effects arising by the fact that the ear canal is occluded in whole or in part by the hearing aid. The so-called occlusion effect is typically associated with an increased sound pressure level of the own voice at low frequencies. A passive measure to reduce the occlusion effect is to minimize the obstruction of the ear canal, this, however, increases the risk of feedback, i.e. reduces the

maximum possible gain provided by the hearing aid. Zurbrügg et al. (2015) proposed a method for active occlusion control in which an ear canal microphone was used. The method provided a significant reduction of both, the objective occlusion effect measured by means of sound pressure level as well as the subjectively perceived occlusion effect.

Further applications exploiting an ear canal microphone are individual sound pressure equalization and transparency. Individual sound pressure equalization is used to determine the sound pressure at the eardrum of the individual ear. Methods estimating the sound pressure at the eardrum using an ear canal microphone have been proposed in Sankowsky-Rothe et al. (2015a) and in Vogl and Blau (2019). In both, one-dimensional electro-acoustic models were used. Denk et al. (2017) investigated how to achieve an acoustically transparent reproduction with a hearing aid like device equipped with an ear canal microphone. A listening test in which the representation of signals coming from an external sound source through the device were compared to a simulated open ear representation revealed that a reliable distinction was not possible.

Finally, a combination of both application scenarios of this thesis the rehabilitative and the diagnostic application could be considered. A hearing aid equipped with an ear canal microphone could be used to check the middle ear status for the individual subject. This could be especially helpful for parents during infancy of their child, when middle ear infections are common.

Bibliography

- Denk, F., Hiipakka, M., Kollmeier, B., and Ernst, S. M. A. (2017). "An individualised acoustically transparent earpiece for hearing devices". In: *International Journal of Audiology* 57.sup3, S62–S70. doi: [10.1080/14992027.2017.1294768](https://doi.org/10.1080/14992027.2017.1294768).
- Hudde, H. and Engel, A. (1998a). "Measuring and Modeling Basic Properties of the Human Middle Ear and Ear Canal. Part I: Model Structure and Measuring Techniques". In: *ACUSTICA/acta acustica* 84.4, pp. 720–738.
- Hudde, H. and Engel, A. (1998b). "Measuring and Modeling Basic Properties of the Human Middle Ear and Ear Canal. Part II: Ear Canal, Middle Ear Cavities, Eardrum, and Ossicles". In: *ACUSTICA/acta acustica* 84.5, pp. 894–913.
- Hudde, H. and Engel, A. (1998c). "Measuring and Modeling Basic Properties of the Human Middle Ear and Ear Canal. Part III: Eardrum Impedances, Transfer Functions and Model Calculations". In: *ACUSTICA/acta acustica* 84.6, pp. 1091–1108.
- Hudde, H., Engel, A., and Lodwig, A. (1999). "Methods for estimating the sound pressure at the eardrum". In: *The Journal of the Acoustical Society of America* 106.4, pp. 1977–1992. doi: [10.1121/1.427945](https://doi.org/10.1121/1.427945).
- Hunter, L. L., Keefe, D. H., Feeney, M. P., Fitzpatrick, D. F., and Lin, L. (2016). "Longitudinal development of wideband reflectance tympanometry in normal and at-risk infants". In: *Hearing Research* 340, pp. 3–14. doi: [10.1016/j.heares.2015.12.014](https://doi.org/10.1016/j.heares.2015.12.014).
- Keefe, D. H., Bulen, J. C., Arehart, K. H., and Burns, E. M. (1993). "Ear-canal impedance and reflection coefficient in human infants and adults." In: *The Journal of the Acoustical Society of America* 94.5, pp. 2617–2638. doi: [10.1121/1.407347](https://doi.org/10.1121/1.407347).
- Keefe, D. H. (2015). "Human middle-ear model with compound eardrum and airway branching in mastoid air cells." In: *The Journal of the Acoustical Society of America* 137 (5), pp. 2698–2725. doi: [10.1121/1.4916592](https://doi.org/10.1121/1.4916592).
- Kringlebotn, M. (1988). "Network Model for the Human Middle Ear". In: *Scandinavian Audiology* 17.2, pp. 75–85. doi: [10.3109/01050398809070695](https://doi.org/10.3109/01050398809070695).
- Merchant, G. R., Horton, N. J., and Voss, S. E. (2010). "Normative Reflectance and Transmittance Measurements on Healthy Newborn and 1-Month-Old Infants". In: *Ear and Hearing* 31.6, pp. 746–754. doi: [10.1097/aud.0b013e3181e68e68](https://doi.org/10.1097/aud.0b013e3181e68e68).
- Møller, A. R. (1961). "Network Model of the Middle Ear". In: *The Journal of the Acoustical Society of America* 33.2, pp. 168–176. doi: [10.1121/1.1908610](https://doi.org/10.1121/1.1908610).
- Nørgaard, K. M. (2022). "A reciprocity method for validating acoustic ear-probe source calibrations". In: *The Journal of the Acoustical Society of America* 152.5, pp. 2652–2663. doi: [10.1121/10.0014959](https://doi.org/10.1121/10.0014959).

- O'Connor, K. N. and Puria, S. (2008). "Middle-ear circuit model parameters based on a population of human ears". In: *The Journal of the Acoustical Society of America* 123.1, pp. 197–211. doi: [10.1121/1.2817358](https://doi.org/10.1121/1.2817358).
- Onchi, Y. (1961). "Mechanism of the Middle Ear". In: *The Journal of the Acoustical Society of America* 33.6, pp. 794–805. doi: [10.1121/1.1908801](https://doi.org/10.1121/1.1908801).
- Sankowsky-Rothe, T., Blau, M., Köhler, S., and Stirnemann, A. (2015a). "Individual Equalization of Hearing Aids with Integrated Ear Canal Microphones". In: *Acta Acustica united with Acustica* 101.3, pp. 552–566. doi: [10.3813/AAA.918852](https://doi.org/10.3813/AAA.918852).
- Shaw, E. A. G. (1977). "Eardrum representation in middle-ear acoustic networks". In: *Meeting of the Acoustical Society of America*. Vol. 62. Suppl. No. 1, p. 12. doi: [10.1121/1.2016028](https://doi.org/10.1121/1.2016028).
- Shaw, E. A. G. and Stinson, M. R. (1981). "Network concepts and energy flow in the human middle ear". In: *Meeting of the Acoustical Society of America*. Vol. 69. 101. T2, p. 43. doi: [10.1121/1.386273](https://doi.org/10.1121/1.386273).
- Vogl, S. and Blau, M. (2019). "Individualized prediction of the sound pressure at the eardrum for an earpiece with integrated receivers and microphones". In: *The Journal of the Acoustical Society of America* 145.2, pp. 917–930. doi: [10.1121/1.5089219](https://doi.org/10.1121/1.5089219).
- Zurbrugg, T., Stirnemann, A., Kuster, M., and Lissek, H. (2015). "Objective and Subjective Validation of an Active Control Approach to Reduce the Occlusion Effect in Hearing Aids". In: *Acta Acustica united with Acustica* 101.3, pp. 502–509. doi: [doi:10.3813/AAA.918847](https://doi.org/10.3813/AAA.918847).
- Zwislocki, J. (1957). "Some Impedance Measurements on Normal and Pathological Ears". In: *The Journal of the Acoustical Society of America* 29.12, pp. 1312–1317. doi: [10.1121/1.1908776](https://doi.org/10.1121/1.1908776).
- Zwislocki, J. (1962). "Analysis of the middle-ear function. Part I: Input impedance". In: *The Journal of the Acoustical Society of America* 34.8, pp. 1514–1523. doi: [10.1121/1.1918382](https://doi.org/10.1121/1.1918382).

Acknowledgments

First of all I would like to thank Prof. Dr. Steven van de Par and Prof. Dr. Matthias Blau for accepting me as a Ph.D. candidate.

I am extremely grateful to Prof. Dr. Matthias Blau for the supervision, guidance and great commitment to creating a really great working environment. In addition to the great professional expertise, which was expressed in a stimulating and inspiring way, it was especially his understanding reactions in difficult moments that made so much possible for me.

I would like to thank Prof. Dr. Steven van de Par for continuous discussions and his advice with a really remarkable sense for the situation.

Furthermore, I would like to thank Prof. Dr. Karsten Plotz for his valuable support.

I would especially like to thank Sven Kissner, Dr. Mina Fallahi, Reinhild Roden, Felix Stärz and Dr. Henning Schepker. Furthermore, I would like to express my gratitude to all members of the Institut für Hörtechnik und Audiologie for the great working environment. Especially Marco Wilmes and Holger Groenewold should be mentioned here.

I especially thank my children. The joy of their curiosity, their interest, but above all, the sharing of their experiences is immeasurable.

Finally, I thank my wife for the emotional but also very practical support that has been such a valuable help. I am grateful to you for so many things and I am always happy about how we grow together.

Curriculum Vitae

Personal	
Name	Mulualem Tobias Sankowsky-Rothe
Date of birth	15-th of November 1974
Place of birth	Showa/Ethiopia
Education	
2016 – 2023	Ph.D. candidate at the University of Oldenburg, Germany
2007 – 2009	Master of Science (M.Sc.) in Hearing Technology and Audiology at the University of Oldenburg, Germany
2001 – 2005	Dipl.-Ing. (FH) in Hearing Technology and Audiology at the University of Applied Sciences of Oldenburg, Germany
Work	
2005 – 2023	Scientific Staff Member at the University of Applied Sciences of Oldenburg, Germany

Erklärung

Hiermit versichere ich, dass ich diese Arbeit selbstständig verfasst habe und keine anderen als die angegebenen Quellen und Hilfsmittel benutzt habe. Die Dissertation hat weder in Teilen noch in ihrer Gesamtheit einer anderen wissenschaftlichen Hochschule zur Begutachtung in einem Promotionsverfahren vorgelegen. Teile der Dissertation wurden bereits veröffentlicht, wie an den entsprechenden Stellen angegeben.

Außerdem versichere ich, dass ich die allgemeinen Prinzipien wissenschaftlicher Arbeit und Veröffentlichung, wie sie in den Leitlinien guter wissenschaftlicher Praxis der Carl von Ossietzky Universität Oldenburg festgelegt sind, befolgt und keine kommerziellen Vermittlungs- oder Beratungsdienste in Anspruch genommen habe.

Oldenburg, den 06.04.2023

M. Tobias Sankowsky-Rothe